isvr Institute of Sound and Vibration Research

# Design of the Controller for a Shape Memory Alloy Adaptive Tuned Vibration Absorber

**E. Rustighi, M.J. Brennan and B.R. Mace**

ISVR Technical Memorandum No 933

May 2004

University of Southampton

# SCIENTIFIC PUBLICATIONS BY THE ISVR

***Technical Reports*** are published to promote timely dissemination of research results by ISVR personnel. This medium permits more detailed presentation than is usually acceptable for scientific journals. Responsibility for both the content and any opinions expressed rests entirely with the author(s).

***Technical Memoranda*** are produced to enable the early or preliminary release of information by ISVR personnel where such release is deemed to the appropriate. Information contained in these memoranda may be incomplete, or form part of a continuing programme; this should be borne in mind when using or quoting from these documents.

***Contract Reports*** are produced to record the results of scientific work carried out for sponsors, under contract. The ISVR treats these reports as confidential to sponsors and does not make them available for general circulation. Individual sponsors may, however, authorize subsequent release of the material.

UNIVERSITY OF SOUTHAMPTON

INSTITUTE OF SOUND AND VIBRATION RESEARCH

DYNAMICS GROUP

# Design of the Controller for a Shape Memory Alloy Adaptive Tuned Vibration Absorber

by

**E. Rustighi, M.J. Brennan and B.R. Mace**

ISVR Technical Memorandum No: 933

May 2004

Authorised for issue by
Professor M.J. Brennan
Group Chairman

## Abstract

The tuned vibration absorber (TVA) is a well-established device to control vibration. Such a device has been designed in several configurations so that it can be automatically tuned in real time. Previously an adaptive tuned vibration absorber (ATVA) has been designed in a beam-like configuration using shape memory alloy (SMA) wire. In the project described in this report a numerical model of the SMA ATVA has been developed in SIMULINK® . A controller for the device has then been designed and optimized using the numerical model. Finally the controller has been implemented experimentally on the real SMA ATVA. The performances of various controllers have been investigated and it is shown that a relatively simple proportional-derivative (PD) controller is effective in controlling an SMA ATVA.

# Contents

# Chapter 1

# Introduction

The tuned vibration absorber (TVA) [1] is a well-established vibration control device, which can be used to suppress a troublesome resonance or to attenuate the vibration of a structure at a particular forcing frequency. Two of the drawbacks of such a device, however, are that it can detune during operation because of changes in forcing frequency, or that there may be differences between the designed and in-situ behaviour. A variable stiffness element can be used to maintain a tuned condition so that the natural frequency of the absorber can be adjusted with time. This can be achieved in a number of ways, for example by altering the pressure in a set of rubber bellows [2], altering the gap between two beams forming a compound cantilever beam [3], adjusting the number of active coils in a coil spring [4] or changing the temperature of a viscoelastic element [5]. The main advantage of a tunable device is that low damping can be used if the tuning is precise and this reduces the need for a large mass [6].

Recently, adaptive tuned vibration absorbers (ATVAs) that exploit the properties of shape memory alloy (SMA) [7] to realize a variable stiffness element in the TVA have been designed as the mechanical properties (the Young's modulus in particular) of SMA change with temperature. Such a material is inherently simple, compact, and can be safely used in spark-free and zero gravity conditions. The main limitations of SMA, however, are the slow response time (the bandwidth is limited due to heating and cooling restrictions and is only a few Hz at best) and the poor energy conversion efficiency when actuated with an electrical signal. Moreover, SMA has no sensing capability (even if the electric resistance value of SMA could be utilized to monitor the phase transformation [8]) and usually it needs a complex control system.

Williams et al [9] realized an ATVA using spring elements composed of three pairs of SMA wires and one pair of steel wires. On-off actuation of

the SMA elements created an ATVA with four discrete tuned frequencies. Characterisation of the absorber showed variation of the natural frequency of the ATVA of approximately 15%. Manual tuning of the ATVA actuation during a stepped-sine base excitation of the primary system showed a wider band of attenuation than was possible with a non-adaptive absorber.

Rustighi et al [10] designed a continuously tunable SMA ATVA in a beam-like configuration. Two parallel SMA wires, electrically connected in order to realise a heating circuit, were glued and supported in the middle, so that the middle of the beams was the connection point of the TVA. The vibrating system could be simplified as a two degree of freedom (2dof) model. Therefore a TVA with beam elements was described using a simple 2dof model. The dynamic behaviour of the TVA was characterized experimentally, and the behaviour, during continuous heating and cooling, was examined and the TVA was shown to be continuously tunable. A change in the tuned frequency of 17.5% was observed between the cold (martensite microstructure) and hot (austenite microstructure) states. The response time of the SMA ATVA was relatively long because of its thermal inertia. However, it is mechanically simple and had a reasonably good performance, despite the tuning parameters being dependent on the current in a strongly nonlinear way.

In order to achieve vibration attenuation four methods can be used, namely passive, adaptive-passive, semi-active and active control. Passive measures are very effective at suppressing vibrations under steady operating conditions, but are not always effective at minimising vibrations over a range of frequencies. On the other hand active control systems, even if very effective, require relatively large amounts of power while providing the control forces. Adaptive-passive and semi-active controls operate by generating a secondary force passively by actively altering the characteristics of the system so the passive system is most effective.

The method for vibration attenuation discussed in this report is adaptive-passive control and involves the use of as SMA ATVA. This type of vibration control is not always as effective as active control, but can be a significant improvement on simple passive control. Moreover, it has the advantages over an active system of requiring a much simpler control and is inherently stable as no dynamic forces are generated actively.

In order to reduce the vibration of a structure by means of a TVA it has to be always precisely tuned, especially if it has a very low loss factor. One method used to automatically tune a TVA is to keep in quadrature the displacement host structure and the displacement of the TVA mass [2, 4, 11].

Long et al [2] proposed an algorithm to vary the stiffness of an ATVA in order to automatically tune it to keep the velocities of the host structure and of the absorber mass in quadrature. The absorber used in the experi-

mental work consisted of a mass supported by an air-mount, whose natural frequency could be adjusted by varying the pressure in the mount. Open-loop control was used to drive the absorber characteristics such that its natural frequency was approximately equal to the excitation frequency, and then a precise algorithm (a proportional controller) was used to fine tune the absorber. The difference between such a control technique and optimal control was discussed. The penalty for tuning the device by setting the velocities to be in quadrature instead of using an optimal control was found to be negligible. As this technique was easy to implement it was the preferred method to tune the absorber.

Kidner and Brennan [11] designed a controller to adaptively tune a beam-like TVA by varying the cross-section of the beam. They employed a fuzzy logic control algorithm using the phase between the velocity of the neutralizer mass and the velocity of the host structure as the control variable. A simple proportional controller was discussed and compared with a fuzzy logic controller. Both controllers were effective in maintaining the tuned condition of the TVA but the fuzzy logic controller was superior to the simple proportional controller due to its improved tracking and smaller steady-state error.

This project deals with the design of the controller of an SMA ATVA. Although SMA has been used to reduce structural vibrations in many different configurations, SMA devices have usually been adapted manually. Many references on the control of SMA actuators, however, can be found.

Choi and Hwang [12] presented a sliding mode controller to reduce the vibration of a building-like flexible structure where four SMA actuators were installed with a certain inclined angle. The SMA actuators were each modelled as a non-linear first order system. The sliding mode controller was designed by treating frequency and damping deviations as uncertain parameters.

In the same way Song [13] designed an active position controller for an SMA wire actuator using a sliding mode based robust approach in order to compensate for the inherent non-linearity associated with such materials.

As the SMA ATVA is a device developed quite recently, there is little literature on controllers for such a device. Williams et al [14] conducted a theoretical stability analysis of an SMA ATVA controlled using the phase difference between the vibration of the TVA and that of the primary structure. They used Lyapunov-based stability analysis to show that the system is stable under proportional plus integral control across the operating range of the SMA ATVA when an integral reset is included in the control algorithm. The integral reset also substantially improved the performance of the system.

This report concerns the design and realization of a adaptive-passive con-

trol for an SMA ATVA built and tested during a previous project [10]. Following this introduction, section two describes the design of such a controller. A numerical model is set up in order to verify the feasibility of the controller and to optimize the controller characteristics. After a review of "standard" controllers some particular controllers are proposed, tested and optimized. Efforts are then focused on a PD (Proportional-Derivative) controller because it is simple and very effective. At the end of the section some considerations on the robustness and effectiveness of the controllers are outlined. In the third section the results of the experimental tests, carried out on the controllers, are presented and comparisons with predicted results are made. Finally, work carried out is summarized and some conclusions drawn.

# Chapter 2

# Design of the controller

This section concerns the numerical modelling of the SMA ATVA and the design of its controller. First a numerical model, set up in SIMULINK® , is described then a review of some possible controllers is presented. Different control techniques are taken in to account and their efficiency is compared using performance indices. An optimal controller is then sought using both manual and automatic optimal parameter searching techniques. The robustness of such controllers is tested by subjecting the system to different types of excitation and varying the characteristics in the system. Finally some conclusions are drawn on the numerical work carried out.

## 2.1 The numerical model

### 2.1.1 The SMA ATVA model

The numerical model developed to design the controller of the SMA ATVA consists of a model of the absorber and a model of the controller. Figure 2.1 shows a block diagram of the controlled system. In this diagram the SMA ATVA block has two outputs, that is the velocity (or it could be acceleration) at the point where the absorber is connected to the host structure, $\dot{x}_h$, and that of the absorber mass, $\dot{x}_a$. From these quantities it is possible to calculate an error function for the controller. In this work this is the cosine of the difference in phase between the displacement of the host structure and the absorber $\phi$. The approach is similar to the standard regulator problem in feedback control (see figure 2.2).

In order to build the SMA ATVA model the block in figure 2.1 has been subdivided in three sub-blocks (see figure 2.2). The first block describes the thermal behaviour of the SMA wire and it has as an output the temperature

of the wire as a function of the current time history that circulates through it. The second block relates the temperature of the wire to the Young's modulus of the material and the last block describes the behaviour of a 2dof model of a beam-like TVA, the details of which are given in reference [10].

The thermal model of the SMA wire is described by the following differential equation [15, 10]

$$\begin{cases} \rho V c_p \dfrac{\mathrm{d}\theta}{\mathrm{d}t} = I^2 R - \alpha A_e(\theta - \theta_a) \\ \theta(t=0) = \theta_a \end{cases} \tag{2.1}$$

where $\rho$ is the density, $V$ is the volume, $c_p$ is the specific heat, $t$ is the time, $\theta$ is the temperature of the wire, $\theta_a$ is the ambient temperature, $I$ is the current in the circuit, $R$ is the electrical resistance of the wire, $A_e$ is the area of heat exchange and $\alpha$ is the convective coefficient. Table 2.1 gives the values used in the numerical calculations. The time constant $\tau$ and the current constant $\beta$ are given by

$$\tau = \frac{\rho V c_p}{\alpha A_e} \tag{2.2}$$

and

$$\beta = \frac{I^2 R}{\alpha A_e} \tag{2.3}$$

To take into account of the latent heat exchanged during the phase transformation, a non constant value of the specific heat is considered, namely

$$c_= \begin{cases} {}_{high}c_p & M_f \leq \theta \leq A_f \\ {}_{low}c_p & \theta < M_f; \theta > A_f \end{cases} \tag{2.4}$$

where $A_f$ and $M_f$ are temperatures of the SMA phase transformation (see [10] for details). The values that the specific heat can assume are given in table 2.1.

The next block in figure 2.2 takes into account how the elastic modulus of the material changes with temperature. The change in the elastic modulus is directly connected to the change in the lattice structure of the material from the cold phase, martensite, to the hot phase, austenite. The Young's moduli of the martensite, $E_m$, and of the austenite, $E_a$, are respectively 40 and 59 GPa [10]. In order to describe such a phase transformation four parameters have to be considered: the temperature at which austenite phase transformation starts and finishes, $A_s$ and $A_f$; the temperature at which martensite phase transformation starts and finishes, $M_s$ and $M_f$. Material tests reveal that the relationship between Young's modulus $E$ and temperature $\theta$ takes the form shown in figure 2.3 [16]. During a full transformation

| | | |
|---|---|---|
| Density | $\rho$ | 6450 kg/m$^3$ |
| Volume | $V$ | $1.3823 \times 10^{-6}$m$^3$ |
| Specific heat | ${}_{low}c_p$ | 322 J/(kg K) |
| | ${}_{high}c_p$ | 2254 J/(kg K) |
| Ambient temperature | $\theta_a$ | 18 °C |
| Electrical resistance | $R$ | 0.1064 Ω |
| Area of heat exchange | $A_e$ | 0.0028 m$^2$ |
| Convective coefficient | $\alpha$ | 41 W/(m$^2$ K) |
| Time constant | $\tau$ | 25.3280 s |
| Current constant | $\beta$ | 0.0371 °C |

Table 2.1: Settings of the numerical model of the thermal model

the functions $E_{M\rightarrow A}(\theta)$, from the martensite to the austenite state, and the function $E_{M\leftarrow A}(\theta)$, from the austenite to the martensite state, are similar to a cosine function given by [17, 10]

$$E_{M\rightarrow A} = \begin{cases} E_m & \theta < A_s \\ \frac{E_m - E_a}{2}\cos(\pi\frac{\theta - A_s}{A_f - A_s}) + \frac{E_m + E_a}{2} & A_s \leq \theta \leq A_f \\ E_a & \theta > A_f \end{cases} \tag{2.5}$$

$$E_{M\leftarrow A} = \begin{cases} E_m & \theta < M_f \\ \frac{E_m - E_a}{2}\cos(\pi\frac{\theta - M_f}{M_s - M_f}) + \frac{E_m + E_a}{2} & M_f \leq \theta \leq M_s \\ E_a & \theta > M_s \end{cases} \tag{2.6}$$

During a partial transformation the Young's modulus takes a value inside the hysteresis loop following the particular behaviour described in [16]. The simulation data used in the numerical simulation of the SMA block are given in table 2.2.

Even though the TVA may be have different shapes it acts like a spring-mass system that is attached to an host structure. If the host structure can be modelled by a mass-like impedance, then the simplified system is a 2dof model (see figure 2.4) comprising the host machine mass and the vibration absorber. The equations of motion of the two masses are

$$m_h\ddot{x}_h + c_a(\dot{x}_h - \dot{x}_a) + k_a(x_h - x_a) = f_h \tag{2.7}$$

$$m_a\ddot{x}_a + c_a(\dot{x}_a - \dot{x}_h) + k_a(x_a - x_h) = 0 \tag{2.8}$$

| | | |
|---|---|---|
| Austenite start temperature | $A_s$ | 45°C |
| Austenite finish temperature | $A_f$ | 67°C |
| Martensite finish temperature | $M_f$ | 35°C |
| Martensite start temperature | $M_s$ | 57°C |
| Martensite Young modulus | $E_m$ | 40 GPa |
| Austenite Young modulus | $E_a$ | 59 GPa |

Table 2.2: Settings of the numerical model of the SMA block

| | | |
|---|---|---|
| Mass of the structure | $m_h$ | 0.0036 kg |
| Active mass of the TVA | $m_a$ | 0.0053 kg |
| Stiffness of the TVA | $k_a$ | 1422 N/m |
| Structural damping of the TVA | $\eta$ | 0.0175 |
| Viscous damping of the TVA | $c_a$ | 0.0481 kg/s |
| Antiresonance frequency | $f_a$ | 82.3 Hz |
| Resonance frequency | $f_r$ | 129.5 Hz |

Table 2.3: Settings of the numerical model of the TVA system

where $m_h$ and $m_a$ are the masses of the host structure and of the absorber, $f_h$ is the force acting on the mass of the host structure, $k_a$ and $c_a$ are the stiffness and the damping coefficient of the absorber. $\ddot{(\,)}$ and $\dot{(\,)}$ are the second and first derivative with respect to time respectively.

In the time domain it is not possible to use hysteretic damping for the damping in the absorber, so viscous damping has been used with a viscous damping coefficient given by

$$c_a = \eta m_a \omega_a = \frac{\eta k_a}{\omega_a} \tag{2.9}$$

where $\eta$ is the material loss factor and $\omega_a$ is the anti-resonance frequency of the point frequency response function (FRF) of the absorber evaluated at the position where it is attached to the host structure. Such a coefficient has been calculated by equating the dissipated energy at the anti-resonance frequency (i.e. $\omega = \omega_a$) because that is the normal working frequency for a properly tuned TVA. Table 2.3 shows the values of the system constants used for the tests carried out.

The global system for the device considered here has a tuned frequency that changes from 82 to 100 Hz passing from the cold to the hot state [10].

### 2.1.2 The error signal

The first operation in the controller block evaluates the error function which is chosen to be the cosine of the phase angle, $\phi$, between the vibration (displacements, velocities or accelerations) of the host and the absorber mass[1].

The velocities of such masses for discrete frequency excitation $\omega$ can be expressed by

$$\dot{x}_h = \dot{X}_h \cos(\omega t) \tag{2.10}$$

$$\dot{x}_a = \dot{X}_a \cos(\omega t - \phi) \tag{2.11}$$

where $\dot{X}_h$ and $\dot{X}_a$ are the amplitudes of the velocities.

The time averaged product of the velocities over one cycle of period $T = 2\pi\omega^{-1}$ can be written as

$$\overline{\dot{x}_h \dot{x}_a} = \frac{1}{T}\int_0^T \dot{x}_h \dot{x}_a \mathrm{d}t = \frac{\dot{X}_h \dot{X}_a}{2}\cos\phi \tag{2.12}$$

Thus the time averaged product of the velocities of the machine and the TVA mass is proportional to the cosine of the phase between the velocities. When the TVA is tuned, the velocities are in quadrature, so their time averaged product is zero and thus $\cos\phi$ is zero. Therefore this signal can be used as an error signal in a control system.

In practice it is more convenient to consider the normalized time averaged product so that the error always lies between -1 and +1 irrespective of the system and the TVA. The normalized time average product of the velocities is given by

$$\mathrm{norm}(\overline{\dot{x}_h \dot{x}_a}) = 2\frac{\overline{\dot{x}_h \dot{x}_a}}{\dot{X}_h \dot{X}_a} = \cos\phi \tag{2.13}$$

Thus the amplitudes of the velocities $\dot{X}_h$ and $\dot{X}_a$, which are obtained by

$$\dot{X}_i = \frac{\pi}{2T}\int_0^T |\dot{x}_i(t)|\mathrm{d}t \quad i = 1, 2 \tag{2.14}$$

have to be calculated as well.

The integral in the previous equation should be calculated over one period. For adaptive-passive controls a control period $T_c$ can be defined as the period at which the controller updates the adaptive device. Usually the control period is much bigger than the period of the structure velocities: $T_c \gg T$. The error signal can also be calculated over the control period since it gives anyways a very good approximation to the actual value.

[1]This tuning is not optimal but coincides with the optimum when the loss factor $\eta = 0$, and is a very good approximation for small damping [2].

### 2.1.3 The controller model

The controller that evaluates the error signal, $\cos\phi$, at every control period, $T_c$, can be used. The general form of the controller algorithm is

$$I_{n+1} = I_n + f(e_n, e_{n-1}, e_{n-2}, \ldots, e_0) \tag{2.15}$$

with the boundaries

$$0 \leq I_{n+1} \leq I_{max} \tag{2.16}$$

where $I_n$ and $e_n$ are the current and the error at the $n$-th time step, $I_{n+1}$ is the current that the controller will generate during the next time step, $I_{max}$ is the maximum current the generator can supply and $e_{n-1}, e_{n-2}, \ldots, e_0$ are the errors previously evaluated. The limitations imposed on the signal $I_{n+1}$ and described by equation 2.16 were achieved in SIMULINK® using a saturation block.

An excitation signal was generated and used to evaluate all the various control algorithms. The excitation frequency was sinusoidal with a frequency that varied linearly from 87 Hz to 95 Hz, from $t$=100 s to $t$=120 s. The simulations were run for a time of 220 s.

All the simulations were conducted using SIMULINK® and the Real-Time Workshop toolbox in order to decrease the computational time. An "ode5" solver with a fixed time step of 0.5 ms (2kHz) was used for the SIMULINK® model. As the tunable range for the device considered here was between 82 and 100 Hz, an excitation frequency of 91 Hz, in the middle of the range, was used to verify effectiveness of the controllers. To test the performance of the controllers a variable frequency between 87 and 95 Hz, whose range was 5 Hz from the boundaries, was also adopted.

A comparison of different control systems, i.e. of different function $f$ in equation 2.15, was carried out in order to find the adaptive control technique most suitable to tune an SMA ATVA. The following section describes the different controller algorithms considered.

## 2.2 The control algorithm

The role of the feedback controller is to generate a control signal that will drive the SMA ATVA and primary system to attain zero error condition $\cos\phi = 0$.

As can be seen above, $\cos\phi$ can be used as an error signal, i.e. at the $n$-th time step in a discrete time control system the error signal is

$$e_n = \cos\hat{\phi} \tag{2.17}$$

where $\cos\hat{\phi}$ is an estimate for the time average given by equation 2.13.

### 2.2.1 P model

Suppose that the current of the SMA ATVA is to be updated every $T_c$ seconds a simple method of adapting the system is by proportional control:

$$I_{n+1} - I_n = -Pe_n \tag{2.18}$$

with the boundaries given by equation 2.16 and where $P$ is a proportional control positive constant and $e_n$ is the error signal signal.

In order to improve the controller an action proportional to an error function can be used:

$$I_{n+1} = I_n - P(e_n + e_n^3 + e_n^5) \tag{2.19}$$

with the boundaries given by equation 2.16 and where $(e_n + e_n^3 + e_n^5)$ is an error function formed from a nonlinear function of the error signal $e_n$. Since equation 2.19 showed better performance it was preferred. For simplicity this control algorithm was called proportional as well.

It can be seen in equation 2.19 that a polynomial combination of the error at the $n$-th time step is multiplied by the proportional control constant. This is intended to compensate for the non-linear relationship that exists between $\cos\phi$ and the stiffness of a TVA when it is tuned [10], as shown in figure 2.5. A fifth order polynomial has been chosen because higher order one does not permit a better approximation of the non-linear relationship notwithstanding the increase in complexity. A similar non linear function could also been obtained using fuzzy logic [11] as discussed in the next subsection.

The period $T_c$ between updates of the stiffness is set to 0.1 s for all the tests. The error at the $n$-th time step is estimated using equation 2.12 integrating over the period of control $T_c$ and normalizing.

### 2.2.2 Fuzzy model

Another simple way to establish a nonlinear mapping between the input error and resulting output action is to use a fuzzy logic controller [11]. Fuzzy output sets, which increase in size linearly as their centre points move away from zero (the tuned condition), were used to compute the change in the current in response to an error. Thus the input function, $\cos\phi$, is mapped using a triangular membership function uniformly distributed (see figure 2.6) while with the output function, the increase in the current $\Delta I$, is mapped using trapezoidal function in which the outer sets are larger (see figure 2.7). The centre set, corresponding to zero error, is very narrow, which reduces the variation in the current. The control surface is then similar to the one

| Input $\cos\phi$ | Output $\Delta I$ |
|---|---|
| Fully negative | Fully negative |
| Negative | Negative |
| Small negative | Small negative |
| Zero | Zero |
| Small positive | Small positive |
| Positive | Positive |
| Fully Positive | Fully Positive |

Table 2.4: The rules of the fuzzy controller

described by the polynomial combination (see figure 2.8). The rules for the fuzzy controller are given in table 2.4.

The main drawback of fuzzy control is that it is more complex to implement because it needs digital control, whereas the proportional controller is analogue and simpler. The use of fuzzy control is usually justified when there are many inputs.

### 2.2.3 PD model

In order to increase damping in the controller and to improve stability a derivative action was added to the proportional control. Therefore, following classical control theory a PD controller, with a proportional control constant $P$ and a derivative control constant $D$, was designed, according to the control law

$$I_{n+1} = I_n - [P(e_n + e_n^3 + e_n^5) + Dd_n] \tag{2.20}$$

with the boundaries given by equation 2.16 and where $d_n$ is the derivative of the error given by

$$d_n = \frac{e_n - e_{n-2}}{2T_c} \tag{2.21}$$

A similar controller has been proposed by Williams et al [14] who referred to it as a PI controller. Assuming a steady-state relationship for the cosine $\cos\phi$ as a function of the stiffness of the SMA ATVA the global system is a first order system driven by equation 2.1. Therefore a steady state control effort is required to maintain the zero error condition and it is realized by inclusion of the integral action in the controller. They incorporated a PI controller into the system by defining the integral of the error as an

augmented state $x_I$:

$$x_I = \int_0^t \cos\phi \, \mathrm{d}\tau \Rightarrow \dot{x}_I = \cos\phi \tag{2.22}$$

The PI controller was then defined by $x_I$:

$$I^2 = -K_P \cos\phi - K_I x_I = -K_P \dot{x}_I - K_I x_I \tag{2.23}$$

where $K_P$ and $K_I$ are the proportional and integral gains.

As equation 2.23 can be obtained by integration of equation 2.20, the two controllers are equivalent. For convenience and in accordance with previous works [2, 10, 11], such a device will be called PD controller henceforth.

### 2.2.4 Continuous control

An alternative is continuous updating of the control. While the previous discrete-time controllers drive the current in the SMA wire by updating it every $T_c$ seconds the continuous-time controller updates the current at the time step of the simulation or at the calculation frequency of the controller. Such a controller was designed in order to simplify the controller and to make it more similar to a classic controller.

The design of such a controller leads to some new difficulties. First the evaluation of the cosine and its normalization cannot be carried out integrating over a single time step. So the integrals for the evaluation and the normalization of the cosine are computed like a common integral but the integral is reset every $T_c$ seconds:

$$\cos\phi = \frac{2}{\dot{X}_h \dot{X}_a T} \int_{nT_c}^{(n+1)T_c} \dot{x}_h \dot{x}_a \mathrm{d}t \quad n = 0, 1, \ldots, \infty \tag{2.24}$$

Moreover, to avoid under- and over-evaluations of the cosine a saturation block constrained at $\pm 1$ was used.

A second problem was observed as large noise that disturbed the output of the controller. Since such a problem resulted from the evaluation of the cosine and its time derivative two low-pass filters were used. The first one was used to filter the cosine function (see figure 2.9). A first order filter with a cut-off frequency of $1/(10T_c)$ (1 Hz in the numerical and experimental test) was adopted:

$$\frac{1}{10T_c s + 1} \tag{2.25}$$

where $s$ is the Laplace variable.

The second filter was used to filter the evaluation of the time derivative of the cosine function, and a cut-off frequency of $1/T_c$ (10 Hz in the numerical and experimental test) was used:

$$\frac{1}{T_c s + 1} \tag{2.26}$$

### 2.2.5 Sliding mode control

Since the sliding mode method is often used to deal with uncertainties in non-linear dynamic systems and to design position control for SMA actuators [12, 13] it was studied to examine its potential.

Two approaches to deal with model uncertainties are robust control and adaptive control. A simple approach to robust control is the so-called sliding mode control methodology. Intuitively it is based on the fact that it is easier to control first order systems, be they nonlinear or uncertain, than it is to control general $n$-th order systems [18]. It is then easy to show that, for the transformed first order problems, "perfect" performance can in principle be achieved in the presence of arbitrary parameter inaccuracies [18]. Such performance, however, is obtained at the price of extremely high control activity. However, the high control activity can be reduced by a modification of the control law or can be used directly (for instance in a system driven by pulse width modulation technique).

Consider a single-input dynamic system

$$x^{(n)} = f(\mathbf{x}) + b(\mathbf{x})u \tag{2.27}$$

where the scalar $x$ is the output of interest (for instance, in position control is the displacement of the actuator), the scalar $u$ is the control input (for instance, the current that passes through the SMA wire), and $\mathbf{x} = [x\ \dot{x}\ \ldots\ x^{(n-1)}]^T$ is the state vector. The function $f(\mathbf{x})$ (in general non linear) is not exactly known, but the extent of the imprecision is upper bounded; similarly, the control gain $b(\mathbf{x})$ is not exactly known, but its sign is known and it is bounded [18]. The control problem is to get the state $\mathbf{x}$ to track a specific time varying state $\mathbf{x}_d = [x_d\ \dot{x}_d\ \ldots\ x_d^{(n-1)}]^T$ in the presence of model imprecision on $f(\mathbf{x})$ and $b(\mathbf{x})$.

Let $\tilde{x} = x - x_d$ be the tracking error so as to define a time-varying surface $S(t)$ in the state-space by the scalar equation $s(\mathbf{x}; t) = 0$, where

$$s(\mathbf{x}; t) = \left(\frac{\mathrm{d}}{\mathrm{d}t} + \lambda\right)^{n-1} \tilde{x} \tag{2.28}$$

and $\lambda$ is a strictly positive constant.

Given the initial condition $\mathbf{x}_d(0) = \mathbf{x}(0)$ the problem of tracking $x \equiv x_d$ is equivalent to that of remaining on the surface $S(t)$ for all $t > 0$. Thus the problem of tracking the $n$-dimensional vector $x_d$ can be reduced to that of maintaining the scalar quantity $s = 0$. So the problem of tracking the $n$-dimensional vector $x_d$ can be replaced by a first order stabilization problem in $s$.

The simplified first order problem of maintaining $s = 0$ can now be achieved by choosing the control law $u$ such that outside of $S(t)$

$$\frac{1}{2}\frac{\mathrm{d}}{\mathrm{d}t}s^2 \leq -\eta|s| \tag{2.29}$$

where $\eta$ is a strictly positive constant. This sliding condition constrains trajectories to point toward the surface $S(t)$.

The system involved in position control can be modelled as a second-order [12] or a third-order system [13]. The SMA actuator system is actually a first order system but it is in series with the model of the structure to which is connected. Since frequency deviation in the excitation force acting on the structure and the SMA hysteresis can be considered as uncertainties, the sliding mode control can be used successfully.

If the assumption that the steady-state relationship between the stiffness and the cosine of the phase difference is valid, the SMA ATVA is just a first order system and the use of the sliding mode control is not necessary. This is the reason why the sliding mode control is not considered further during this work.

## 2.3 Choice and optimization of the controller

### 2.3.1 Setting of performance indices

In order to compare the performances of several control systems a performance index is needed. A classical general index is the integral of the absolute value of the error, IAE, given by [19]

$$\mathrm{IAE} = \int_0^\infty |e(t)|\mathrm{d}t \tag{2.30}$$

Such an index can be modified in order to be adapted to the problem of tuning a SMA ATVA. So considering the ratio between the absolute values of the displacement of the host structure without, $x_h^{free}(t)$, and with the controller, $x_h^{control}(t)$, subjected to the same excitation, the performance index

$\psi$ can be defined as

$$\psi = \frac{\int_0^\infty |x_h^{free}(t)| \mathrm{d}t}{\int_0^\infty |x_h^{control}(t)| \mathrm{d}t} \tag{2.31}$$

There are other indices, and for vibration control purposes, the time required for the system to tune within some limit of its optimal value is another possibility [19]. For instance the settling time $t_s$ can be defined as the time required for the system to settle within the band $\pm 0.1$ of the error (see figure 2.10).

### 2.3.2 Comparison of controller performances

In order to compare the performance of the different controllers, they were tested with the TVA subjected to the same excitation in each case. Two different kinds of excitation were chosen. The first was a constant frequency excitation of 91 Hz, in the middle of the tunable range of the ATVA. The second was an excitation with a frequency changing from 87 to 95 Hz between the 100-th and 120-th second of the simulation (see figure 2.11). Such a frequency range was chosen as its limits were 5 Hz from the limits of the tunable range.

Firstly the P controller was tested and a constant $P = 0.6$ was set. Figure 2.12 shows the response of the system to the constant frequency excitation. The velocity of the host mass was reduced to the optimal value after 50 s from the beginning of the simulation (see figure 2.12(a)). Even if the amplitude of the host mass velocity is much reduced, the cosine of the phase angle (figure 2.12(c)) oscillates around zero and the controller is quite active (figure 2.12(e)). Figure 2.13 shows the response to the variable frequency excitation. A similar oscillation in the error and in the controller output was recorded between 50 and 100 s and between 120 and 220 s. During the transient the system did not respond so quickly and a small increase in the host structure velocity was recorded.

The fuzzy controller was then tested. The output of the controller was amplified with a constant equal to that of the P controller in order to have comparable results. Its behaviour was quite similar to the proportional controller already depicted. Figure 2.14 shows the response to the constant frequency excitation while figure 2.15 shows the response to the variable frequency excitation. The oscillation was still recorded but with a lower frequency even if with a greater amplitude. The responsiveness of the two systems can be seen to be roughly the same.

A PD controller with a proportional constant $P = 0.6$ and a derivative constant $D = 0.9$ was considered. Figure 2.16 shows the results for constant

frequency excitation. The amplitude of the velocity is effectively reduced after 50 s (figure 2.16(a)) and the performance is comparable to that obtained with the P controller. The error reaches a steady state-value after only about 60 s and maintains this value for the rest of the simulation (figure 2.16(c)) so that the controller is much less active (figure 2.16(e)). Figure 2.17 shows the response to the variable frequency excitation. The performance of the controller was very good and the controller maintained a small amplitude of the host structure during the transition time (figure 2.17(a)).

Finally the continuous PD controller was considered. The value of the proportional constant was $P = 5 \times 10^{-4}$ and that of the derivative constant was $D = 5 \times 10^{-3}$. Figure 2.18 shows the performance of such a controller for constant frequency excitation while figure 2.19 shows the result of the simulation for a variable frequency excitation. Even with this controller the reduction in the velocity of the host structure was very effective. Nevertheless the error tended to zero very slowly like a first order system with a high damping. Moreover during the change in the frequency the controller reacted in a noisy and erratic way (see figure 2.19(e)) even if the amplitude of the velocity of the host structure was kept small.

### 2.3.3 Ad-hoc optimization

From the comparison shown in the previous section the PD controller has the best performance. It was decided to optimize its parameters, i.e. the proportional and derivative constants, $P$ and $D$. In this section manual optimization is presented while in the next section an automatic optimization procedure is presented.

In order to find the optimal value for the constants $P$ and $D$ of the controller 16 controllers were considered varying such constants between 0.0 and 0.9 with increments of 0.3. Each controller was subjected to a variable excitation frequency from 95 to 87 Hz from 100 to 120 s of the simulation that took 220 s in total.

For each controller its performance index was calculated. Table 2.5 shows the performance indices $\psi$ calculated using equation 2.31. Table 2.6 shows the averaged settling time obtained as a mean value between the two settling times measured during the first 100 s and after the change in the excitation frequency, i.e. after 120 s.

Moreover the responses of the systems obtained by varying the constants value are pictured graphically in tables in order to see the differences in the controller actions. Figure 2.20 shows the velocity, figure 2.21 the error, figure 2.22 the time derivative of the error and figure 2.23 the current demanded by the controller.

| | $D = 0.0$ | $D = 0.3$ | $D = 0.6$ | $D = 0.9$ |
|---|---|---|---|---|
| $P = 0.0$ | 1.0000 | 0.9999 | 0.8387 | 0.8852 |
| $P = 0.3$ | 0.6725 | 0.5311 | 0.6219 | 0.6177 |
| $P = 0.6$ | 0.6400 | 0.5409 | 0.6183 | 0.6090 |
| $P = 0.9$ | 0.6227 | 0.5297 | 0.5691 | 0.6116 |

Table 2.5: Performance index $\psi$ of PD controller with different constant values

| | $D = 0.0$ | $D = 0.3$ | $D = 0.6$ | $D = 0.9$ |
|---|---|---|---|---|
| $P = 0.0$ | 160.0000 s | 160.0000 s | 160.0000 s | 160.0000 s |
| $P = 0.3$ | 160.0000 s | 144.0000 s | 138.9000 s | 123.7500 s |
| $P = 0.6$ | 159.5000 s | 142.0000 s | 130.9500 s | 120.3500 s |
| $P = 0.9$ | 160.0000 s | 141.3500 s | 123.8000 s | 131.5500 s |

Table 2.6: Average settling time of PD controller with different constant values

The controller with the best performance index $\psi$ is the controller with the constants $P = 0.3$ and $D = 0.3$ while the controller with the best averaged settling time is the controller with the constants $P = 0.6$ and $D = 0.9$. The reduction of the amplitude of the host mass velocity performed by the first one seemed to be more effective (see figure 2.20) but also the activity of the controller has to be examined. In fact the action of the first controller was not so damped and the error took longer to reach the $\pm 0.1$ band (see figure 2.21). Consequently the activity of the power supply is more limited with the second (see figure 2.23).

As the PD controller with the time constants $P = 0.6$ and $D = 0.9$ presents the lower averaged settling time and there is less activity it is considered to be the best one.

### 2.3.4 Optimizing using the Genetic Algorithm (GA)

Genetic Algorithms (GAs) are stochastic global search and optimization methods that mimic the metaphor of natural biological evolution. GAs operate on a population of potential solutions applying the principle of survival of the fittest to produce successively better approximations to a solution. At each generation of a GA, a new set of approximations is created by the process of selecting individuals according to their level of fitness in the problem domain and reproducing them using operators borrowed from natural

genetics. This process leads to the evolution of populations of individuals that are better suited to their environment than the individuals from which they were created, just as in natural adaptation [20].

GAs have been shown to be an effective strategy in the off-line design of control systems by a number of practitioners. They can be used both to establish the structure of the controller and to set the numerical values of the controller [21]. Such techniques are used in an attempt to find the optimal values of the constants $A_c$, $B_c$, $C_c$ and $D_c$ in the following controller:

$$I_{n+1} = I_n - (A_c e_n + B_c e_n^3 + C_c e_n^5 + D_c d_n) \tag{2.32}$$

with the boundaries given by equation 2.16. Beside these four constants, the update time of the controller, $T_c$, has been considered in the optimization process as the fifth gene.

Although there are many good public-domain genetic algorithm packages none of these provide an environment that is immediately compatible with existing tools in the control domain. The MATLAB® Genetic Algorithm Toolbox [22] aims to make GAs accessible to the control engineer. This allows the retention of existing modelling and simulation tools for building objective functions and allows the user to make direct comparisons between genetic methods and traditional procedures [23].

The Genetic Algorithm Toolbox for MATLAB® , developed at the Department of Automatic Control and Systems Engineering of the University of Sheffield, is freely available to download and has been utilized to carry out the automatic optimization of the controller.

Two tests were carried out. The first used the IAE as the fitness function in the GA while the latter test used the settling time. The first test was carried out seeking constants $A_c$, $B_c$, $C_c$ and $D_c$ in the range $[0; 3]$, while the update time was between 0.1 and 0.5 s. To each individual of the offspring was imposed an excitation variable from 100 and 120 s from 87 to 97 Hz. Each simulation took 220 s. Figure 2.24(a) shows how the performance index IAE develops from a generation to the other while figure 2.24(b) shows the value of the controller constants of the best individual. The GA process was stopped after the thirtieth offspring. Each generation was composed of twenty individuals. Examining the performance index it is clear that it did not vary significantly from one generation to an other. So there are some doubts of the effectiveness of the use of the IAE as a performance index.

The result of the same optimization process was carried out using the settling time as the performance index are shown by figure 2.25. Here the settling time seems to be more influenced by changing the coefficients. In order to evaluate the settling time $t_s$ each individual was tested with an excitation force with a variable frequency from 100 and 120 s from 87 to 97 Hz.

| Controller constants | Test 1 - IAE | Test 2 - $t_s$ |
|---|---|---|
| $A_c$ | 1.3 | 3 |
| $B_c$ | 2.1 | 3 |
| $C_c$ | 1.1 | 1.75 |
| $D_c$ | 2.7 | 1.2 |
| $T_c$ | 0.5 s | 0.1 s |

Table 2.7: Result of the GA optimizations

So two settling time can be calculated: one for the first excitation frequency and the other for the exciation frequency after 120 s. In the algorithm the mean value of these was used.

The constants found for the best individual of the thirtieth generation are shown in table 2.7.

## 2.4 Testing the robustness of the controller

### 2.4.1 Broad-band excitation

In order to check the robustness of the controller it was subjected to broad-band excitation. The PD controller with constants $P = 0.6$ and $D = 0.9$ was studied. The excitation was a white noise filtered by a band pass filter with cut-off frequencies of 87 and 95 Hz.

The results were very unsatisfactory. The error was always evaluated with a mean value very close to +1. The time derivative even if it has a zero mean value was too noisy. The controller drove a current so small than the wire was not heated.

The controller does not work in presence of noise excitation but this is not very important, as the TVA is not designed to cope with broad-band excitation but with single frequency sinusoidal excitation.

### 2.4.2 Changing the system dynamics

Another analysis was carried out to test the robustness of the controller; it was applied to different systems. Figure 2.26 shows the basic model and two other models used for comparison. These are introduced to include the dynamics of the host structure. The values of the constants of the basic 2dof system utilized in the design process (figure 2.26(a)) are shown in table 2.3. A new model was obtained grounding the host mass $m_h$ by the spring

| State | Frequencies | Original Model | Grounded Model | 3dof Model |
|---|---|---|---|---|
| Cold | Resonance freq. | (0;129) Hz | (53;154) Hz | (0;90;168) Hz |
| | Antiresonance freq. | (82) Hz | (82) Hz | (82;100) Hz |
| Hot | Resonance freq. | (0;157) Hz | (64;187) Hz | (0;110;204) Hz |
| | Antiresonance freq. | (100) Hz | (100) Hz | (100;100) Hz |

Table 2.8: Natural frequencies of the modified systems; antiresonance frequencies are referred to the host structure mass $m_1$

$k_h = k_a^{\text{cold}}$ and the damper $c_h = c_a$ (figure 2.26(b)). A 3dof model was then obtained by adding a third mass $m_0 = m_h$ instead of grounding the mass $m_h$. The new resonance and antiresonance frequencies are shown in table 2.8. The antiresonance frequencies relate to the mass $m_h$ because it is the vibration of this mass that has to be reduced.

Such systems were excited with a variable frequency excitation force, from 87 to 95 Hz between 100 and 120 s, and applied to the mass $m_h$. Finally the same force was applied to the mass $m_0$ of the 3dof model. Figure 2.27 shows the response of the basic system subject to such an excitation when the PD controller is on. Figure 2.28 shows the response of the grounded system. The behaviour of this system is very similar to the basic one. Only a small difference can be found in the amplitude velocity of the absorber mass (compare figure 2.27(b) with figure 2.28(b)).

Figure 2.29 shows the response of the 3dof model excited on the mass $m_h$ while the figure 2.30 shows the response when the same excitation is applied to the mass $m_0$. When the excitation is applied to the mass $m_h$ there is no difference in the performance of the controller, but when the excitation is applied to the mass $m_0$ a small decrease in the performance is noted. Both the velocity amplitude of the host structure $m_h$ and of the absorber mass $m_a$ are greater (figure 2.30(b) notes an increase in the axis limits).

The performance of the controller is hardly affected by changes in the system if the excitation frequency is applied directly to the host structure. The performance can worsen a little if the excitation is not directly applied to the host structure at the position where the absorber is attached.

### 2.4.3 Changing the hysteresis

Now the influence of the amplitude of the hysteresis field in the SMA is investigated. Increasing the hysteresis gap weakens the direct relationship between stiffness and temperature.

The measured broadness of the hysteresis gap was 10°C (see table 2.2). The first series of experiment were carried out with a system without hysteresis. Figures 2.31, 2.32 and 2.33 show the velocity, the cosine and the current of the system for different value of the constants of the PD controller. These figures can be compared to figures 2.20, 2.21 and 2.23.

The performance of the controller is increased markedly. Nonetheless the PD controller chosen seems to be still the best.

Then some simulations were carried out increasing the hysteresis gap to 20°C. The increase in the hysteresis gap causes the phase transformation of the material to take longer. So in order to see the adaptation of the ATVA within the same simulation time the transformation temperatures were decreased by 10°C. The second part of the simulation took too much time and maybe a decrease in specific heat during the phase transformation would be a better way to investigate this effect. Figures 2.34, 2.35 and 2.36 show the velocity, the cosine and the current recorded during the simulations.

Even if the increase of the system seems to worsen the performance of the controller it does not affect its effectiveness.

### 2.4.4 Changing the rate of change of the excitation frequency

In order to investigate the performance of the PD controller to different excitations it was simulated imposing a variable frequency excitation force with different rates of change in the frequency. Figures 2.37, 2.38 and 2.39 show the velocity of the host structure, the cosine and the current of the simulations carried on with a variable frequency excitation from 97 to 87 Hz. The change in the frequency started at 70 s and finished at a different value from 71 s to 220 s. The adaptation to the decrease in the frequency is strictly related to the cooling properties of the system. It seems that the more gentle the frequency changes the better is the performance of the controller.

Figures 2.40, 2.41 and 2.42 show the same results but when the excitation changes from 87 to 97 Hz. Now the performance of the system is more correlated to the current that the power supply can generate in order to heat the SMA ATVA. Since the amplitude of the host structure velocity was kept small also with high rate in the frequency change (see figure 2.40), it is clear that the performance of the controllers are very good.

## 2.5 Summary

A numerical model of a SMA ATVA already designed and built has been established. Then some controllers for such SMA ATVA have been designed and tested on the numerical model. A comparison between different kinds of controller showed that the PD controller gives the best results.

Such a controller has been optimized, manually and automatically, using genetic algorithms. Finally the robustness of such a controller has been tested.

The simulations carried out showed a good performance and robustness of the chosen PD controller. Nevertheless it seems that every controller that sets the cosine of the phase angle between the velocity of the host structure and the velocity of the absorber mass (error function) to zero can work. In fact when the error function is in the band $\pm 0.5$ the amplitude of the host structure is strongly reduced.

## 2.6 Figures

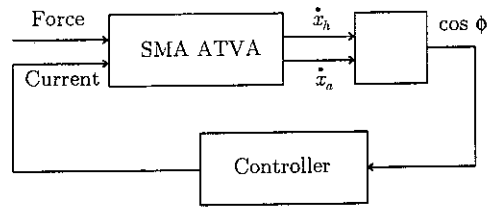


Figure 2.1: Sketch of the regulator

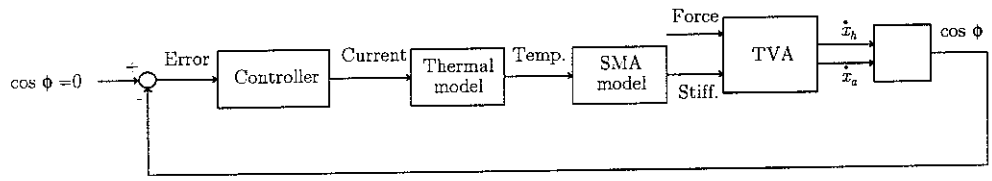


Figure 2.2: Block diagram of the regulator

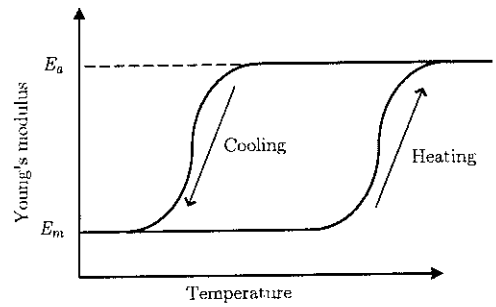


Figure 2.3: Model of the elastic modulus change with temperature in SMA

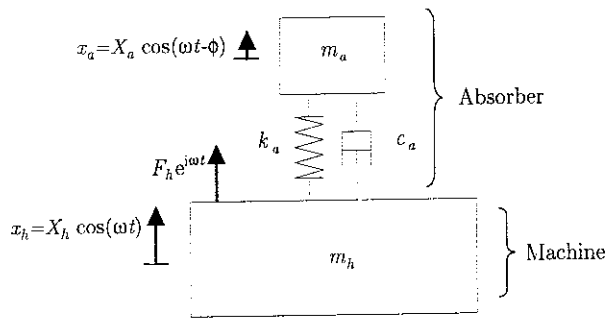


Figure 2.4: Vibration absorber fitted to a machine

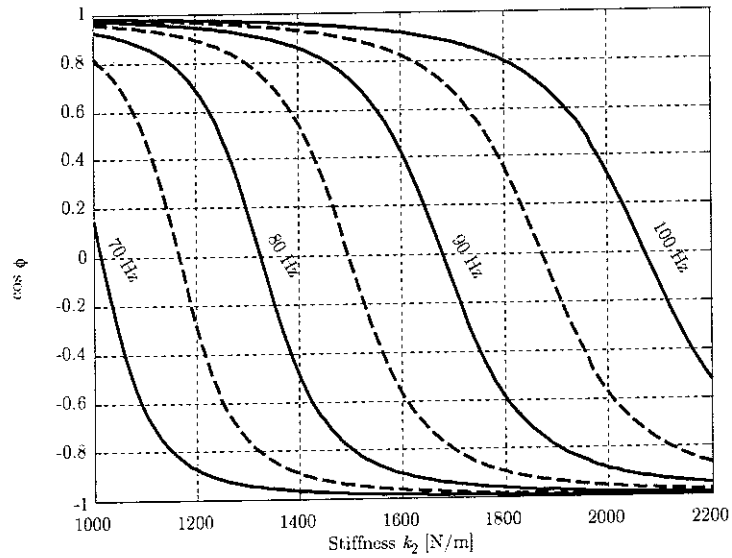


Figure 2.5: The cosine of the phase difference vs. absorber stiffness at different excitation frequencies ($m_h$=0.0036 kg; $m_a$=0.0053 kg; $\eta$=0.1)

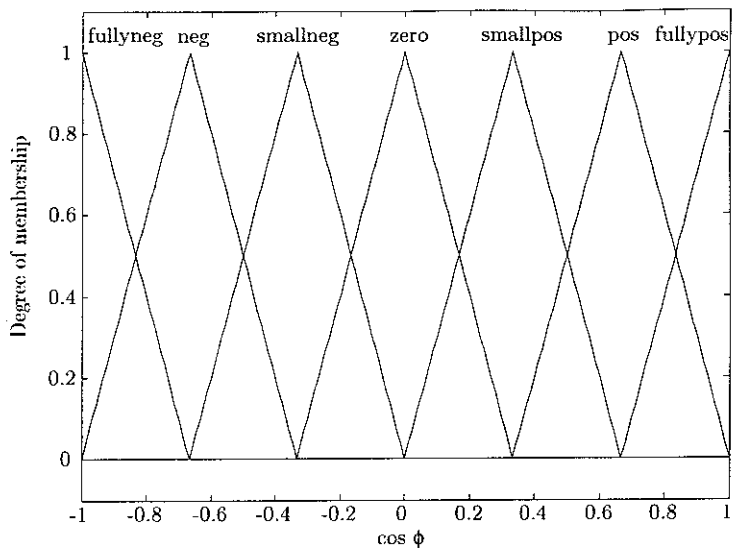


Figure 2.6: Membership functions of the input variable in the fuzzy controller

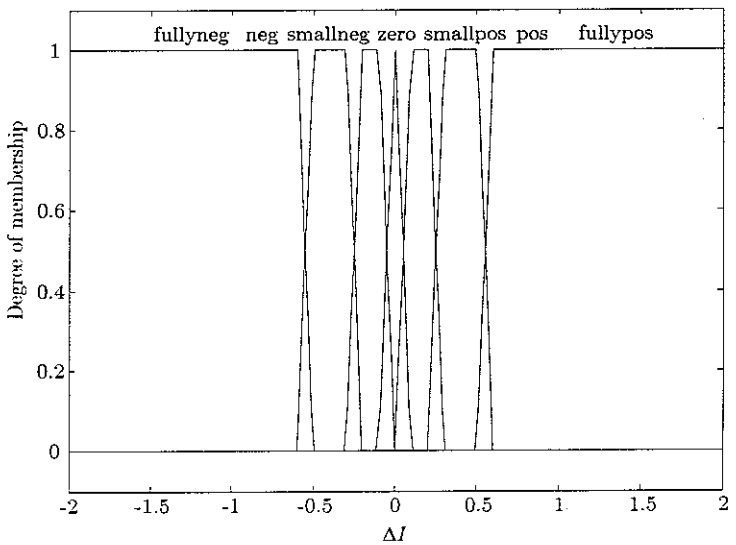


Figure 2.7: Membership functions of the output variable in the fuzzy controller

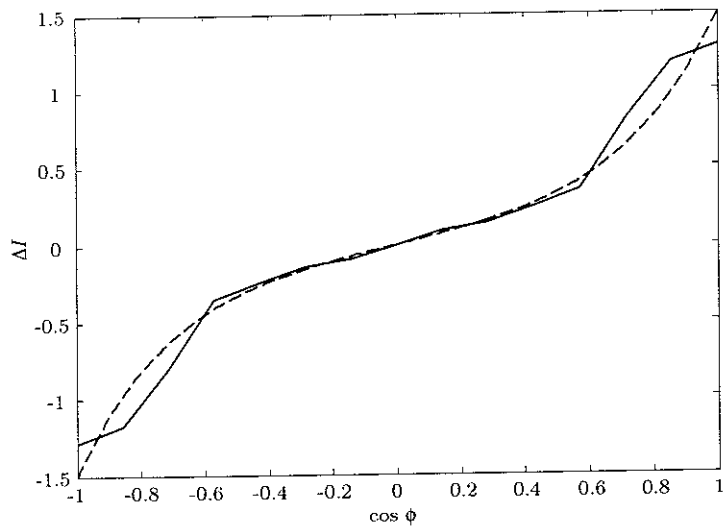


Figure 2.8: Control surface of fuzzy and P controllers: — fuzzy controller; - - - P controller with constant $P = 0.5$

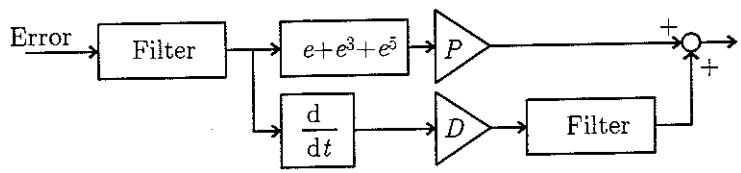


Figure 2.9: Sketch of the continuous controller

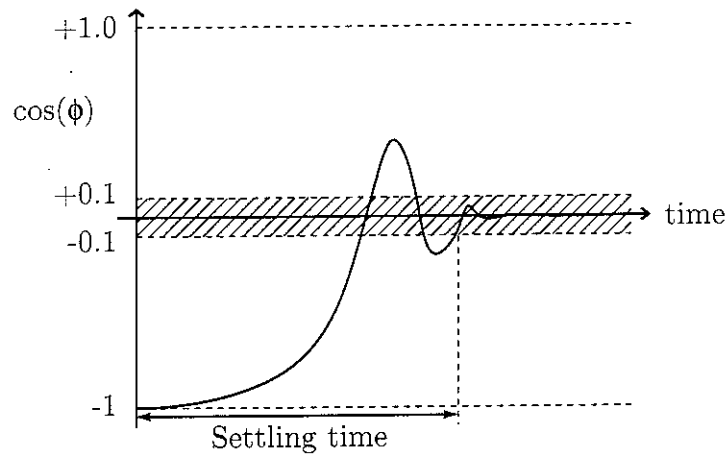


Figure 2.10: The settling time

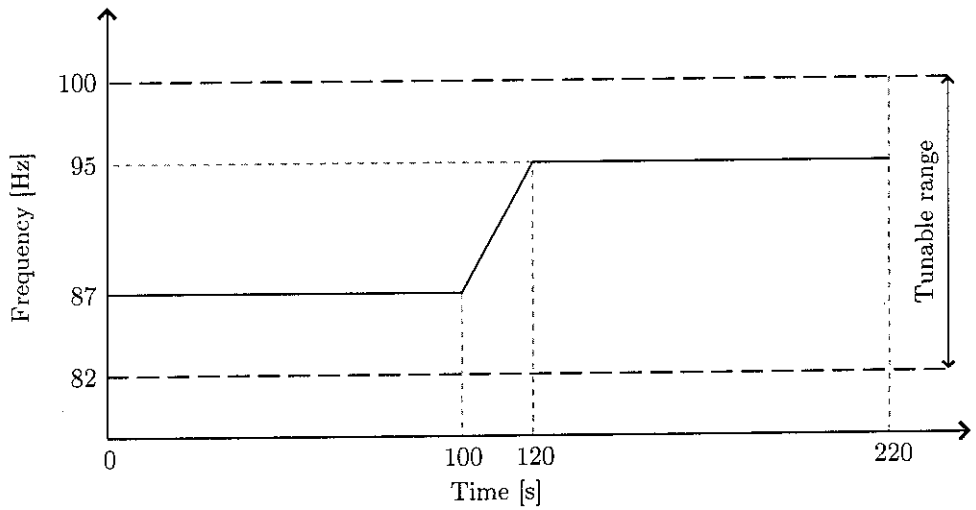


Figure 2.11: The excitation frequency

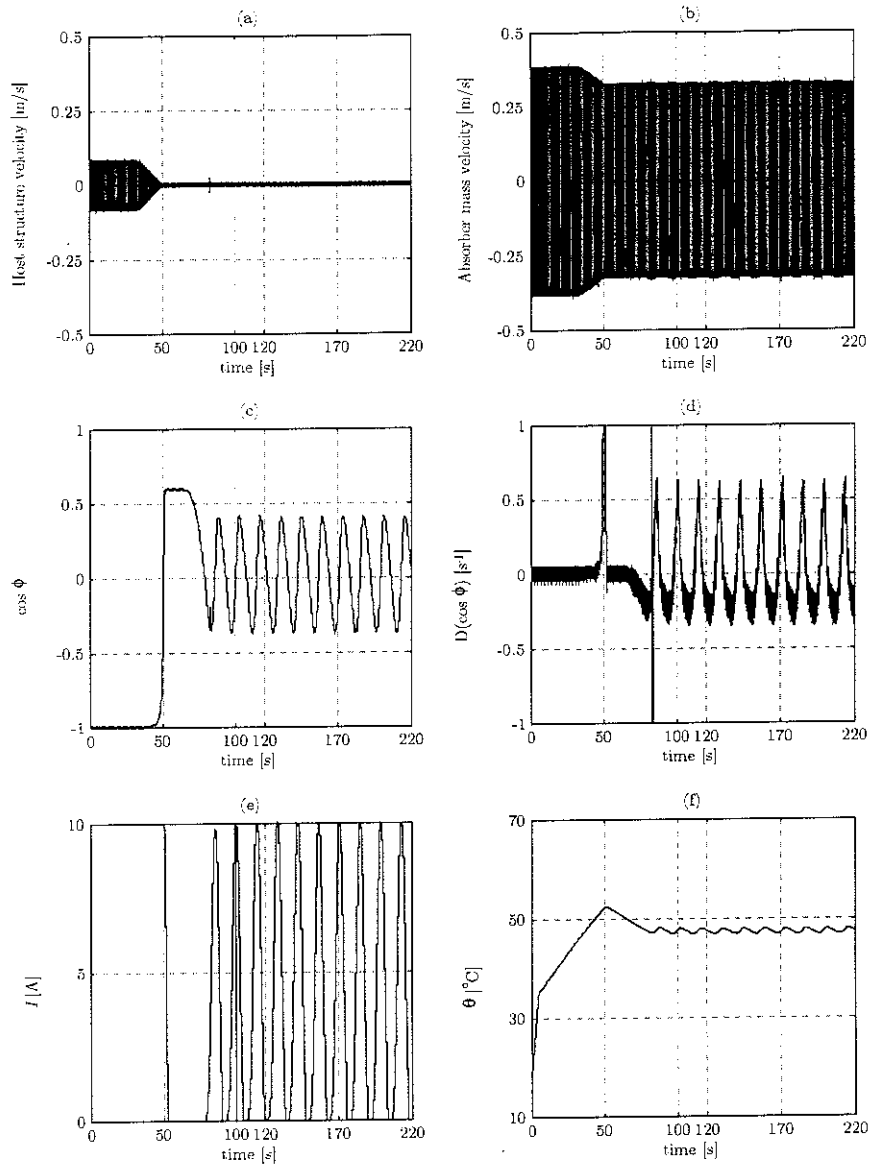


Figure 2.12: Performance of the P controller for a 91 Hz constant frequency excitation: (a) velocity of the host structure, (b) velocity of the TVA, (c) $\cos\phi$, (d) $\mathrm{d}(\cos\phi)/\mathrm{d}t$, (e) current supplied to the SMA wire, (f) temperature of the SMA wire

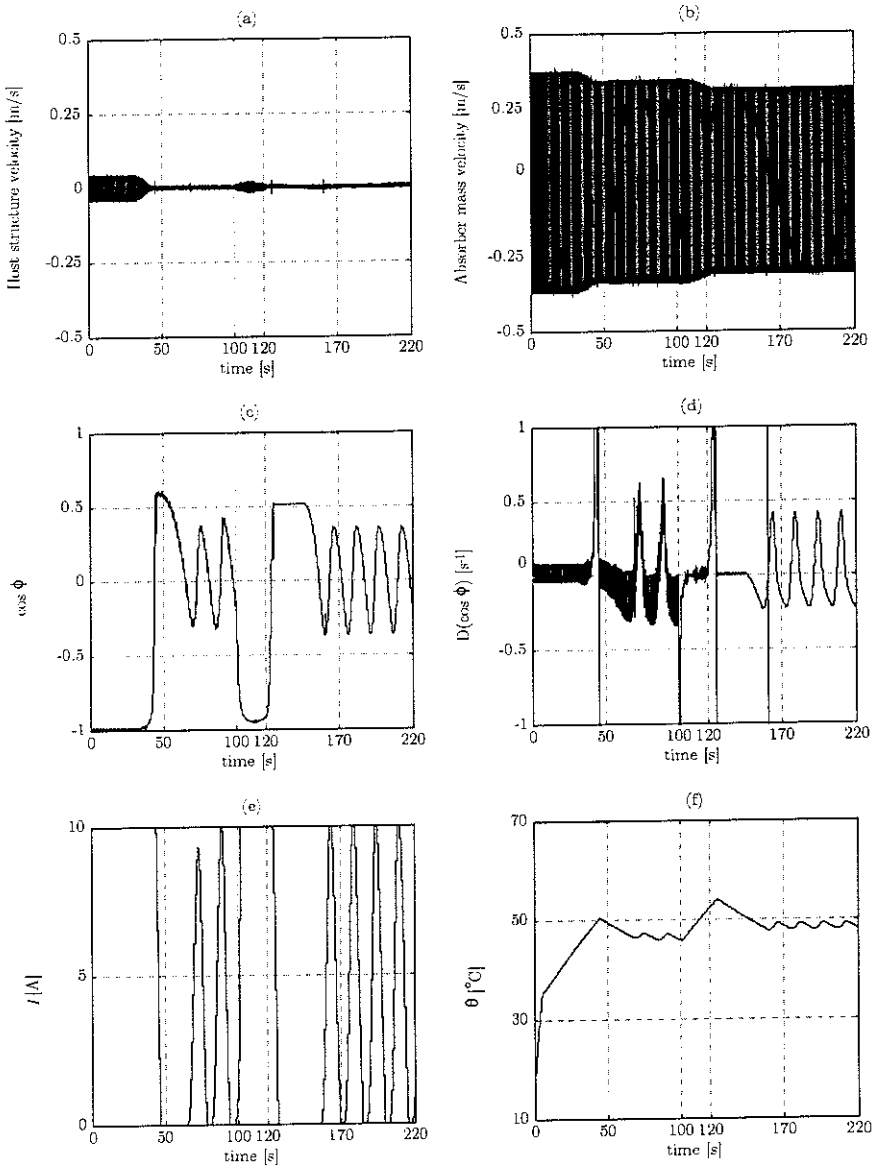


Figure 2.13: Performance of the P controller for a variable frequency excitation from 87 to 95 Hz: (a) velocity of the host structure, (b) velocity of the TVA, (c) $\cos\phi$, (d) $\mathrm{d}(\cos\phi)/\mathrm{d}t$, (e) current supplied to the SMA wire, (f) temperature of the SMA wire

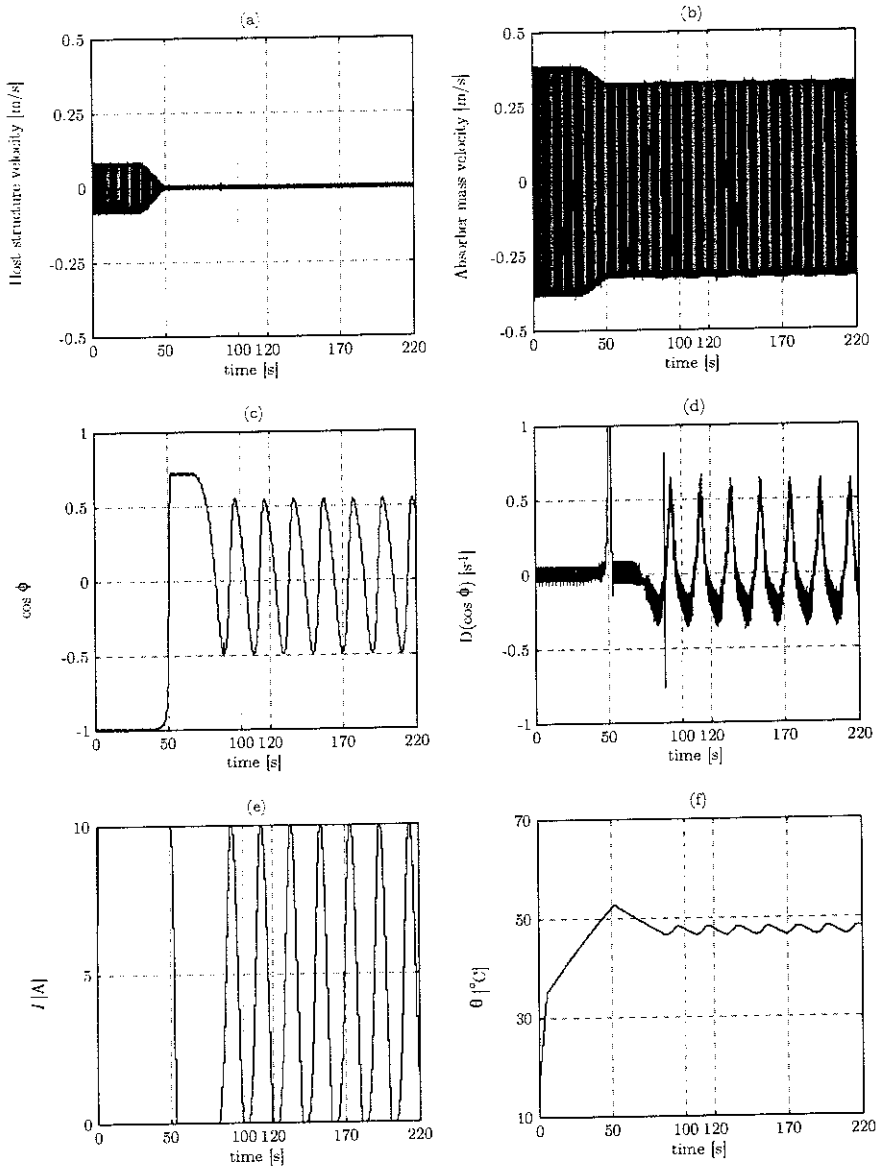


Figure 2.14: Performance of the fuzzy controller for a 91 Hz constant frequency excitation: (a) velocity of the host structure, (b) velocity of the TVA, (c) $\cos\phi$, (d) $\mathrm{d}(\cos\phi)/\mathrm{d}t$, (e) current supplied to the SMA wire, (f) temperature of the SMA wire

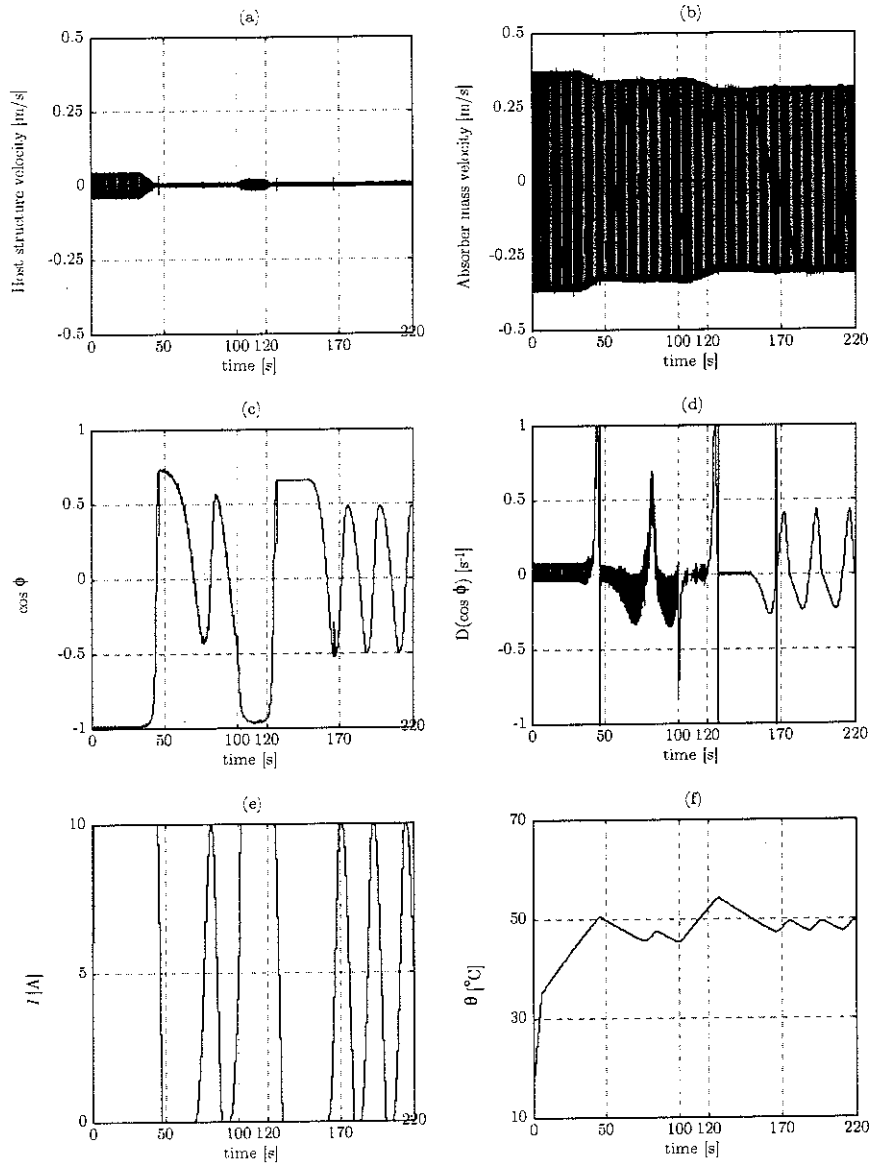


Figure 2.15: Performance of the fuzzy controller for a variable frequency excitation from 87 to 95 Hz: (a) velocity of the host structure, (b) velocity of the TVA, (c) $\cos\phi$, (d) $\mathrm{d}(\cos\phi)/\mathrm{d}t$, (e) current supplied to the SMA wire, (f) temperature of the SMA wire

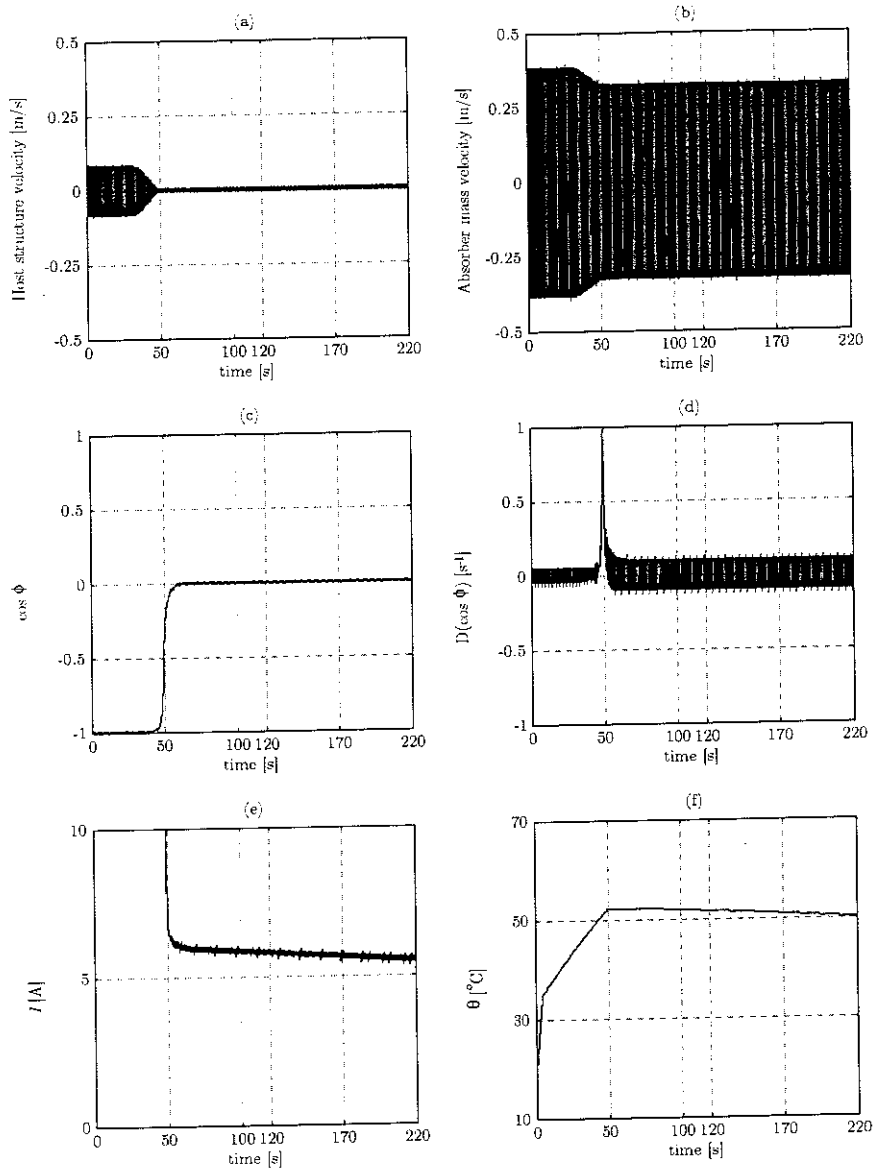


Figure 2.16: Performance of the PD controller for a 91 Hz constant frequency excitation: (a) velocity of the host structure, (b) velocity of the TVA, (c) $\cos\phi$, (d) $\mathrm{d}(\cos\phi)/\mathrm{d}t$, (e) current supplied to the SMA wire, (f) temperature of the SMA wire

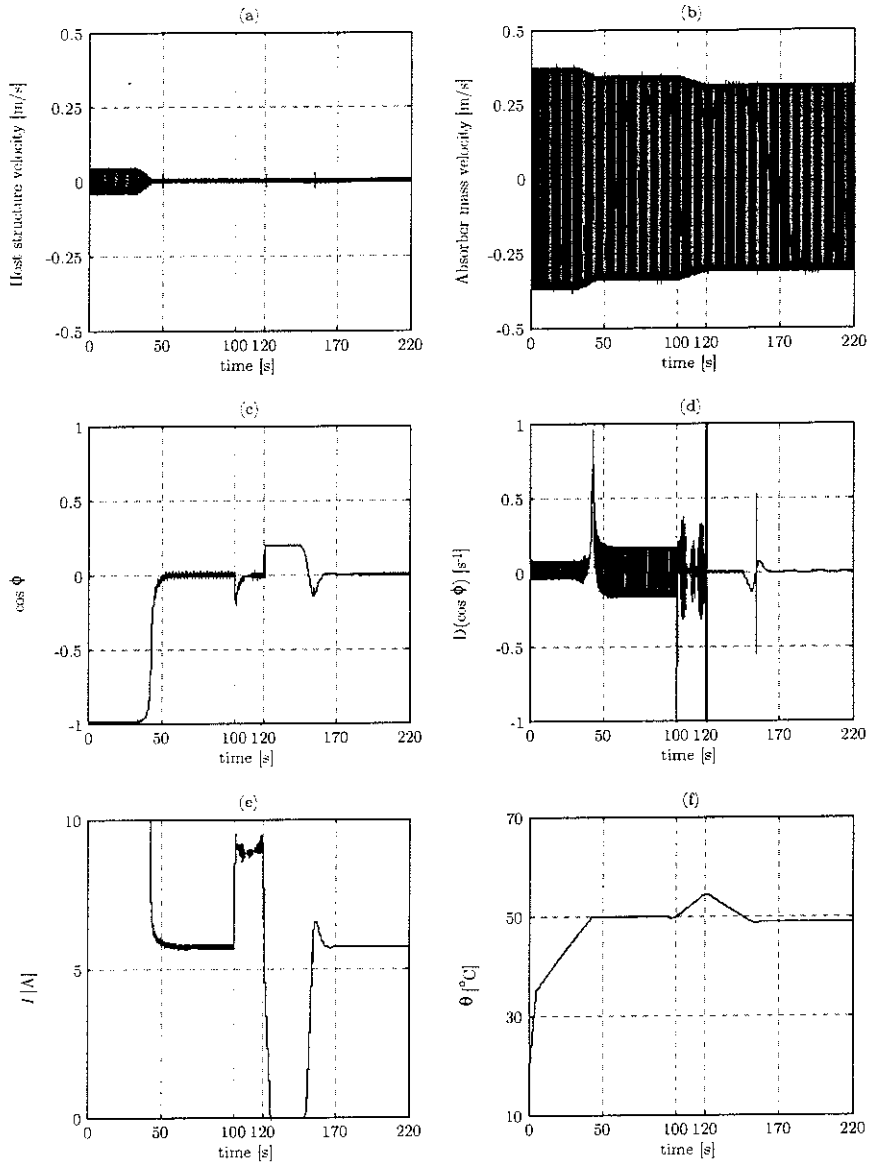


Figure 2.17: Performance of the PD controller for a variable frequency excitation from 87 to 95 Hz: (a) velocity of the host structure, (b) velocity of the TVA, (c) $\cos\phi$, (d) $\mathrm{d}(\cos\phi)/\mathrm{d}t$, (e) current supplied to the SMA wire, (f) temperature of the SMA wire

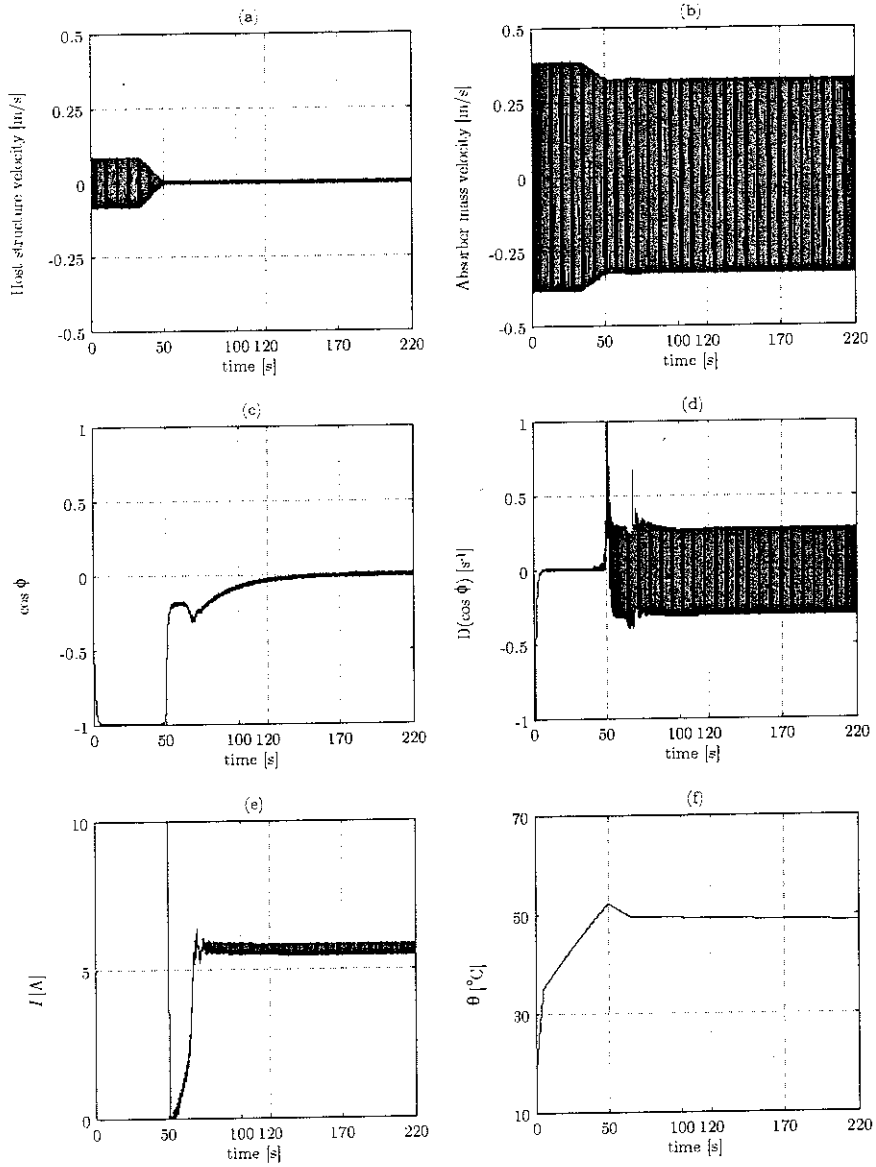


Figure 2.18: Performance of the continuous PD controller for a 91 Hz constant frequency excitation: (a) velocity of the host structure, (b) velocity of the TVA, (c) $\cos\phi$, (d) $\mathrm{d}(\cos\phi)/\mathrm{d}t$, (e) current supplied to the SMA wire, (f) temperature of the SMA wire

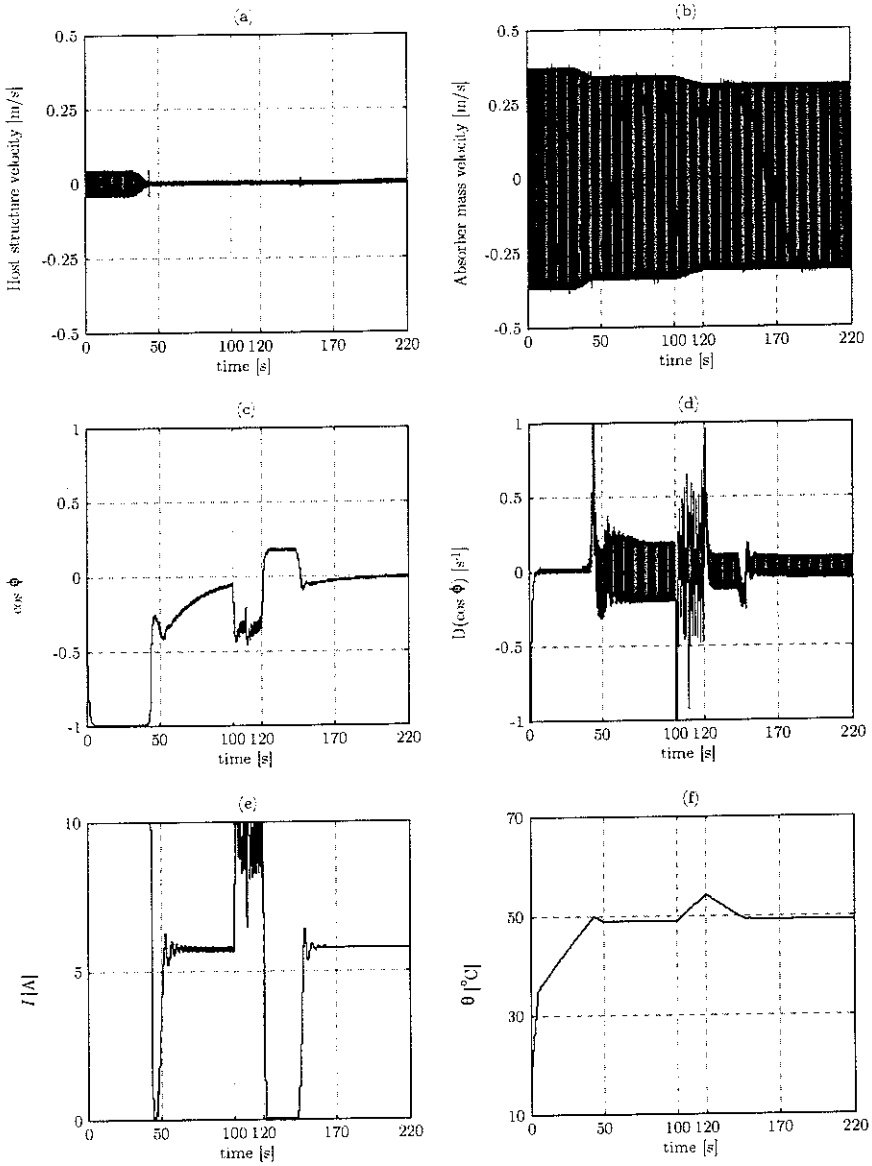


Figure 2.19: Performance of the continuous PD controller for a variable frequency excitation from 87 to 95 Hz: (a) velocity of the host structure, (b) velocity of the TVA, (c) $\cos\phi$, (d) $\mathrm{d}(\cos\phi)/\mathrm{d}t$, (e) current supplied to the SMA wire, (f) temperature of the SMA wire

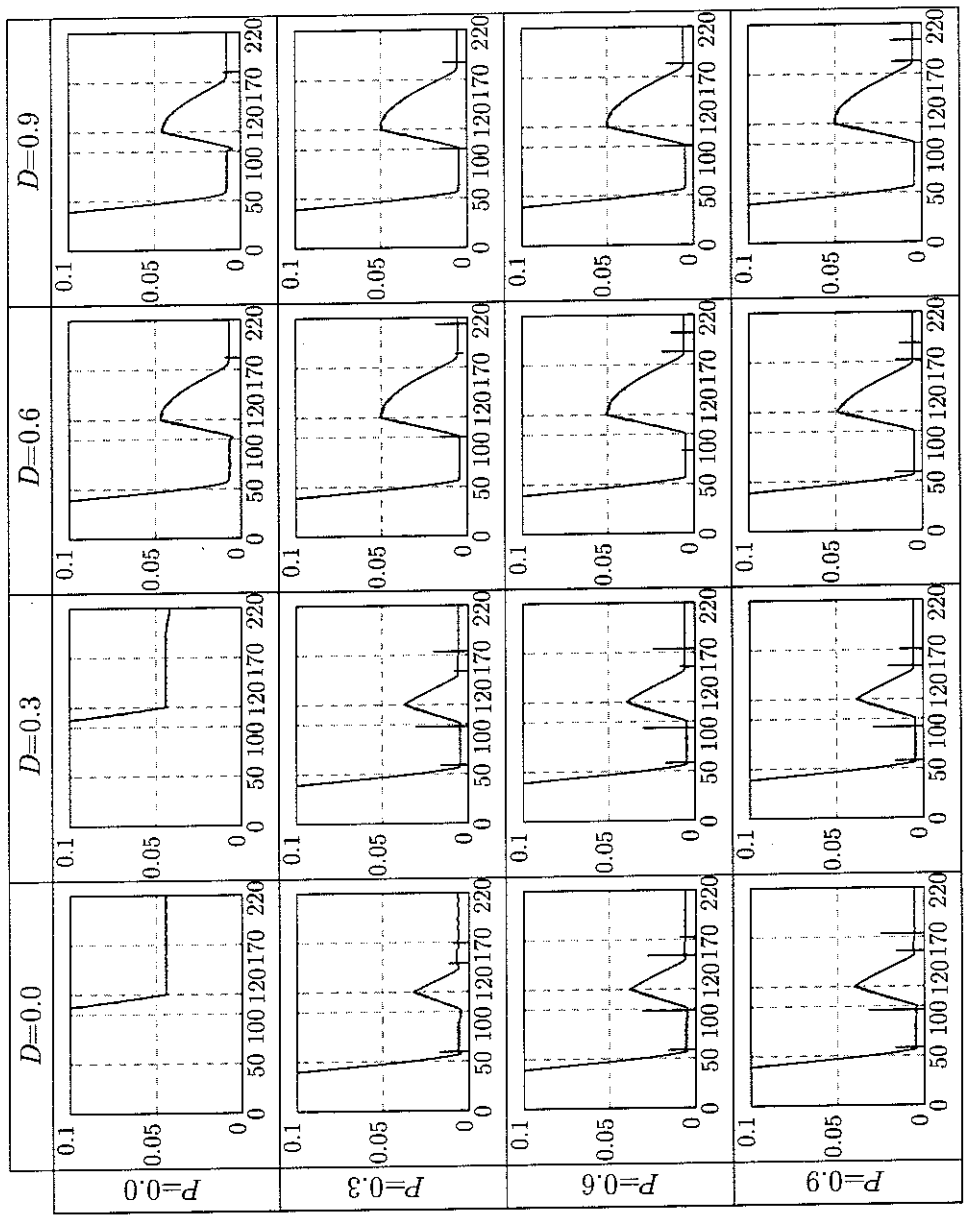


Figure 2.20: Simulation of PD controllers with different constant values: tracks of the amplitude of the host structure velocity [m/s]

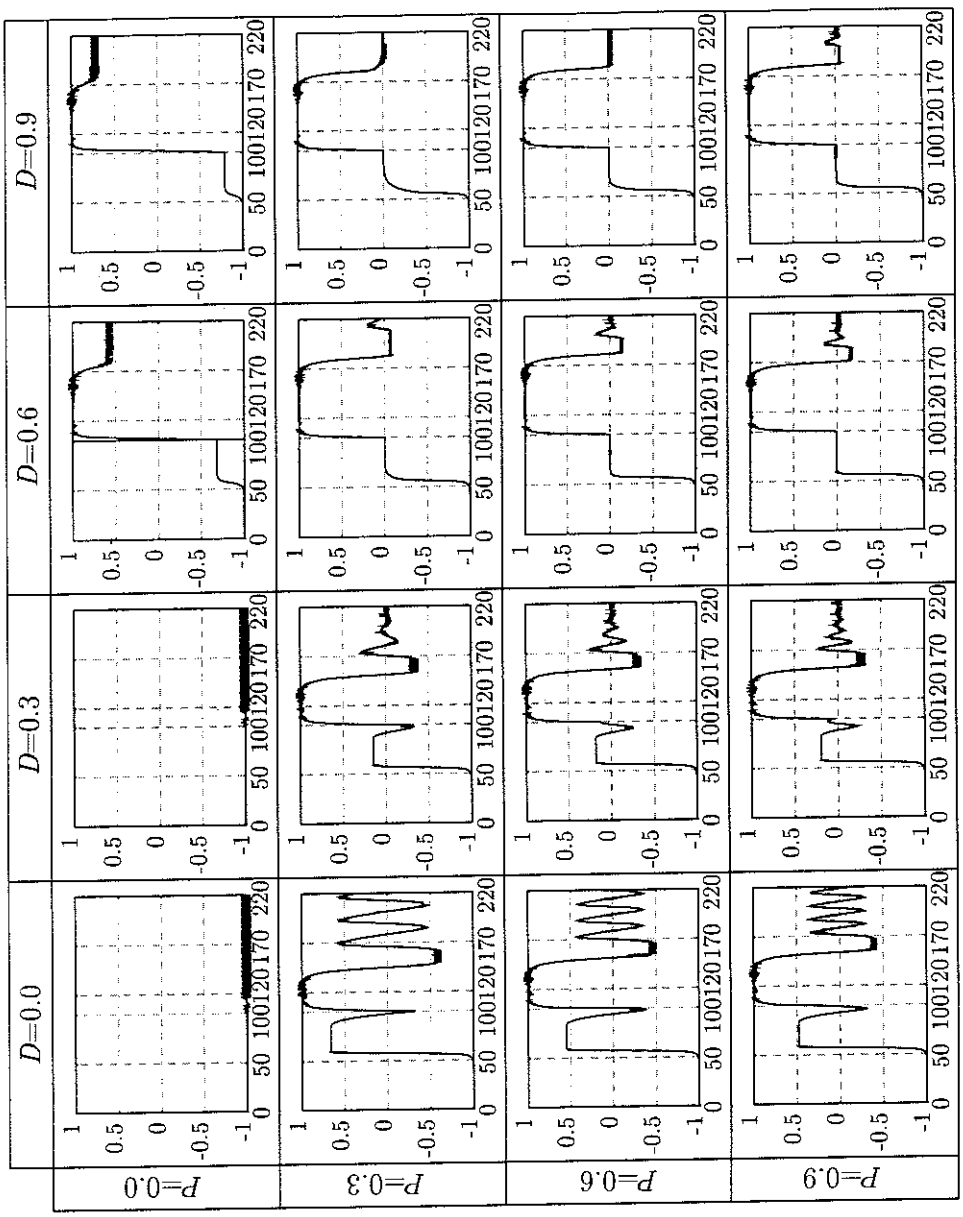


Figure 2.21: Simulation of PD controllers with different constant values: error tracks

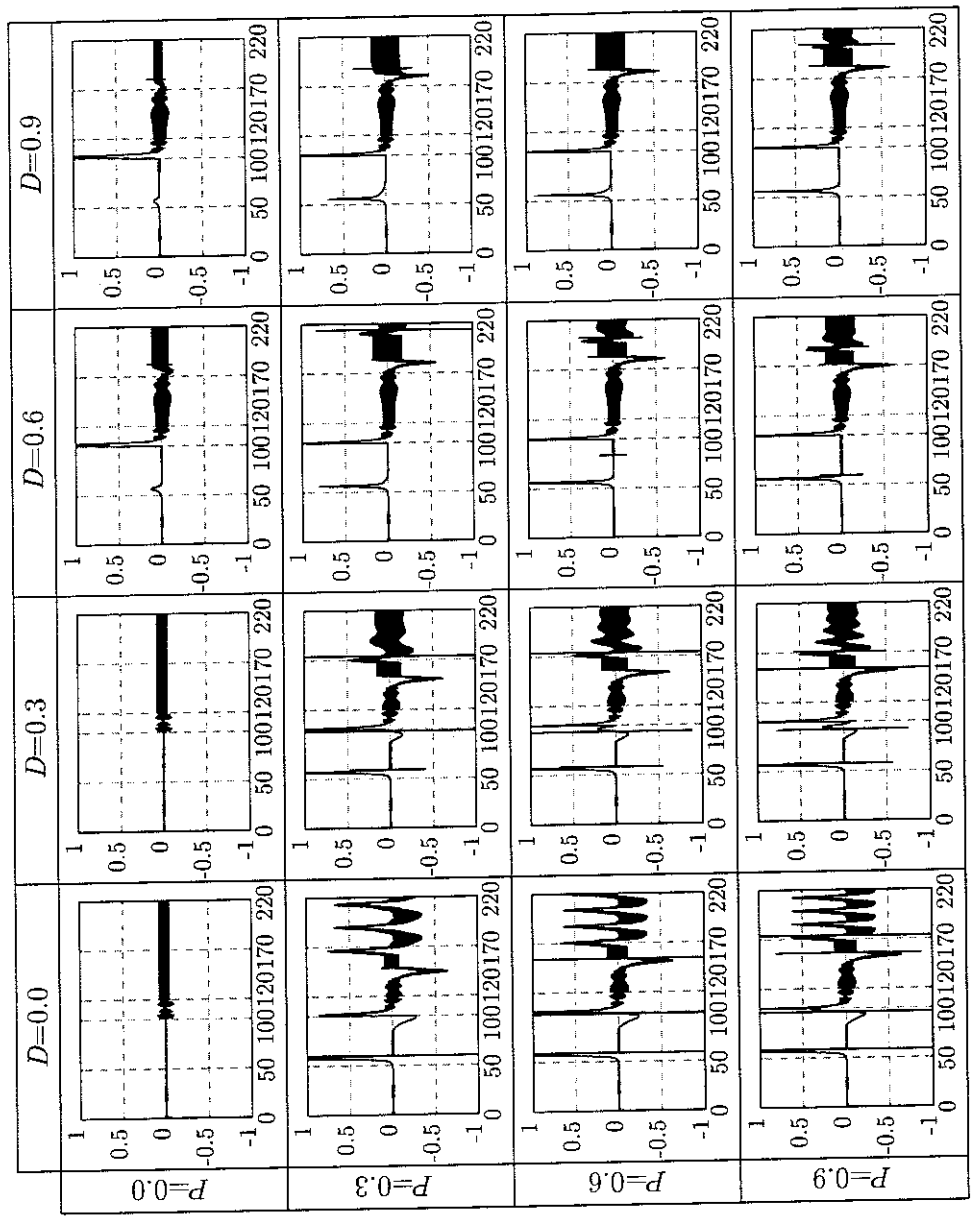


Figure 2.22: Simulation of PD controllers with different constant values: error time derivative tracks [1/s]

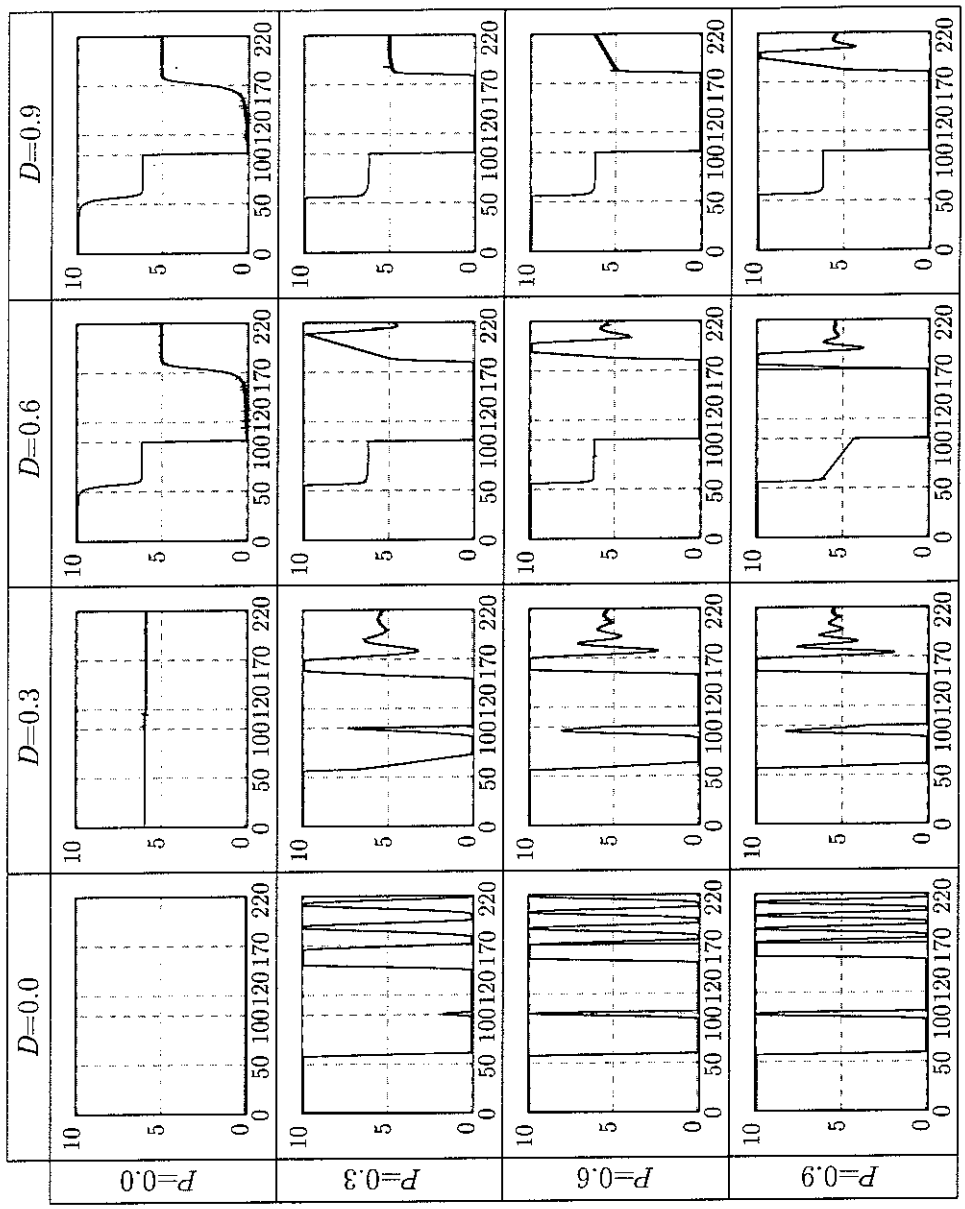


Figure 2.23: Simulation of PD controllers with different constant values: current tracks [A]

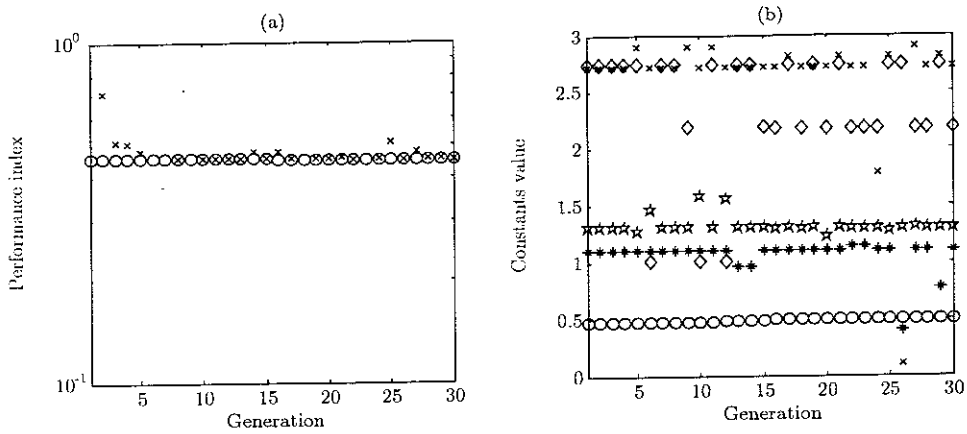


Figure 2.24: GA optimization of the controller using the IAE performance index. (a) Performance of the population: ∘ best; × worst. (b) Values of the controller constants: ⋆ $A_c$: ◇ $B_c$; ∗ $C_c$; × $D_c$; ∘ $T_c$

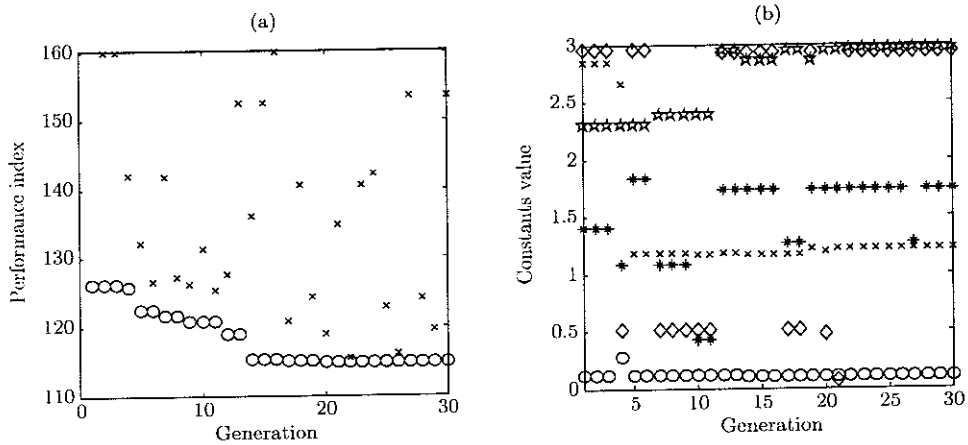


Figure 2.25: GA optimization of the controller using the settling time performance index. (a) Performance of the population: ∘ best; × worst. (b) Values of the controller constants: ⋆ $A_c$: ◇ $B_c$; ∗ $C_c$; × $D_c$; ∘ $T_c$

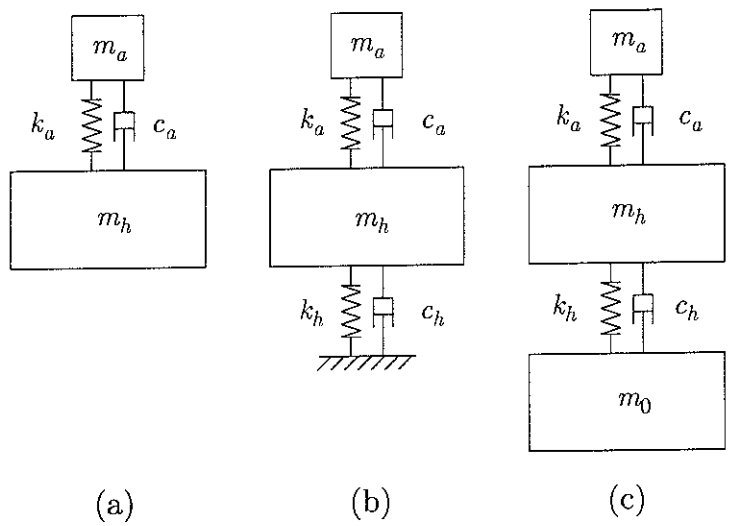


Figure 2.26: Models of the systems considered: original model (a), grounded model (b) and 3dof model (c)

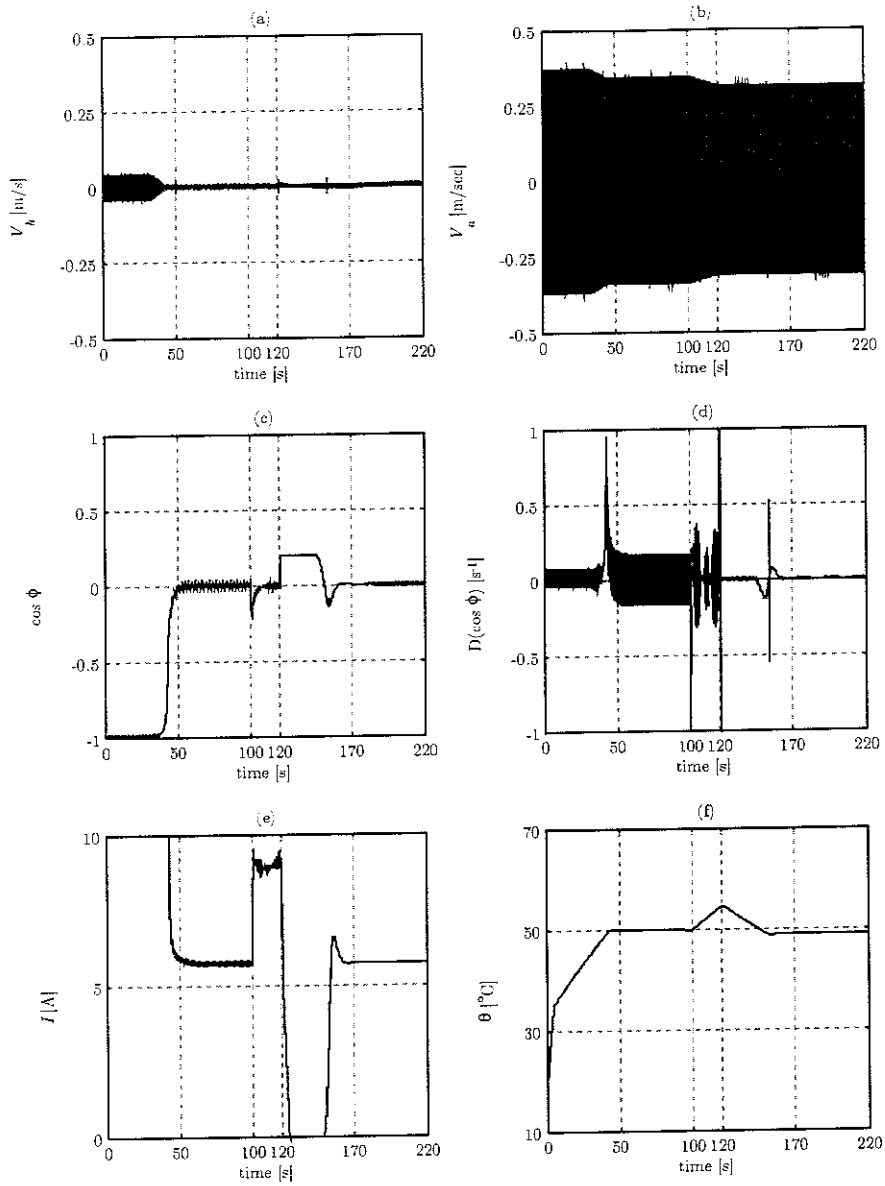


Figure 2.27: Performance of the TVA on a free 1dof system: (a) velocity of the host structure, (b) velocity of the TVA, (c) $\cos\phi$, (d) $\mathrm{d}(\cos\phi)/\mathrm{d}t$, (e) current supplied to the SMA wire, (f) temperature of the SMA wire

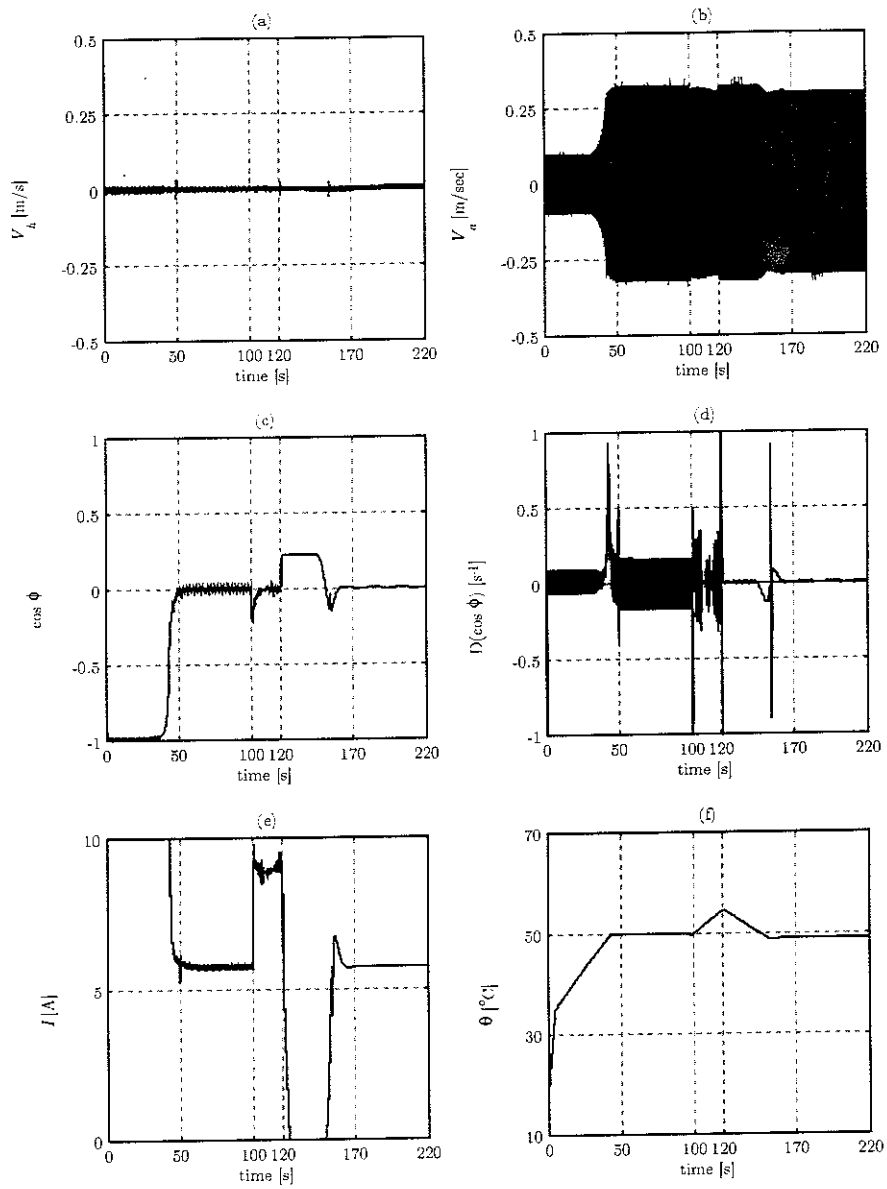


Figure 2.28: Performance of the TVA on a grounded 1dof system: (a) velocity of the host structure, (b) velocity of the TVA, (c) $\cos\phi$, (d) $\mathrm{d}(\cos\phi)/\mathrm{d}t$, (e) current supplied to the SMA wire, (f) temperature of the SMA wire

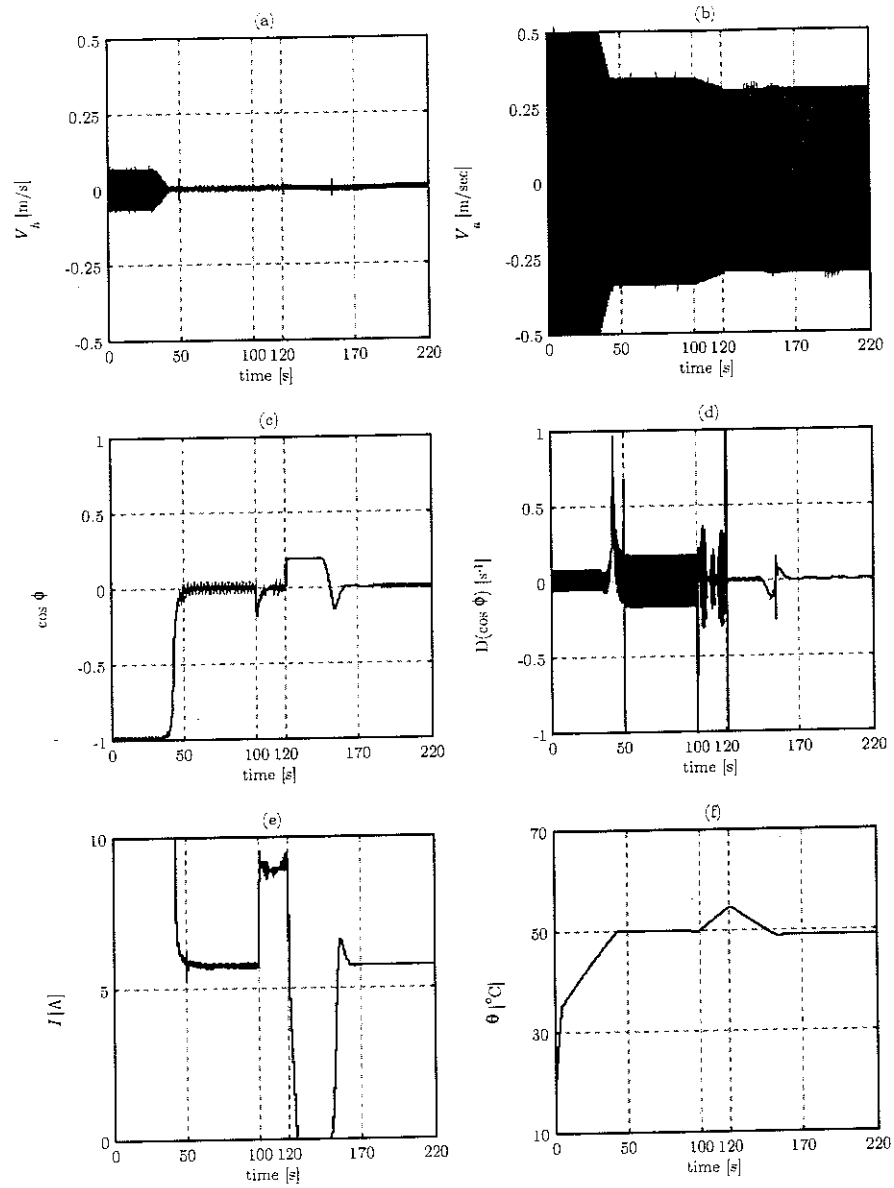


Figure 2.29: Performance of the TVA on a 2dof system exciting $m_1$: (a) velocity of the host structure, (b) velocity of the TVA, (c) $\cos\phi$, (d) $\mathrm{d}(\cos\phi)/\mathrm{d}t$, (e) current supplied to the SMA wire, (f) temperature of the SMA wire

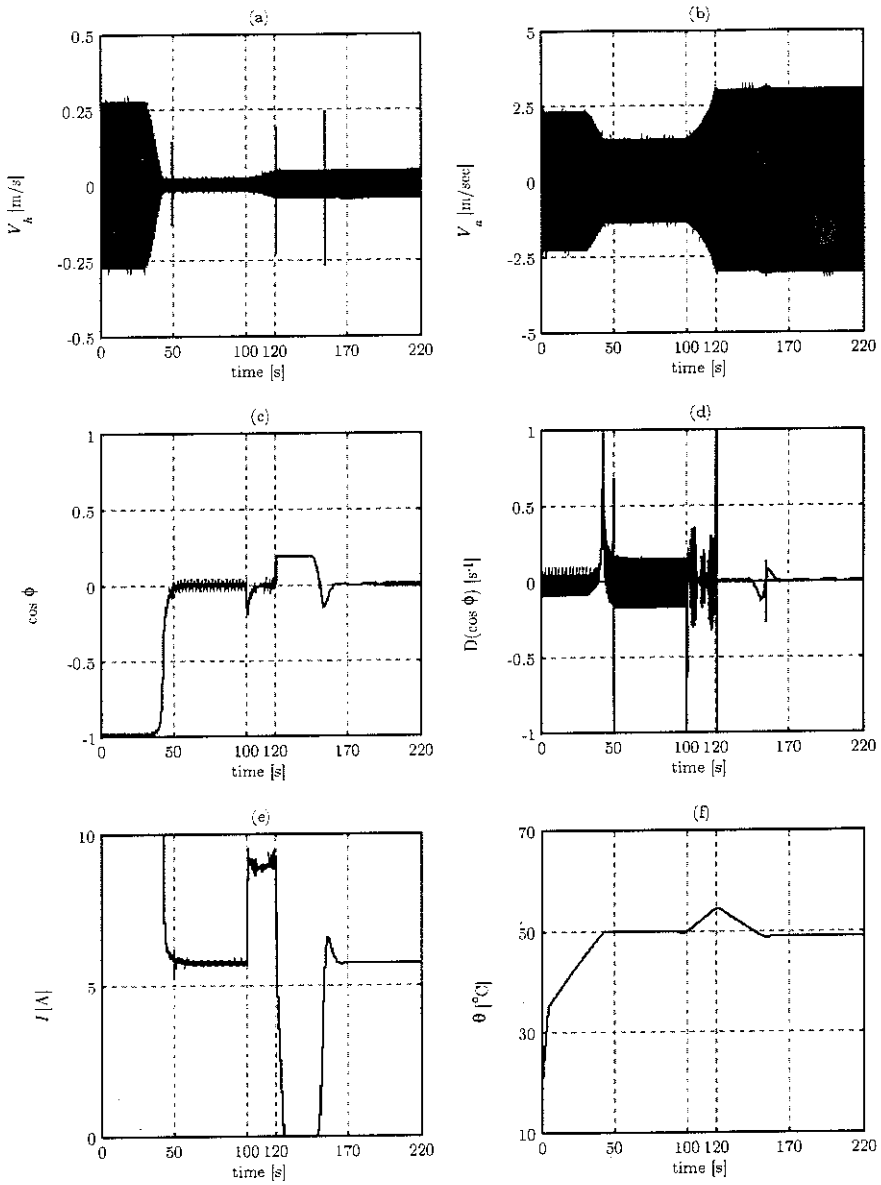


Figure 2.30: Performance of the TVA on a 2dof system exciting $m_0$: (a) velocity of the host structure, (b) velocity of the TVA, (c) $\cos\phi$, (d) $\mathrm{d}(\cos\phi)/\mathrm{d}t$, (e) current supplied to the SMA wire, (f) temperature of the SMA wire

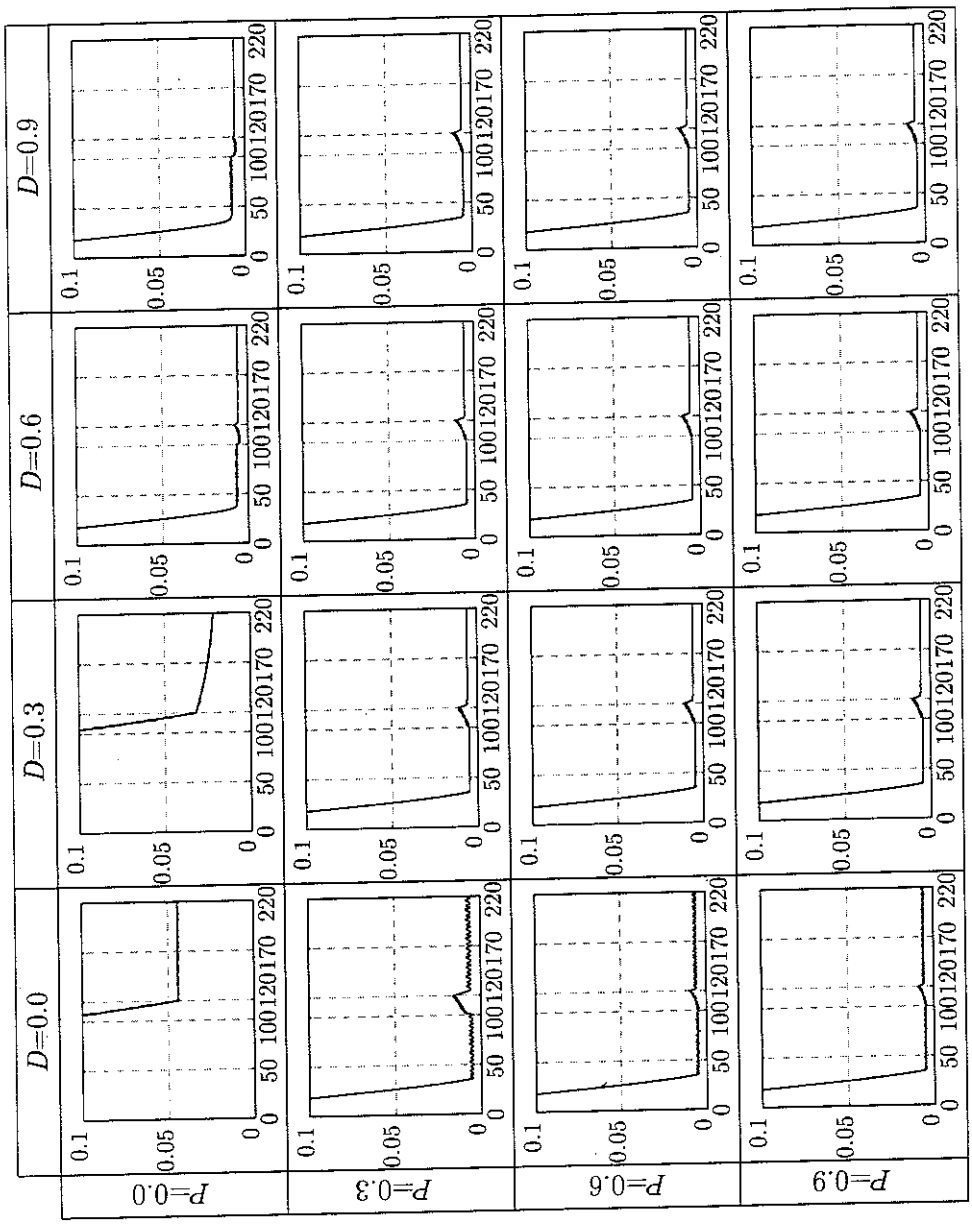


Figure 2.31: Simulation of PD controllers with different constant values and no hysteresis: tracks of the amplitude of the host structure velocity [m/s]

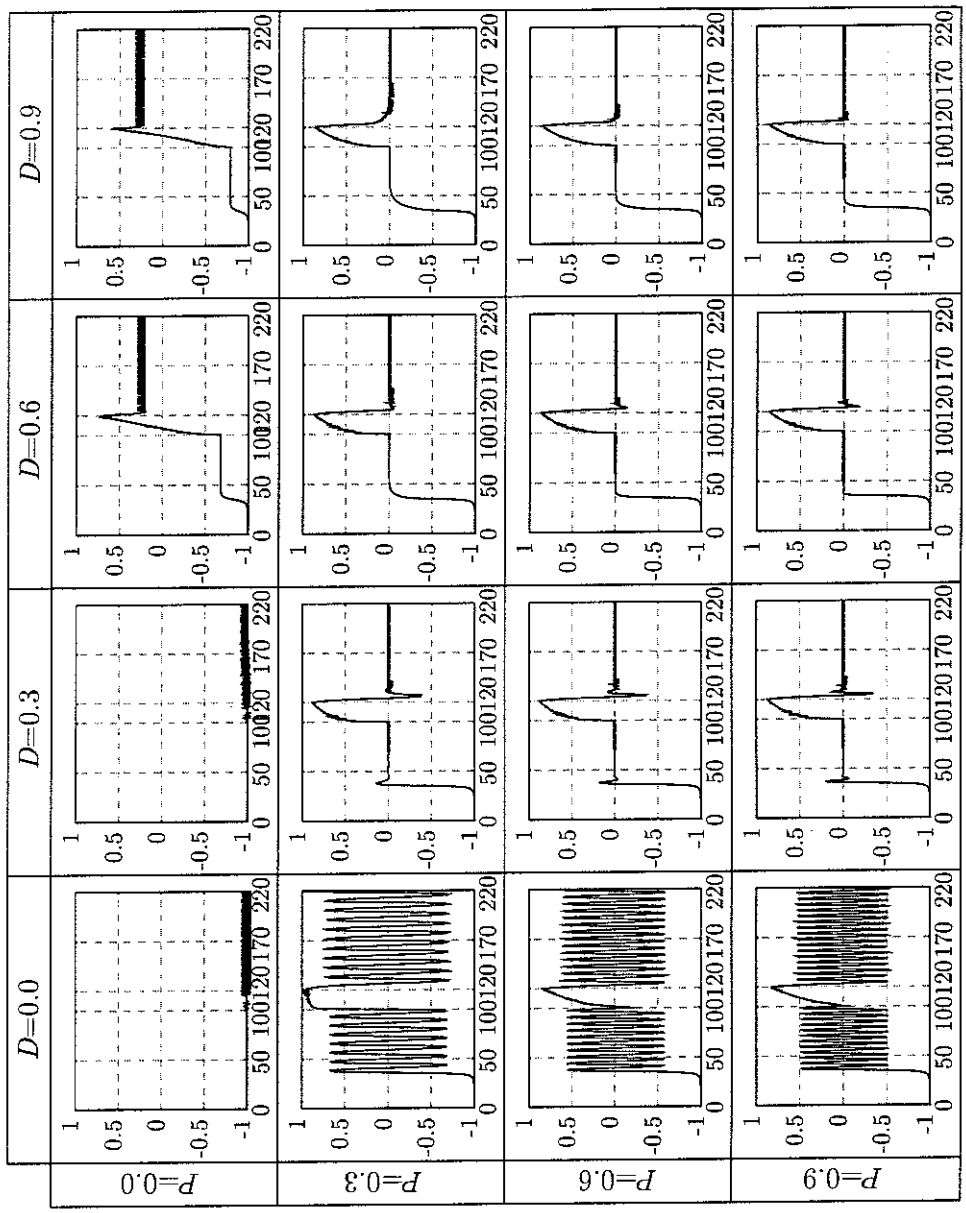


Figure 2.32: Simulation of PD controllers with different constant values and no hysteresis: error tracks

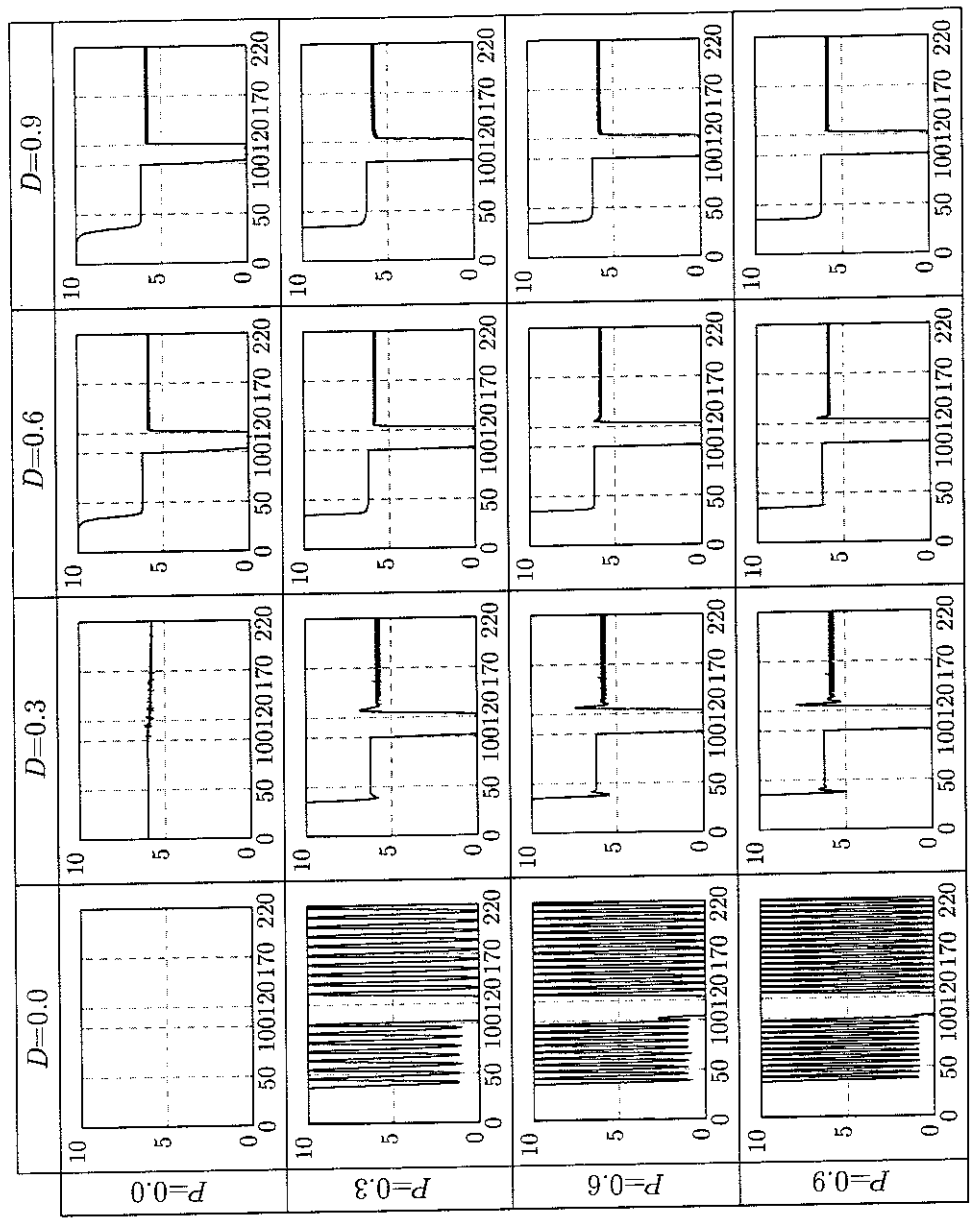


Figure 2.33: Simulation of PD controllers with different constant values and no hysteresis: current tracks [A]

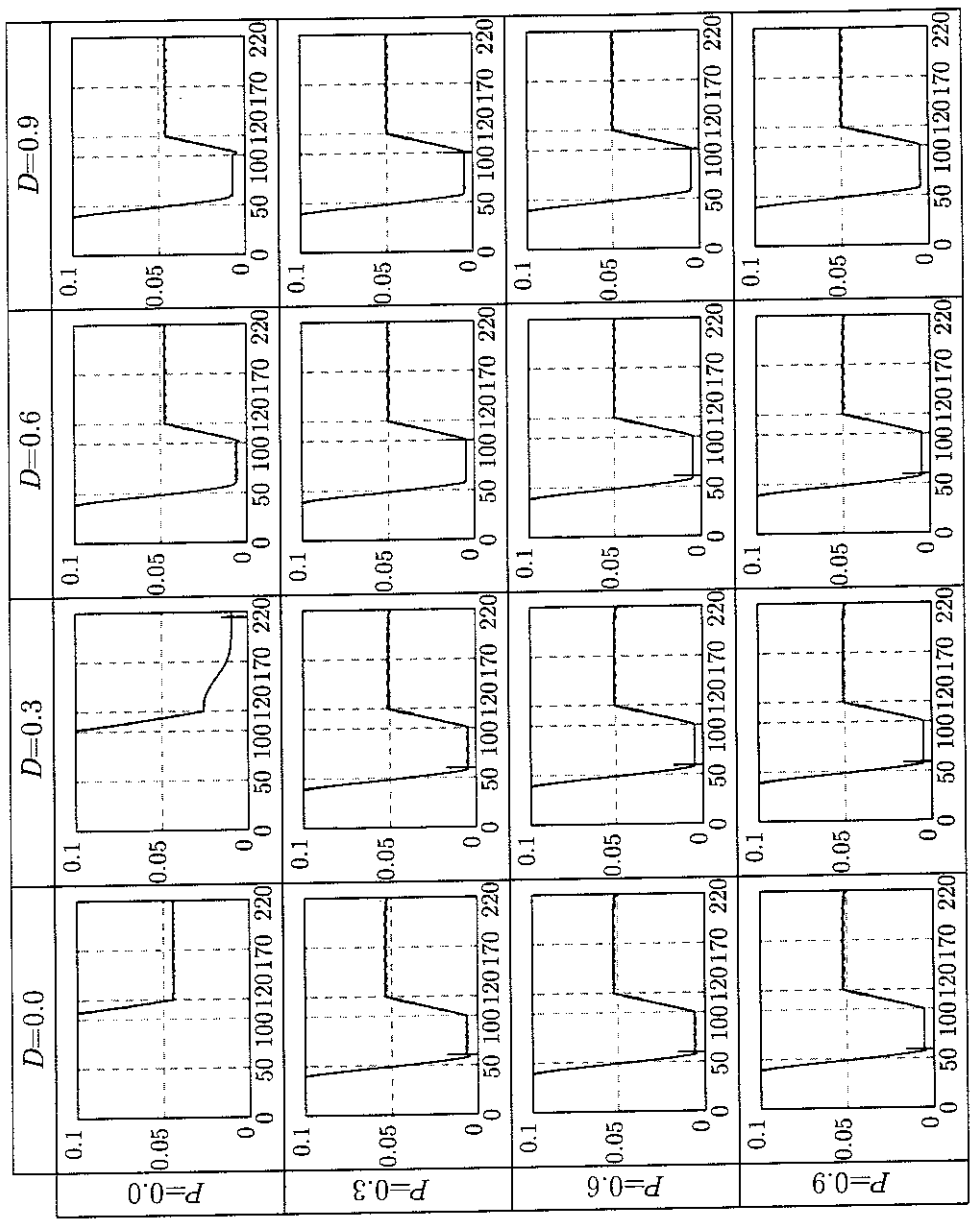


Figure 2.34: Simulation of PD controllers with different constant values and a big hysteresis field: tracks of the amplitude of the host structure velocity [m/s]

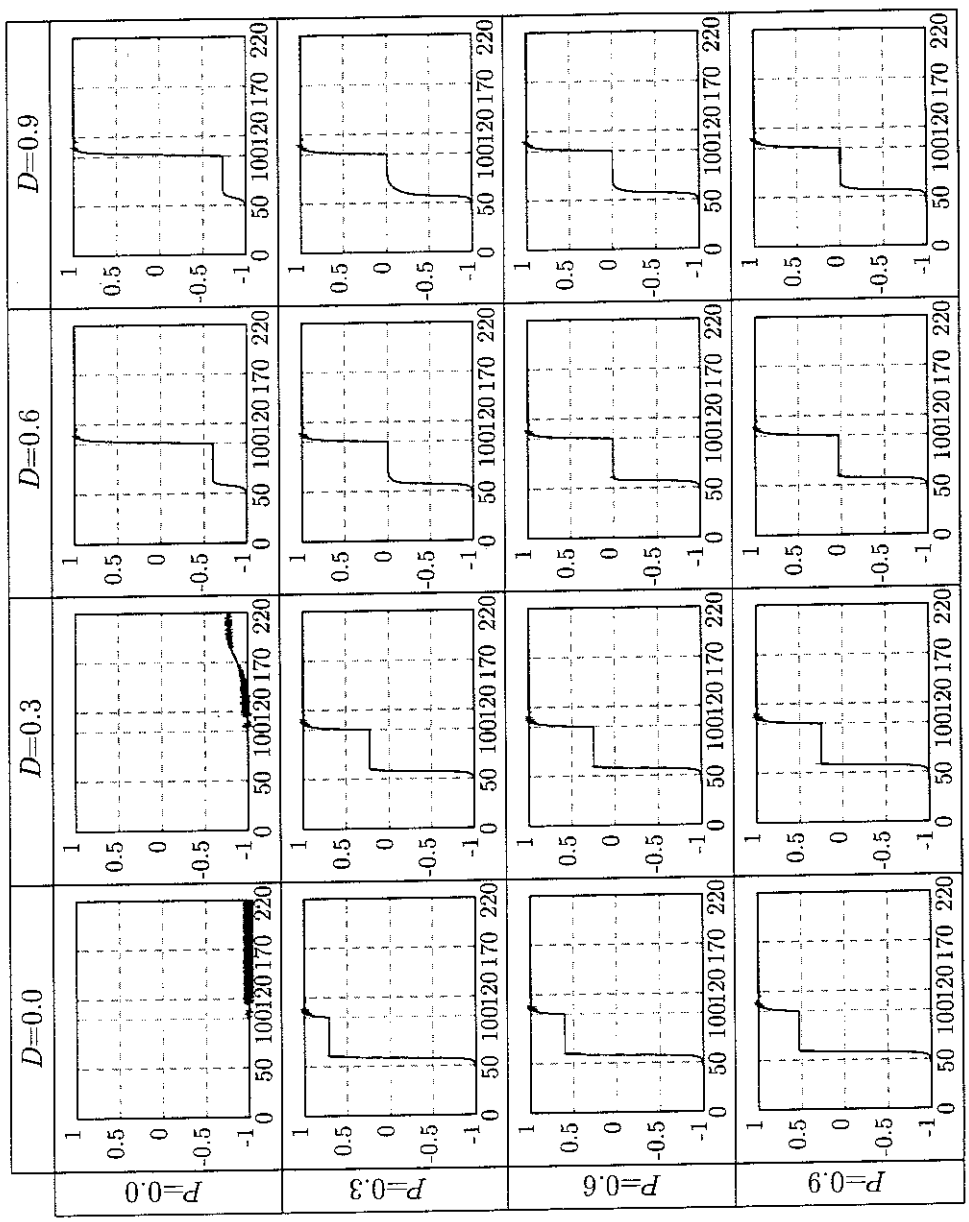


Figure 2.35: Simulation of PD controllers with different constant values and a big hysteresis field: error tracks

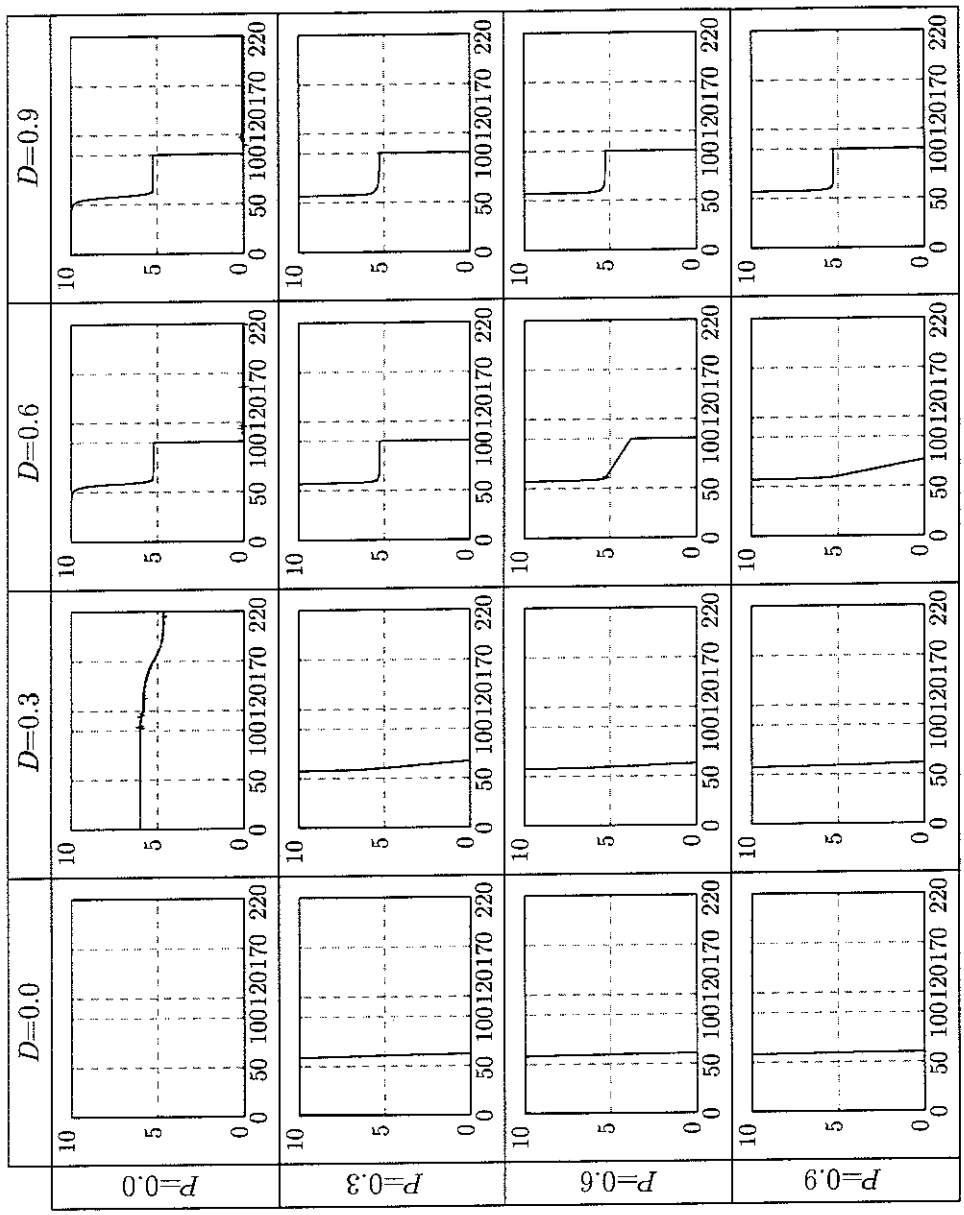


Figure 2.36: Simulation of PD controllers with different constant values and a big hysteresis field: current tracks [A]

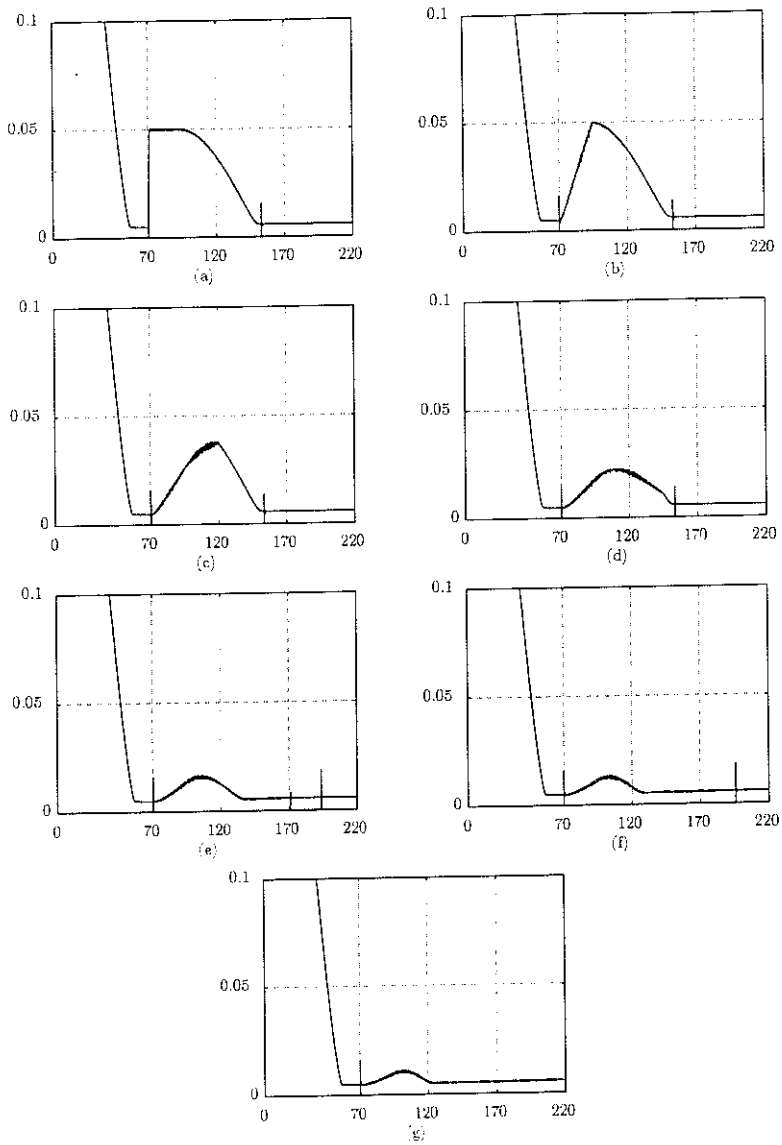


Figure 2.37: Simulation of PD controllers working with different excitation down: velocity tracks [m/s] as function of time [s]; variable frequency excitation from 97 to 87 Hz between 70 s and 71 s (a), 95 s (b), 120 s (c), 145 s (d), 170 s (e), 195 s (f) or 220 s (g)

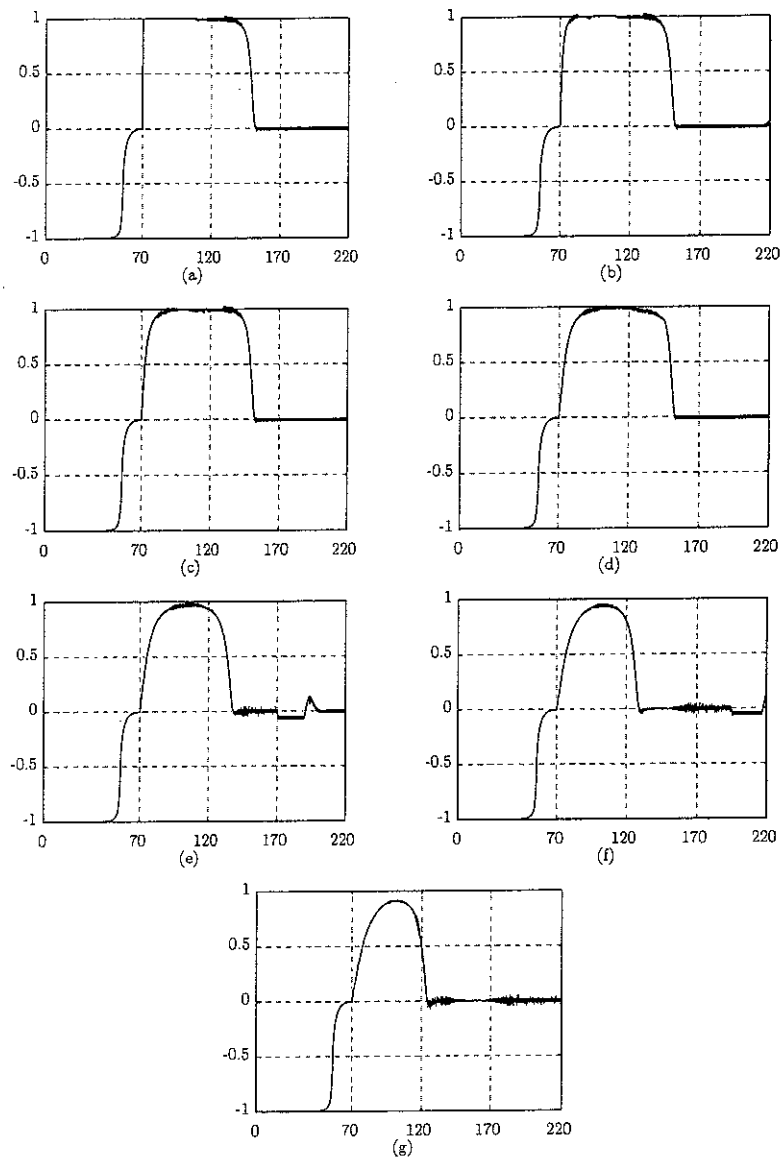


Figure 2.38: Simulation of PD controllers working with different excitation down: error tracks as function of time [s]; variable frequency excitation from 97 to 87 Hz between 70 s and 71 s (a), 95 s (b), 120 s (c), 145 s (d), 170 s (e), 195 s (f) or 220 s (g)

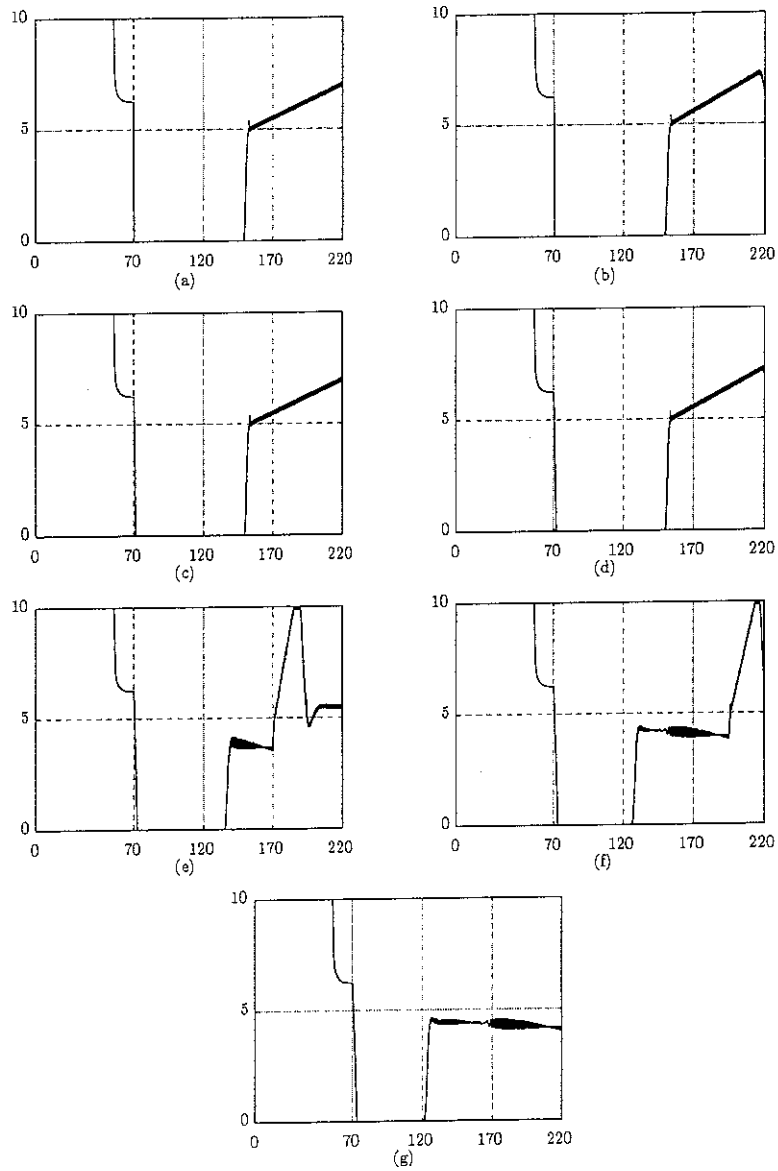


Figure 2.39: Simulation of PD controllers working with different excitation down: current tracks [A] as function of time [s]; variable frequency excitation from 97 to 87 Hz between 70 s and 71 s (a), 95 s (b), 120 s (c), 145 s (d), 170 s (e), 195 s (f) or 220 s (g)

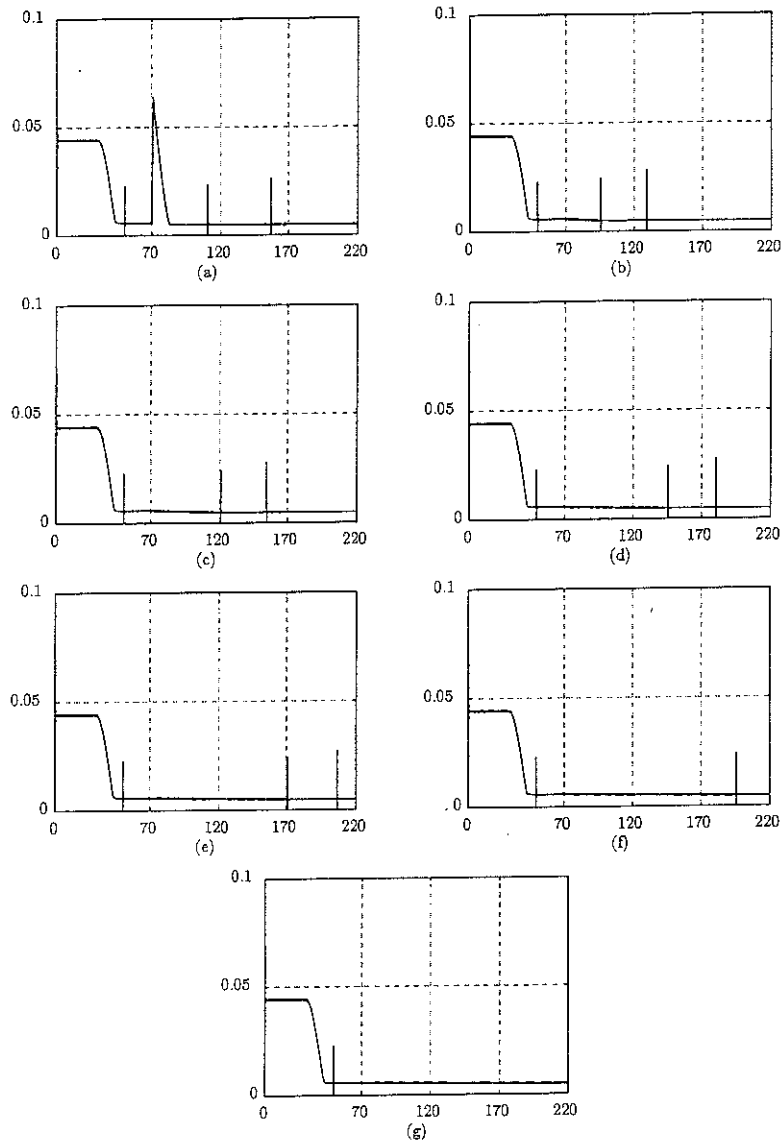


Figure 2.40: Simulation of PD controllers working with different excitation down: velocity tracks [m/s] as function of time [s]; variable frequency excitation from 87 to 97 Hz between 70 s and 71 s (a), 95 s (b), 120 s (c), 145 s (d), 170 s (e), 195 s (f) or 220 s (g)

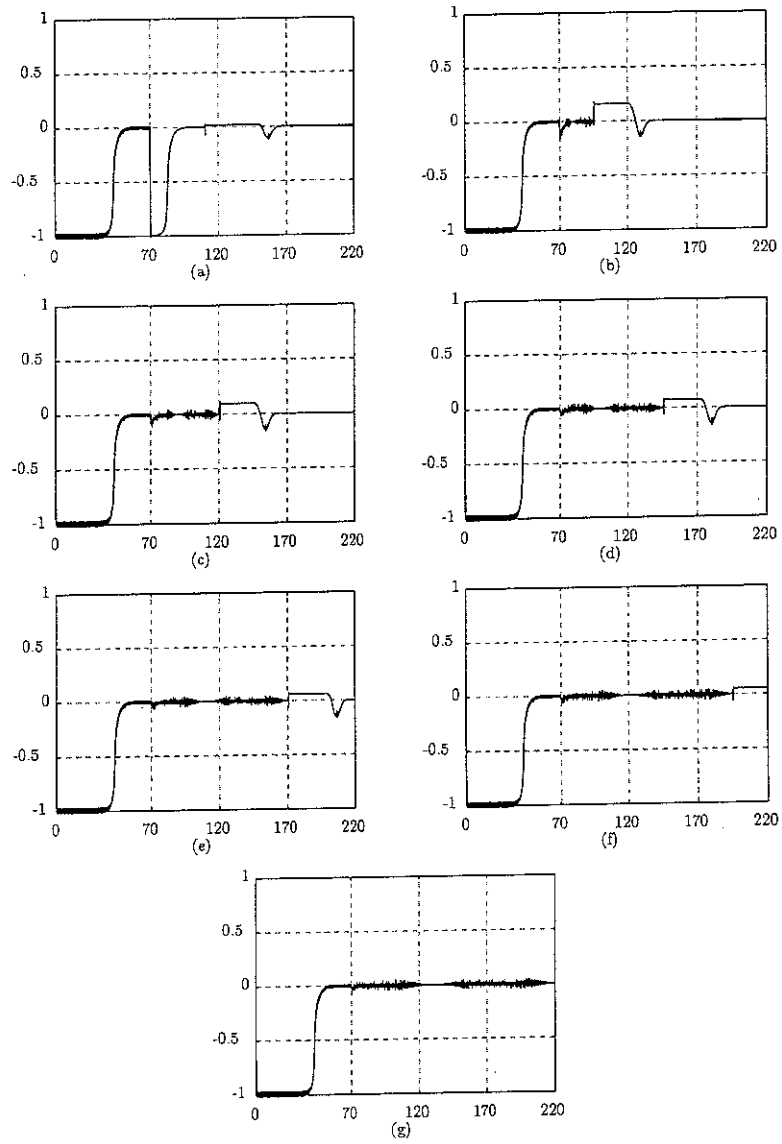


Figure 2.41: Simulation of PD controllers working with different excitation down: error tracks as function of time [s]; variable frequency excitation from 87 to 97 Hz between 70 s and 71 s (a), 95 s (b), 120 s (c), 145 s (d), 170 s (e), 195 s (f) or 220 s (g)

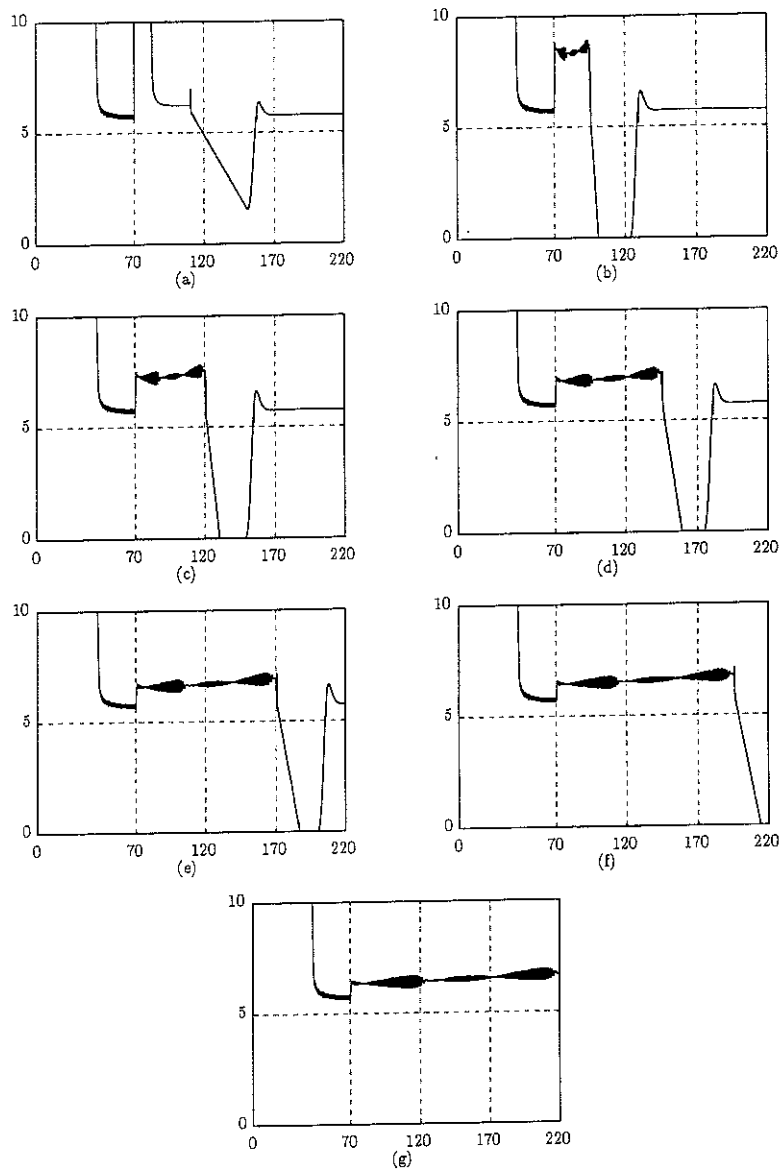


Figure 2.42: Simulation of PD controllers working with different excitation down: current tracks [A] as function of time [s]; variable frequency excitation from 87 to 97 Hz between 70 s and 71 s (a), 95 s (b), 120 s (c), 145 s (d), 170 s (e), 195 s (f) or 220 s (g)

# Chapter 3

# Experimental work

## 3.1 The test rig

During the numerical simulations presented in the previous chapter several controllers were designed and studied. The control algorithms were applied to a real SMA ATVA which was built and tested during earlier work [10].

The controllers were implemented in SIMULINK® using the Real Time Workshop and Real-Time Windows Target toolboxes. The use of such toolboxes permits exploitation of the controller SIMULINK® boxes already designed for numerical simulations. Moreover such software allowed the type of controller and constants of each controller to be changed from one test to another.

The PC on which the software was installed, was also equipped with an I/O Board for analog and digital data acquisition (NI "National Instruments" PCI-MIO-16E-4) and a BNC adapter (NI BNC-2110). Thus the controller, implemented on the PC, could receive the signals from the SMA ATVA (accelerations of the host structure and of the TVA) and send the appropriate control signal to the heating circuit of the absorber. The SIMULINK® program also generated the signal used to drive the shaker. Figure 3.1 shows the connections of the several pieces of equipment used in the experiments while figure 3.2 shows a picture of the experimental layout.

The SMA ATVA was built using two parallel SMA wires which were 2 mm diameter and 230 mm long [10]. The tunable range of the device was between 63.9 Hz (below 35°C) and 77.6 Hz (above 67°C). The tunable range recorded during the actual tests was between 52 and 66 Hz. The difference was due to the addition of an accelerometer at each end of the beam that forms the TVA. These were required for control purposes but were not used during the absorber characterization. The performance of the ATVA could be predicted

by adding a 1 g mass at each end of the beam in order to take into account of the mass of the accelerometers, the glue and the connection leads. Figure 3.3 shows the results of this new prediction while figure 3.4 shows how the predicted tunable range depends on the temperature.

The controllers utilized the signals gathered from the accelerometer in the middle (host structure acceleration) and the accelerometers at the ends of the beam (TVA acceleration) to calculate the current that must pass through the SMA wire. In the middle an impedance head, PCB ICP® 288D01 with a voltage sensitivity of about -10.2 $mVs^2/m$, was used whereas at the ends of the beam two PCB ICP® 352C22 accelerometers were used. These had a weight of 0.5 gm, a voltage sensitivity of about 10 $mVs^2/m$ and an operating temperature range from -54 to +121 °C. They were bonded to the beam using cyanoacrylate adhesive. Only one accelerometer was necessary for the controller action, and the other one was used as a dummy mass in order to maintain the symmetry of the structure.

The heating current was generated by a power supply Lambda ZUP10-20 with a power of 20 W that could generate a maximum voltage of 10 V or a maximum current of 20 A. The power supply has an analog current remote control, i.e. a signal between 0 and -4 Volts can drive a current from 0 to 21 A (105% of the full rated output current). So the conversion coefficient from Ampere (generated) and Volt (supplied to the supply remote control port) is $-1/5.25$ [A/V].

Although the acquisition of accelerometer signals and the control of the power supply was straightforward, the signals supplied to the shaker was contaminated with high frequency noise. The D/A conversion generated high frequency component in the signal due to its faceted shape after the analog reconstruction. So the signal was passed through a low-pass filter, Kemo® BenchMaster VBF 8, set to a cut-off frequency of 150 Hz, well above the tunable range of the SMA ATVA.

Lastly a thermocouple was placed on the SMA wire near the middle of the ATVA in order to check the temperature of the absorber during the experiments.

## 3.2 Experimental procedure

After the set up of equipment and SIMULINK® programs some preliminary tests were carried out in order to check the tunable range and the performance of the controller algorithms inside this range.

In the first series of experiments the SMA ATVA was excited at a constant frequency for a period of 220 s for each test. The excitation frequency

was then varied from 50 up to 67 Hz, increasing it by 1 Hz at a time. The controller was switched on at the beginning of the test and it brought the temperature of the wire from a starting temperature around the ambient temperature to the "tuned" temperature. All the experiments were carried out at an ambient temperature of about 16-17°C and starting at a temperature of the wire up to 22-24°C. The sampling frequency was set to 1 kHz (corresponding to a sampling period of 0.001 s). A buffer of 50000 points was used so that a full buffer contained 50 s of data. The full buffer was downloaded to a file so that at the end of the experiment five files were recorded, each containing 50 seconds except the last one that contained only 20 seconds.

During preliminary tests the controller that showed the best performance in the numerical simulations was implemented. So a PD controller was employed, with an update of the current value every 0.1 s. The constant $P$ was set to 0.6 and the constant $D$ to 0.9.

From these preliminary tests it was determined that the tunable range was between 52 and 66 Hz. Above 66 Hz the controller was not working properly and it carried on heating the SMA ATVA even if the vibration of the base was not reduced. Below 52 Hz the behaviour of the test rig was not fully predictable. In fact between 50 and 52 Hz the system was sometimes tunable. The phenomenon was not fully explained but could be related to the "over-softening" behaviour observed during the characterization of the device [10] which can broaden the tunable range. Below 50 Hz the controller did not work properly. It cooled the SMA wire to the ambient temperature even if this has no effect on the vibration reduction. Nevertheless the reliable tunable range was between 52 and 66 Hz and in this range the controller was working properly and each test was repeatable.

In order to show the behaviour of the controller when the system was excited inside the tunable range the results of three tests are reported. The first was carried out at the lower end of the tunable range (52 Hz), the second one in the middle (59 Hz) and the last one at the upper end (66 Hz) in order to cover the whole range. Figures 3.5 and 3.6 show the results of the test carried out with an excitation frequency of 52 Hz. Figure 3.5(a) shows the effectiveness of the controller in reducing the acceleration of the host structure after 25 s. Figure 3.5(b) shows the acceleration of the absorber mass during the test. This acceleration had almost the same amplitude during the test although it had a mean value different from zero in the first 50 s. Such a drift in the acceleration of the absorber was recorded for all the tests carried out and it had no effect on the performance of the controller. Later in this section, a possible explanation of this phenomenon is given. Figure 3.6 shows the activity of the controller during the test. In particular figure 3.6(a) shows

the evaluation of the cosine of the phase angle between the host structure and absorber accelerations. It's evident that the evaluation of the error function, is not influenced by the ambient noise or by the oscillations in the absorber acceleration. Figure 3.6(b) shows the current generated by the power supply during the test. At the beginning of the test the current is at its maximum in order to bring the temperature of the SMA to the required value as soon as possible. After a small drop in the current it rises again in order to reach a steady state value of around 4.5 A. Finally figure 3.6(c) shows the derivative of the error. Such a function is noisier than the other function, because of its numerical derivation, but during the steady state condition, i.e. after 50 s, it has a null mean value.

It is clear that the numerical model describes the real system quite well. Therefore the model described in the previous chapter can be used to predict the behaviour of different devices and design the respective controllers. Moreover the PD controller works quite well inside all the tunable range and tests show that it is possible to use SMA to realize and control a continuous ATVA.

Figures 3.7 and 3.8 show the results of the test carried out with an excitation frequency of 59 Hz. The steady state value was reached after a longer transient at about 60 s. The "wobbling" in the acceleration of the absorber mass was still present and it seems to worsen the evaluation of the error during the first ten seconds. The "tuned" current, i.e. the current at the steady state, was about 5.5 A. Figures 3.9 and 3.10 show the results of the test carried out with an excitation frequency of 66 Hz. The steady state was reached after 120 s after the test had begun. The oscillation in the absorber acceleration seems to generate an erroneous evaluation of the error in the first 10 s. Fortunately this did not influence the action of the controller greatly and it kept the current supply to the maximum value permitted (10 A). The "tuned" current was now about 9 A.

During the numerical simulation the derivative term was shown to be essential in reducing the controller activity. A test with a $P$ constant of 0.6 and $D = 0$ constant was carried out. The results are shown in figures 3.11 and 3.12. It can be seen that the acceleration of the masses of the host structure and of the absorber are roughly equal to those with the PD controller (compare figure 3.11 with figure 3.7). Examination of the activity of the controller, however, shows the importance of the derivative term. The error reaches the desired value (zero) only after 160 s and after some damped oscillation around the steady state value. In the respective numerical test, the system never reached the desired value but it kept oscillating around this value without any decay. The oscillation around the "tuned" value is also present in the current supplied by the current generator (see figure 3.12(b)).

A result similar to that using the P controller was obtained using the fuzzy controller. In figure 3.13 and in figure 3.14 such results are shown. With the fuzzy controller the system reaches a steady state value after an even longer time (greater than 200 s). Moreover the acceleration of the absorber mass has a persistent oscillation that is probably due to the stronger activity of the power supply. Comparing figure 3.13(b) and 3.14(b) it is evident that the oscillations are related to the increases in the current. It is possible that the variation of the electrical field generated by the current inside the SMA wire degrades the performance of the accelerometer that is separated by the SMA wire only by a thin glue layer. However, even if the result is similar to the previous one, the P controller is preferable because can be implemented using an analogue circuit.

The PD controller was continuously implemented also in a configuration in which it updated at the sampling frequency. The constant $P$ was set to $5 \times 10^{-4}$ and $D$ to $5 \times 10^{-3}$. The controller worked and the amplitude of the host structure mass was effectively reduced in the same manner the P controller with a 0.1 s update frequency (see figure 3.15). However figure 3.16(a) shows that the system was slower in reaching the tuned condition, taking about 100 s. The current that the controller generated seems to stay around the steady state value but with more noise and oscillations (see figure 3.16(b)). The evaluation of the derivative term seems quite good and not too noisy (figure 3.16(c)) which was probably due to the filter constants. It can be concluded that a longer update period for an SMA ATVA seems favourable.

In order to complete the performance analysis of the PD controller some more tests were carried out applying a variable frequency excitation. The force applied in the first test was a force with a constant frequency of 60 Hz for the first 100 s, then the frequency shifted linearly from 60 Hz to 65 Hz in 20 s. Then the frequency of the excitation stayed constant till the end of the simulation, that is from the 120-th second to the 220-th second of the test, as shown in figure 3.17(a). Figure 3.17 shows the effectiveness of the controller in keeping the acceleration of the host structure very small. Figure 3.18 shows the actions that the controller took during the test. In particular figure 3.18(c) shows that the "tuned" current is about 5 A for the 60 Hz excitation frequency and is about 7 A for the 65 Hz excitation frequency. During the transient, from the 100-th second, the controller drove the maximum current in order to heat the device as soon as possible. Unfortunately these current values are only indicative of the SMA state because of the hysteresis between temperature and Young's modulus, in fact the same value of the elastic modulus can be obtained with different temperatures.

A second test with a variable frequency excitation was carried out by

varying linearly the frequency from 65 Hz to 60 Hz, again between the 100-th and 120-th second of the test (see figure 3.19(a)). Figures 3.19 and 3.20 show the results of such a test. Figure 3.20(a) shows that the system did not reach the tuned condition during the first 100 s of constant 65 Hz excitation but that the amplitude of the acceleration of the host structure was already substantially reduced (see figure 3.19(b)). During the next 20 s the current was switched off in order to cool the wire as quickly as possible (see figure 3.20(b)). Even if the system reached the tuned condition after 150 s (see figure 3.20(a)) the amplitude of the host structure remained small also during the transient period (see figure 3.19(b)).

In section 2.3.4 genetic algorithms (GA) were used in order to find the optimal constants of the controller. Table 2.7 shows the results of two GA optimal constant searches. The constants in the table refer to equation 2.32. The first GA optimum search was carried out using the IAE performance index while the second one was carried out using the settling time performance index. Such results were also used in experimental tests in order to verify the effectiveness and the usefulness of the GA.

Figure 3.21 shows the results of the controller determined by the first GA search. The reduction in the host structure acceleration does not seem to be different from that obtained with the PD controller with the constants empirically chosen (see figure 3.7). Figure 3.22 shows the activity of the controller. The results are similar to those given by figure 3.8 but the $\cos\phi$ shows a small over-shoot before reaching the desired value. Such a small over-shoot has the effect of causing a small interruption in the current supply at about 65 s from the beginning of the test. Moreover the driven current seems a little more noisy. Since the results are very similar to that obtained with an empirical optimization, the use of a GA optimum searching method does not seem to be very useful in this case.

Figure 3.23 shows the result of the test carried out on the controller obtained by the second GA search. The use of such a controller does not improve the performance of that already reported. Instead $\cos\phi$ and its derivative appear to be less noisy (see figure 3.24). In the same way the supplied current appears less noisy and less fluctuating. As the update time period, $T_c$, seems to be important to the controller activity, it is advisable to take it in account during the optimization, even in the manually designed controller.

The oscillation in the measured acceleration of the absorber mass has shown not to be a problem in the controller effectiveness. In fact the evaluation of the $\cos\phi$ is made using both the host structure and absorber accelerations (see equation 2.12). If only one of the signal has a mean value different from zero the evaluation of the cosine is computed without any error. The

problem in the evaluation occurs when both the accelerations signals have a mean value different from zero. Even though this situation was not recorded during the experimental tests it is likely to occur when cheap accelerometers are used. So a very simple solution is suggested. In fact if the signals are passed through high-pass filters before they are passed to the block for the evaluation of the error function a very good result can be obtained. Figure 3.25 shows the results of a test carried out with a constant excitation frequency of 59 Hz filtering the acceleration signals. The high-pass filter was implemented in SIMULINK® and was a simple second order system with a cut-off frequency of 1 Hz given by

$$\frac{s^2}{s^2+s+1} \tag{3.1}$$

where $s$ is the Laplace variable. Figure 3.26(a) shows $\cos\phi$ evaluated by the system. The evaluation is computed without any error but the effectiveness of the controller is not improved (compare figure 3.8 to figure 3.26).

## 3.3 Discussion

The experiments showed that it is possible to use SMA to realize and control a continuous ATVA and that industrial application is feasible. The PD control algorithm designed in the previous section proved to be very effective and reliable with the real system. The performance of such a controller was compared to those of some other controllers but none of these has showed an improved performance. Moreover, as the controller proposed can be implemented using a analogue system, it is potentially cheaper and more durable.

The proposed numerical model describes the real system quite well and can be used to predict the behaviour of other similar devices and to design the respective controllers. However the model does not describe all the real system characteristics. In fact using only a P controller the controlled SMA ATVA reached the desired value but with a damped oscillation of the current, but the numerical results showed a constant oscillation around the steady state value.

The PD controller worked quite well within all the tunable frequency range. However, if the host structure was excited outside the tunable range the controller tried to force the device to tune itself anyway. So if the excitation is below the tunable range the controller overcools the SMA ATVA down to the ambient temperature; if the excitation frequency is above of the tunable range, the controller overheats the device up to the steady state

temperature related to the maximum current. Such behaviour is not a problem, however, because it does not affect the effectiveness of the controller. It starts working again properly when the excitation moves inside the tunable range again. Nonetheless in order to improve the readiness of the device the controller should always keep the SMA ATVA inside the tunable range. For instance the controller could be improved by also providing a measure of the excitation frequency. So the controller can update the current value only when the excitation frequency is inside the tunable range.

## 3.4 Figures

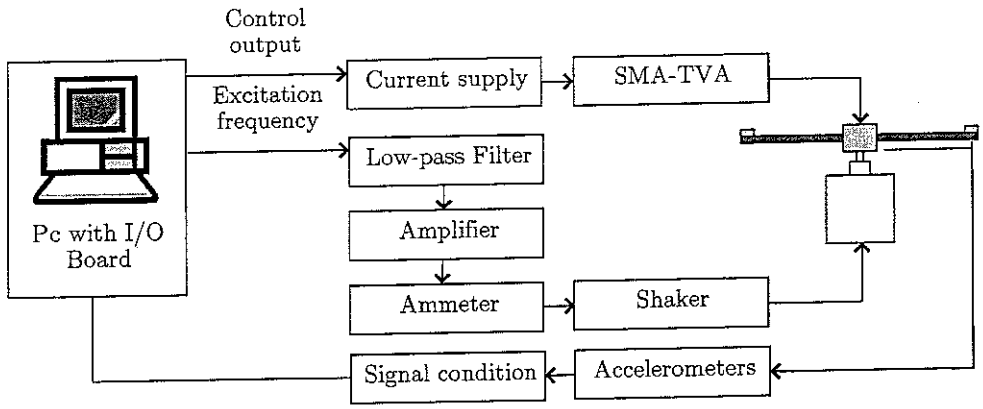


Figure 3.1: Flow diagram of the test rig connections

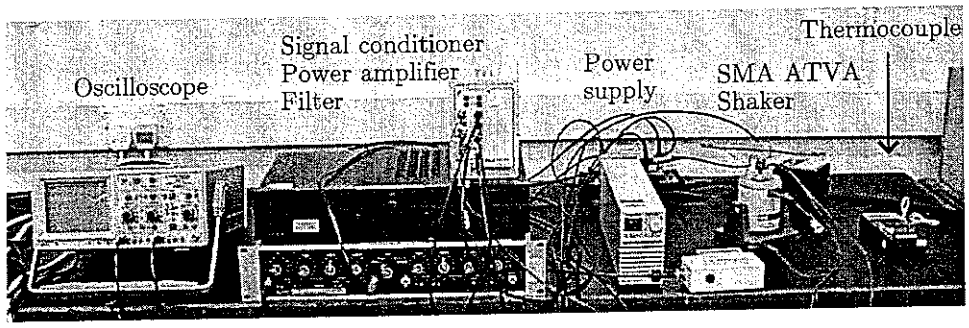


Figure 3.2: Photograph of the test rig bench

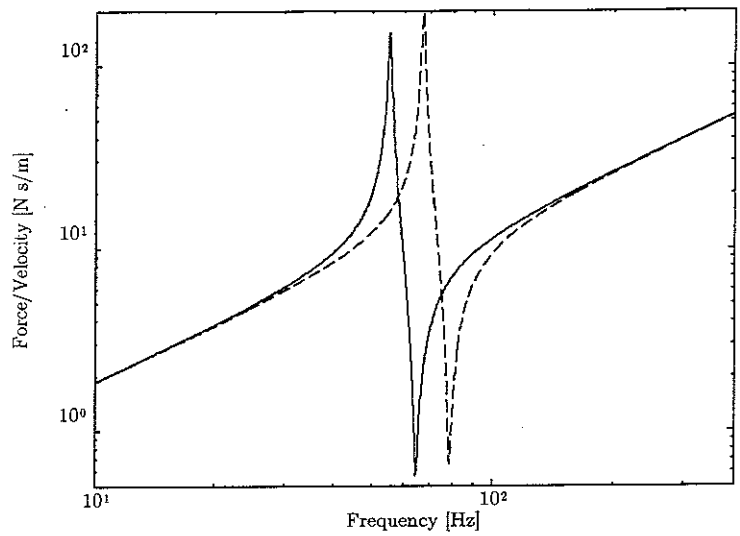


Figure 3.3: Predicted variation of impedance FRF from the cold to the hot state: — cold state; - - - hot state

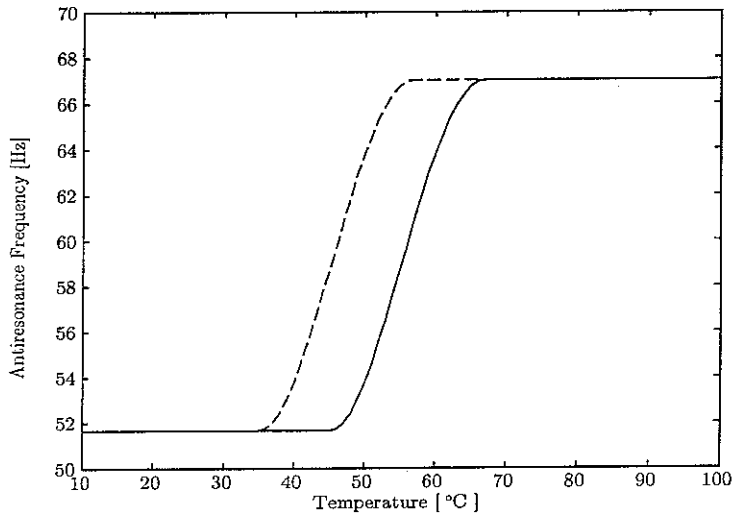


Figure 3.4: Variation of the antiresonance frequency with temperature: — heating; - - - cooling

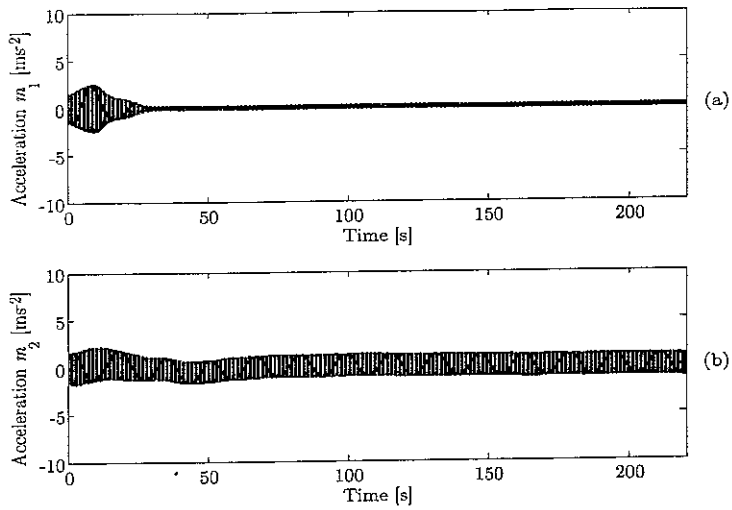


Figure 3.5: Effectiveness of the PD controller for a 52 Hz excitation frequency: acceleration of the host structure (a) and of the TVA (b)

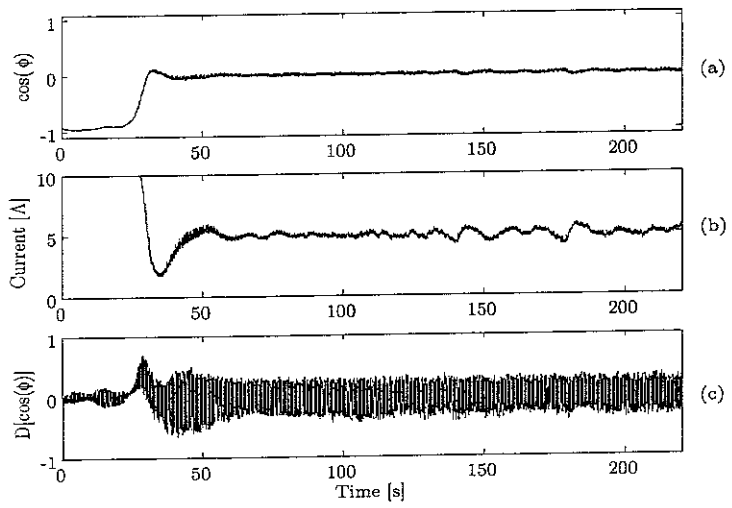


Figure 3.6: PD Controller activity for a 52 Hz excitation frequency: cosine of the acceleration phase difference $\cos\phi$ (a), current (b) and time derivative of $\cos\phi$ (c)

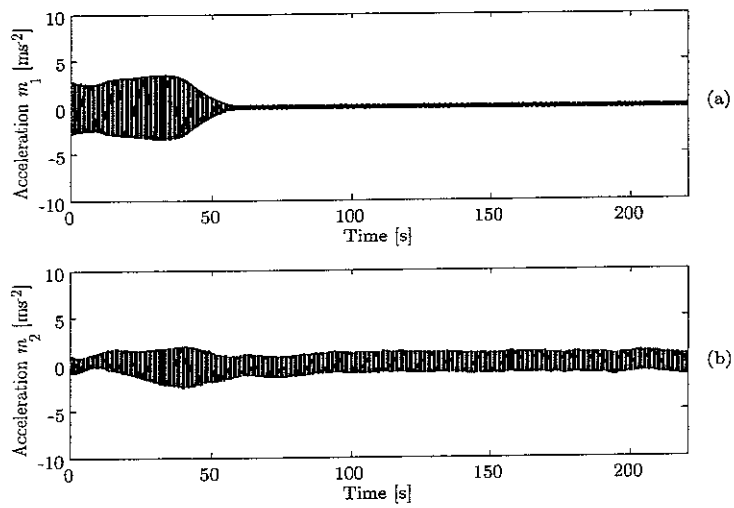


Figure 3.7: Effectiveness of the PD controller for a 59 Hz excitation frequency: acceleration of the host structure (a) and of the TVA (b)

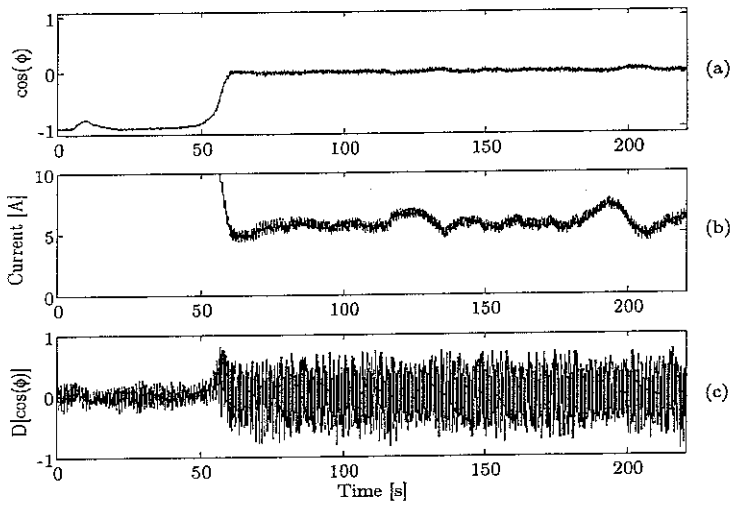


Figure 3.8: PD Controller activity for a 59 Hz excitation frequency: cosine of the acceleration phase difference $\cos\phi$ (a), current (b) and time derivative of $\cos\phi$ (c)

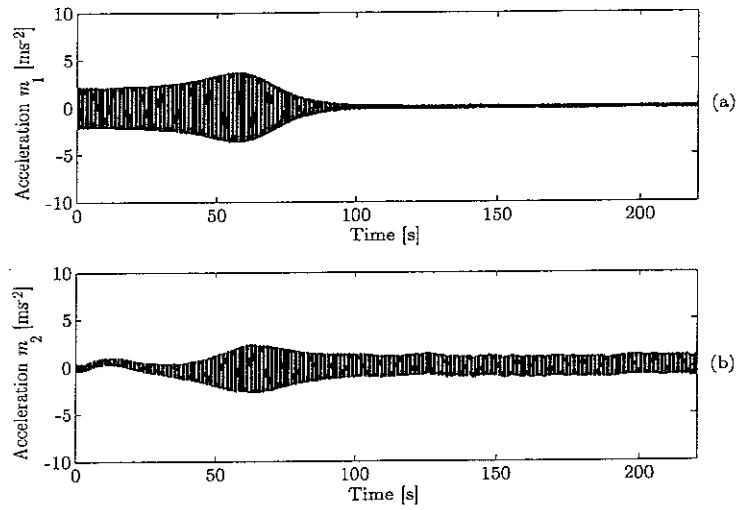


Figure 3.9: Effectiveness of the PD controller for a 66 Hz excitation frequency: acceleration of the host structure (a) and of the TVA (b)

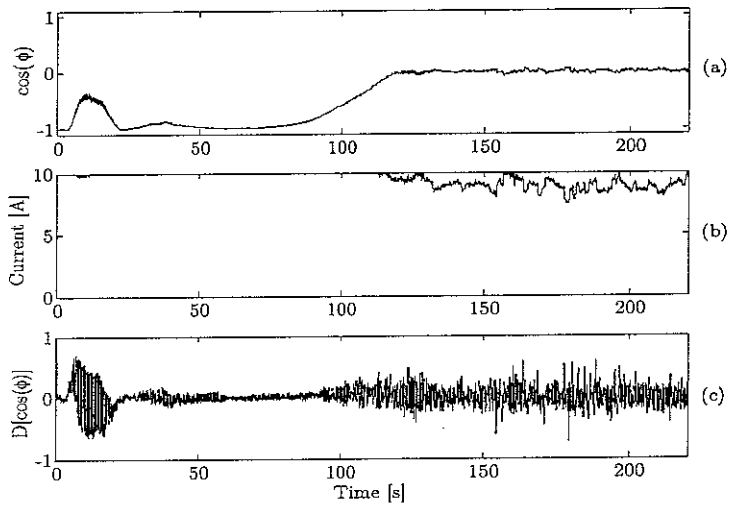


Figure 3.10: PD Controller activity for a 66 Hz excitation frequency: cosine of the acceleration phase difference $\cos\phi$ (a), current (b) and time derivative of $\cos\phi$ (c)

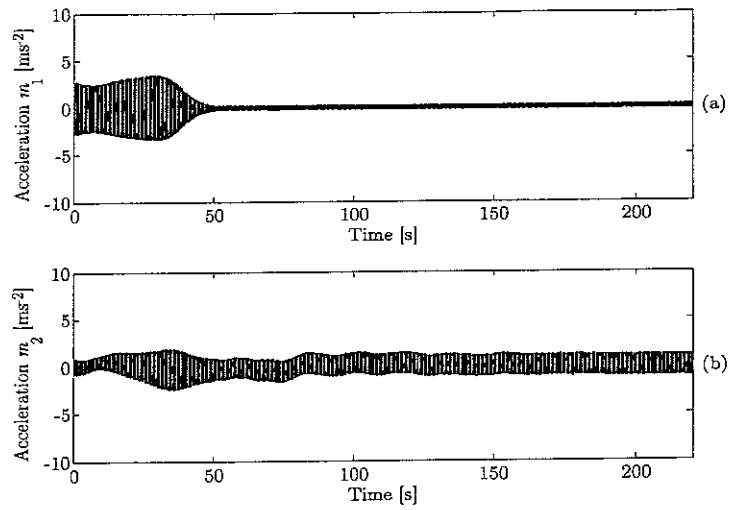


Figure 3.11: Effectiveness of the P controller for a 59 Hz excitation frequency: acceleration of the host structure (a) and of the TVA (b)

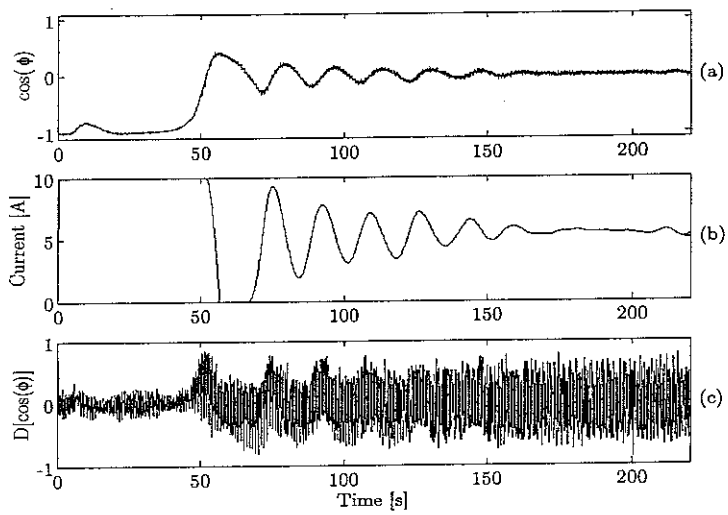


Figure 3.12: P Controller activity for a 59 Hz excitation frequency: cosine of the acceleration phase difference $\cos\phi$ (a), current (b) and time derivative of $\cos\phi$ (c)

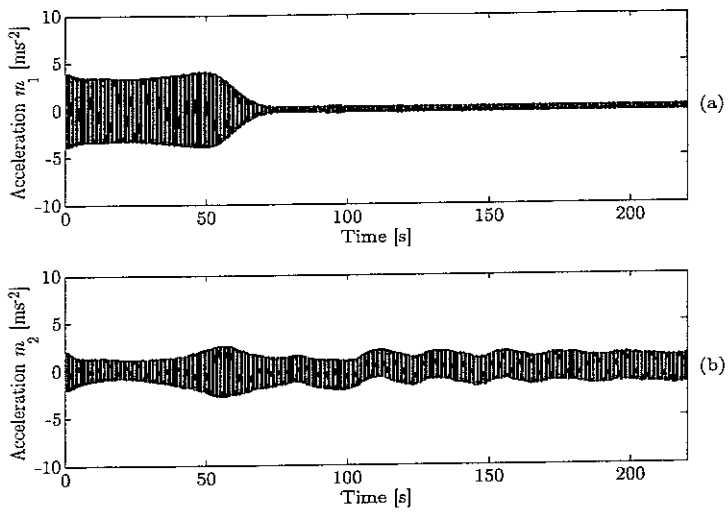


Figure 3.13: Effectiveness of the fuzzy controller for a 59 Hz excitation frequency: acceleration of the host structure (a) and of the TVA (b)

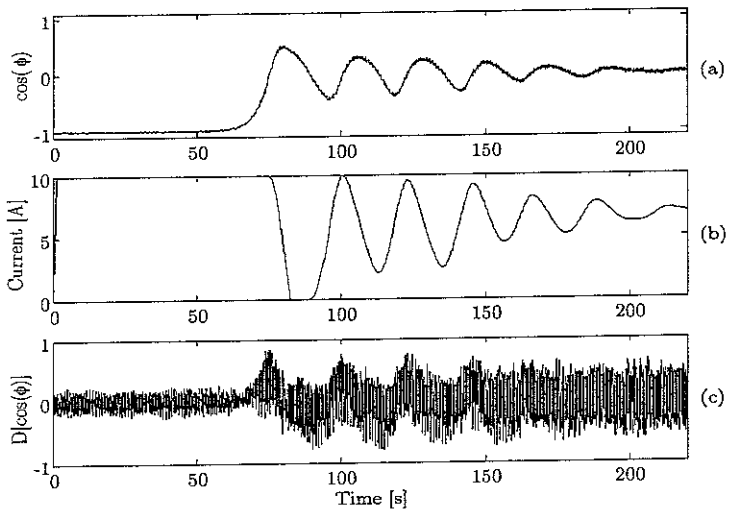


Figure 3.14: Fuzzy controller activity for a 59 Hz excitation frequency: cosine of the acceleration phase difference $\cos\phi$ (a), current (b) and time derivative of $\cos\phi$ (c)

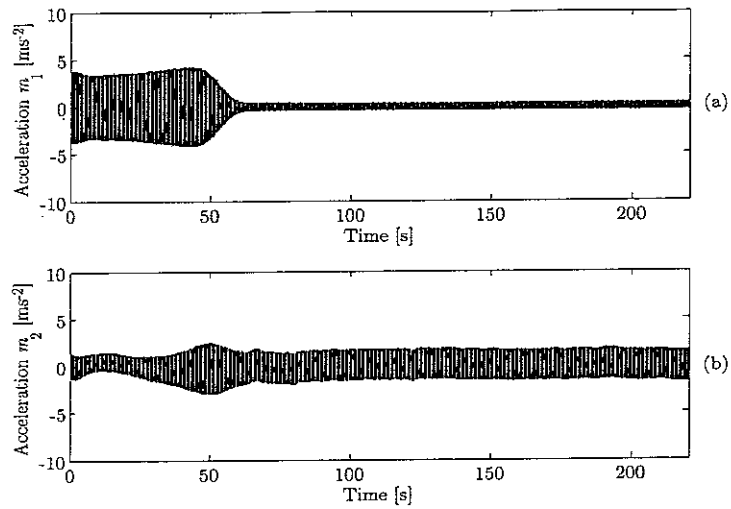


Figure 3.15: Effectiveness of the continuous PD controller for a 59 Hz excitation frequency: acceleration of the host structure (a) and of the TVA (b)

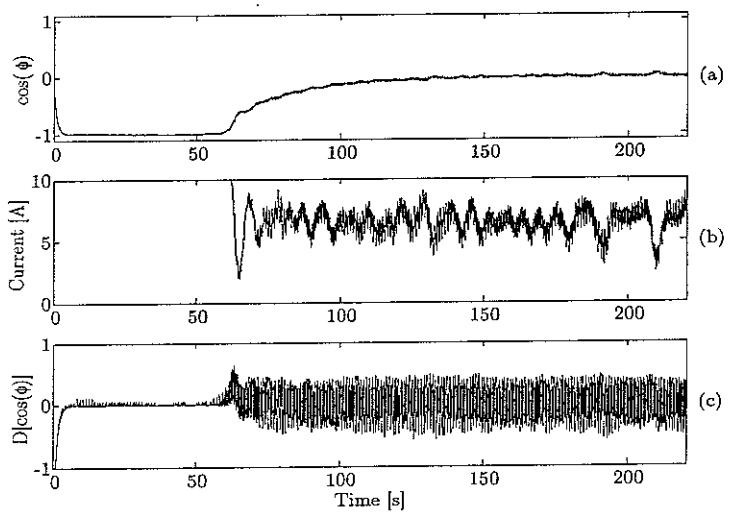


Figure 3.16: PD continuous controller activity for a 59 Hz excitation frequency: cosine of the acceleration phase difference $\cos\phi$ (a), current (b) and time derivative of $\cos\phi$ (c)

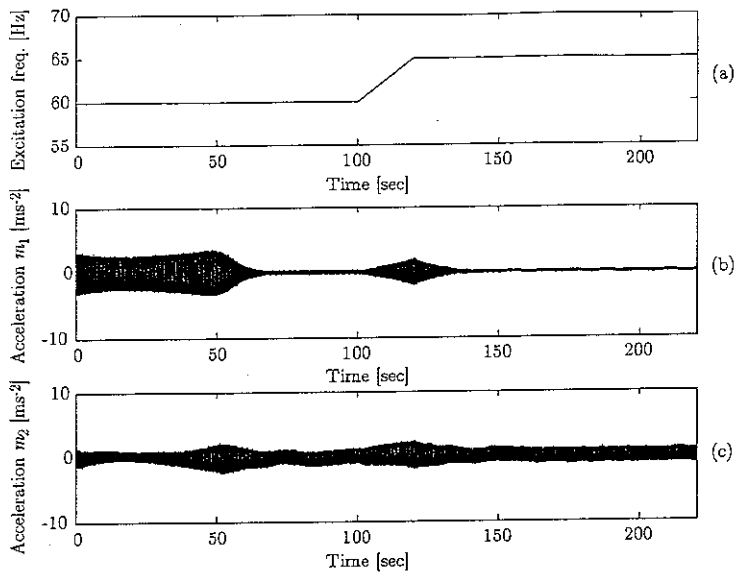


Figure 3.17: Effectiveness of the PD controller for a variable excitation frequency from 60 to 65 Hz: excitation frequency (a), acceleration of the host structure (b) and of the TVA (c)

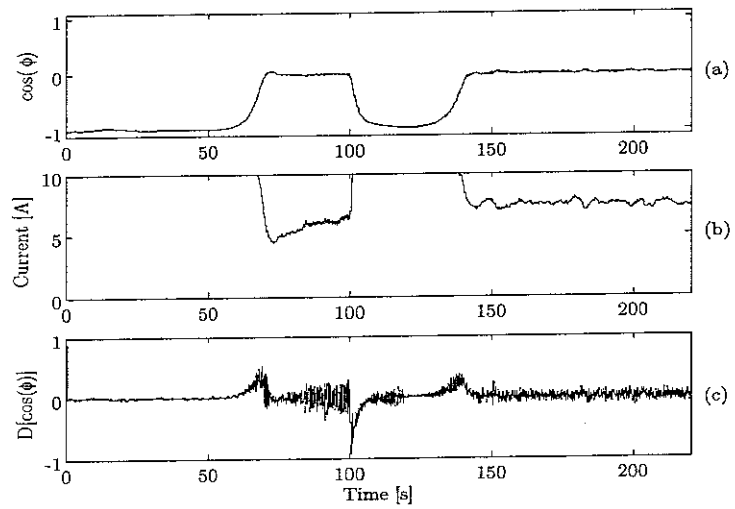


Figure 3.18: PD controller activity for a variable excitation frequency from 60 to 65 Hz: cosine of the acceleration phase difference $\cos\phi$ (a), current (b) and time derivative of $\cos\phi$ (c)

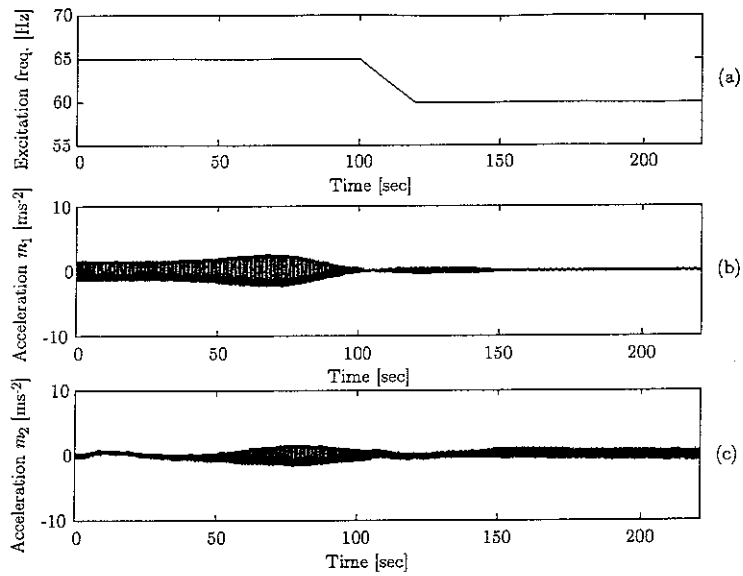


Figure 3.19: Effectiveness of the PD controller for a variable excitation frequency from 65 to 60 Hz: excitation frequency (a), acceleration of the host structure (b) and of the TVA (c)

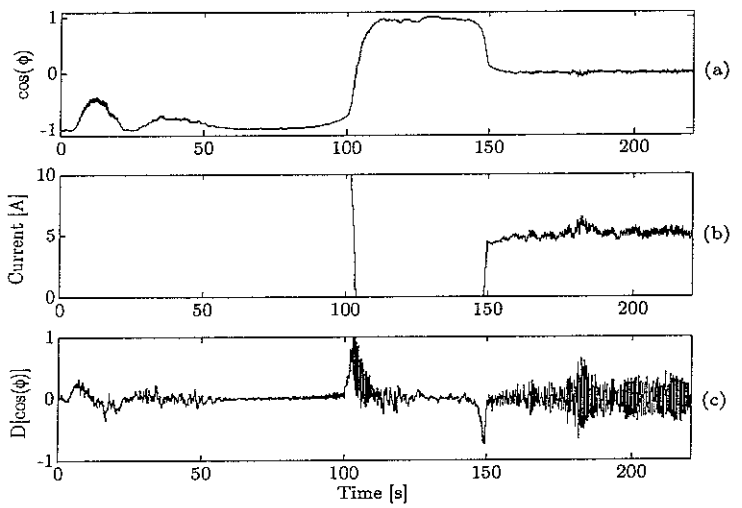


Figure 3.20: PD controller activity for a variable excitation frequency from 65 to 60 Hz: cosine of the acceleration phase difference $\cos\phi$ (a), current (b) and time derivative of $\cos\phi$ (c)

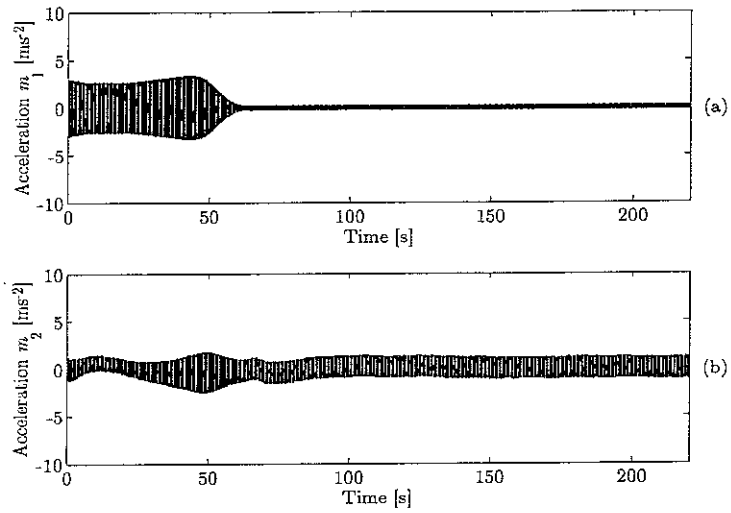


Figure 3.21: Effectiveness of the PD controller optimized by GA using the IAE performance index for a 59 Hz excitation frequency: acceleration of the host structure (a) and of the TVA (b)

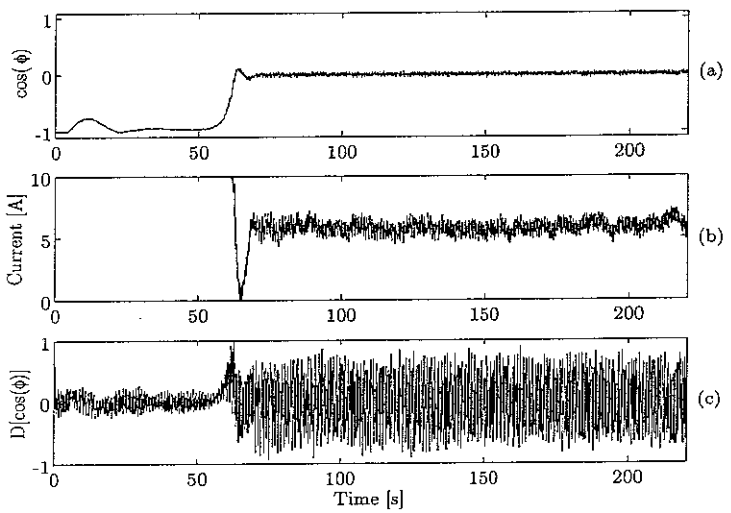


Figure 3.22: PD controller activity optimized by GA using the IAE performance index for a 59 Hz excitation frequency: cosine of the acceleration phase difference $\cos\phi$ (a), current (b) and time derivative of $\cos\phi$ (c)

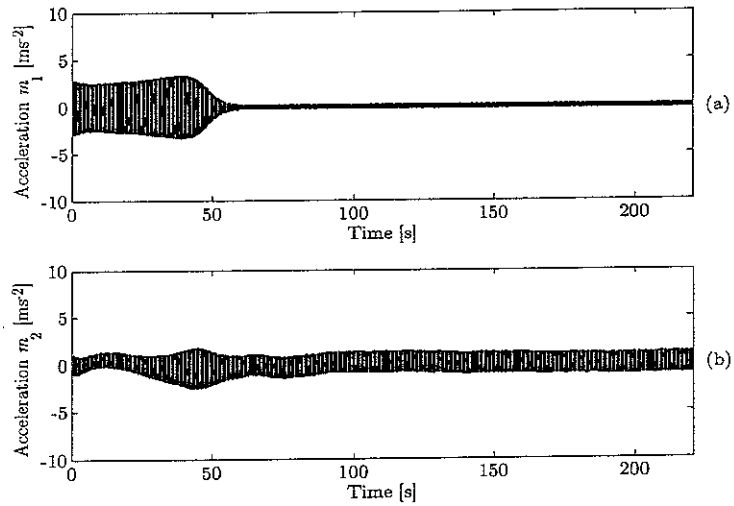


Figure 3.23: Effectiveness of the PD controller optimized by GA using the settling time performance index for a 59 Hz excitation frequency: acceleration of the host structure (a) and of the TVA (b)

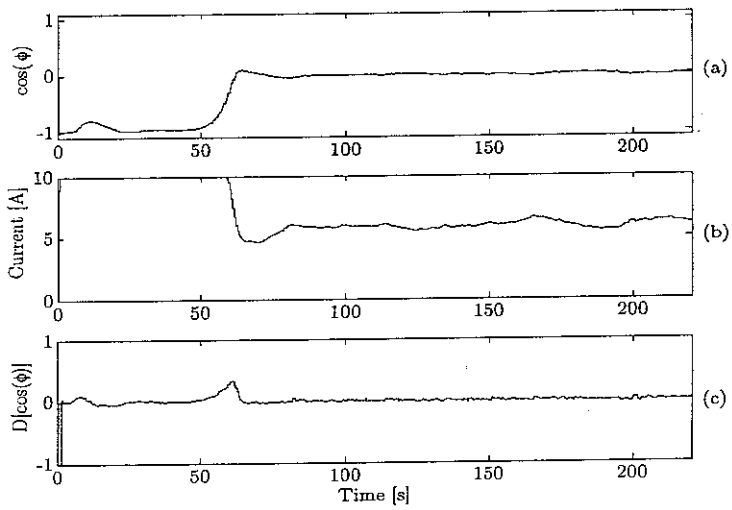


Figure 3.24: PD controller activity optimized by GA using the settling time performance index for a 59 Hz excitation frequency: cosine of the acceleration phase difference $\cos\phi$ (a), current (b) and time derivative of $\cos\phi$ (c)

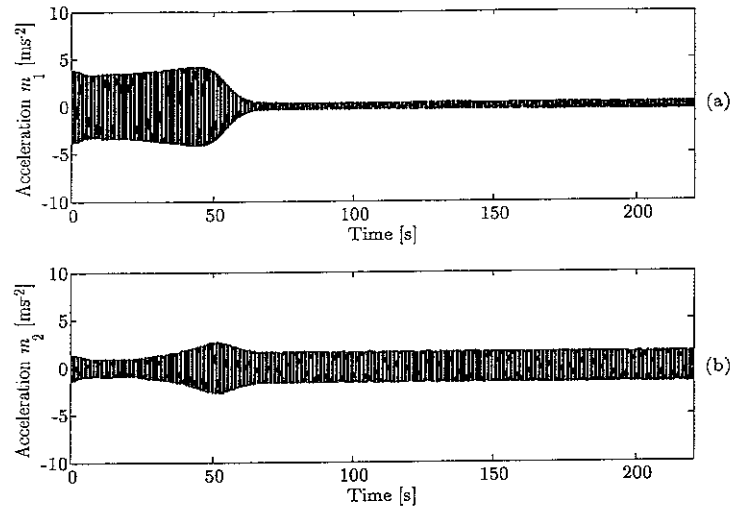


Figure 3.25: Effectiveness of the PD controller for a 59 Hz excitation frequency applying an high-pass filter to accelerations: acceleration of the host structure (a) and of the TVA (b)

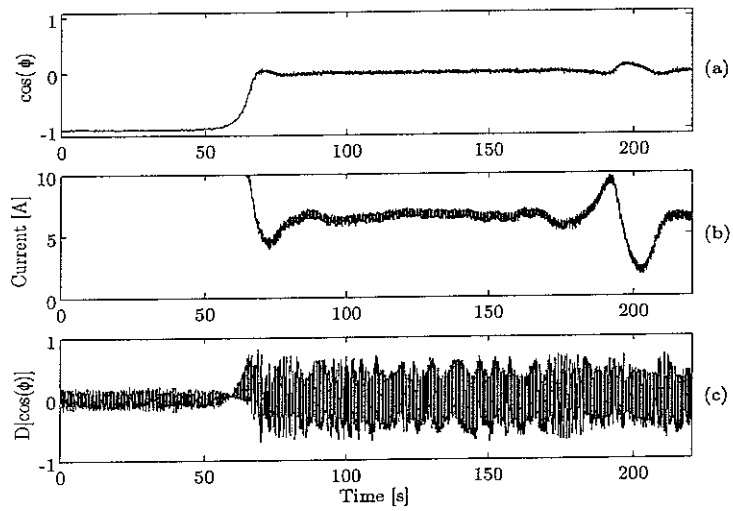


Figure 3.26: PD Controller activity for a 59 Hz excitation frequency applying an high-pass filter to accelerations: cosine of the acceleration phase difference $\cos\phi$ (a), current (b) and time derivative of $\cos\phi$ (c)

# Chapter 4

# Conclusions

In previous work an adaptive tuned vibration absorber (ATVA) has been designed, built and tested in a beam-like configuration using a shape memory alloy (SMA) wire. In the work described in this report the numerical model for the real-time control of such an SMA ATVA has been set up and implemented in SIMULINK® .

Different controllers for the SMA ATVA have been designed and tested on the numerical model. After a comparison of the different kinds of controllers the PD controller was shown to have a better performance. The fuzzy controller had good performance in reducing the amplitude of the oscillation of the host structure but not in the reduction of the error function. P controller showed a performance very similar to the fuzzy controller but with a simpler algorithm. Lastly the continuous controller showed to be effective but with a great settling time.

The constants of the PD controller were optimized, first manually and then automatically using genetic algorithms. The controller optimized automatically did not show better performance than that optimized manually. Following this the robustness of the controller was investigated.

Finally the controller was tested on the real SMA ATVA using the Real Time Workshop. The PD control algorithm proved to be very effective and reliable also with the real system. The performance of such a controller was compared to other controllers but none of these has showed better performance. The results of the experimental analysis were very similar to those of the numerical simulations. Moreover, as the controller proposed is achievable in an analogue way, it is potentially cheaper and more durable.

The tests showed that it is possible to use SMA to realize and control a continuous ATVA. The performances of SMA ATVA makes industrial applications feasible although there are some drawbacks, such as the unexplained over-softening behaviour, observed during the previous work, and the large

time constant, due to the thermal dynamics of the system.

The proposed numerical model describes the behaviour of the real system quite well and can be used to predict the behaviour of other similar devices and to design the respective controllers.

# References


[1] J.P. Den Hartog. *Mechanical vibrations.* Dover Publications, Inc, New York, 4th edition, 1956.

[2] T. Long, M.J. Brennan, and S.J. Elliott. Design of smart machinery installations to reduce transmitted vibrations by adaptive modification of internal forces. *Proceedings of the Institution of Mechanical Engineers, Journal of Mechanical Engineering Science*, 212(I):215–228, 1998.

[3] M.J. Brennan. Actuators for active vibration control - tunable resonant devices. In *Proceedings of the 4th European Conference on Smart Materials and Structures*, Harrogate, U.K., 1998.

[4] M.A. Franchek, M.W. Ryan, and R.J. Bernhard. Adaptive passive vibration control. *Journal of Sound and Vibration*, 189(5):565–585, 1995.

[5] K.E. Smith. Smart tuned mass dampers. In *Active Materials and Adaptive Structures: Proceedings of the ADPA/AIAA/ASME/SPIE Conference*, Alexandria, Virginia, 1991.

[6] M.J. Brennan. Vibration control using a tunable vibration neutralizer. *Proceeding of the Institution of Mechanical Engineering, Journal of Mechanical Engineering Science*, 211(C):91–108, 1997.

[7] D.E. Hodgson, M.H. Wu, and R.J. Biermann. *Tenth ed. Metals Handbook*, volume 2, chapter Shape Memory Alloys. http://www.sma-inc.com/SMAPaper.html.

[8] K. Yang and L.C. Gu. A novel robot hand with embedded shape memory alloy actuators. *Proceedings of the Institution of Mechanical Engineers, Journal of Mechanical Engineering Science*, 216(C):737–745, 2002.

[9] K. A. Williams, G. Chiu, and R. Bernhard. Adaptive-passive absorber using shape-memory alloys. *Journal of Sound and Vibration*, 249(5):835–848, 2002.

[10] E. Rustighi, M.J. Brennan, and B.R. Mace. Design on an adaptive vibration absorber using shape memory alloy. Technical Memorandum 920, University of Southampton, Institute of Sound and Vibration Research, 2003.

[11] M.R.F. Kidner and M.J. Brennan. Varying the stiffness of a beam-like neutralizer under fuzzy logic control. *Transaction of the ASME, Journal of Vibration and Acoustics*, 124:90–99, 2002.

[12] S.B. Choi and J.H. Hwang. Structural vibration control using shape memory actuators. *Journal of Sound and Vibration*, 231(4):1168–1174, 2000.

[13] G. Song. Robust position regulation of a shape memory alloy wire actuator. *Proceedings of the Institution of Mechanical Engineers, Journal of Mechanical Engineering Science*, 216(I):301–308, 2002.

[14] K. A. Williams, G. Chiu, and R. Bernhard. Stability analysis of a shape memory alloy adaptive tuned vibration absorber under pi control with anti-windup. In *ASME International Mechanical Engineering Congress and Exposition*, New York, 2001.

[15] A. Baz, K. Imam, and J. McCoy. Active vibration control of flexible beams using shape memory actuators. *Journal of Sound and Vibration*, 140(3):437–456, 1990.

[16] A.V. Srinivasan and D.M. McFarland. *Smart Structures, Analysis and Design.* Cambridge University Press, 2001.

[17] C. Liang and C.A. Rogers. Design of shape memory alloy springs with applications in vibration control. *Journal of Intelligent Material Systems and Structures*, 8:314–322, 1997.

[18] J.-J.E. Slotine and W. Li. *Applied nonlinear control.* Prentice-Hall, Inc., 1991.

[19] Richard Dorf and Richard Bishop. *Modern Control Systems.* Prentice Hall, 2001.

[20] A. J. Chipperfield and P. J. Fleming. The MATLAB genetic algorithm toolbox. *IEE Colloqium on Applied Control Techniques Using MATLAB*, 1995/014, January 1995.

[21] Alen Varšek, Tanja Urbančič, and Bodgan Filipič. Genetic algorithms in controller design and tuning. *IEEE Transactions on Systems, Man and Cybernetics*, 23(5):1330–1339, Sep-Oct 1993.

[22] A. J. Chipperfield, P. J. Fleming, and C. M. Fonseca. Genetic algorithm tools for control systems engineering. In *Adaptive Computing in Engineering Design and Control*, Plymouth, UK, September 21-22 1994.

[23] Andrew Chipperfield, Peter Fleming, Hartmut Pohlheim, and Carlos Fonseca. *Genetic Algorithm TOOLBOX v1.2 User's Guide.* 1994.